COMPARISON OF DISPERSIVE AND NON-DISPERSIVE NUMERICAL LONG WAVE MODELS AND HARBOR AGITATION

A THESIS SUBMITTED TO
THE GRADUATE SCHOOL OF NATURAL AND APPLIED SCIENCES
OF
MIDDLE EAST TECHNICAL UNIVERSITY

BY

ALİ ÖZBAY

IN PARTIAL FULFILLMENT OF THE REQUIREMENTS
FOR
THE DEGREE OF MASTER OF SCIENCE
IN
CIVIL ENGINEERING

JUNE 2012

Approval of the thesis

COMPARISON OF DISPERSIVE AND NON-DISPERSIVE NUMERICAL LONG WAVE MODELS AND HARBOR AGITATION

submitted by **ALİ ÖZBAY** in partial fulfillment of the requirements for the degree of **Master of Science in Civil Engineering Department, Middle East Technical University** by,

Prof. Dr. Canan Özgen _____
Dean, Graduate School of **Natural and Applied Sciences**

Prof. Dr. Güney Özcebe _____
Head of Department, **Civil Engineering**

Prof. Dr. Ahmet Cevdet Yalçıner _____
Supervisor, **Civil Engineering Dept., METU**

Examining Committee Members:

Prof. Dr. Ayşen Ergin _____
Civil Engineering Dept., METU

Prof Dr. Ahmet Cevdet Yalçıner _____
Civil Engineering Dep., METU

Prof. Dr. İsmail Aydın _____
Civil Engineering Dept., METU

Assoc. Prof. Dr. Utku Kanoğlu _____
Engineering Sciences Dept., METU

Dr. Işıkhan Güler _____
Civil Engineering Dept., METU

Date: **22.06.2012**

I hereby declare that all information in this document has been obtained and presented in accordance with academic rules and ethical conduct. I also declare that, as required by these rules and conduct, I have fully cited and referenced all material and results that are not original to this work.

Name, Last name : Ali Özbay

Signature :

ABSTRACT

COMPARISON OF DISPERSIVE AND NON-DISPERSIVE NUMERICAL LONG WAVE MODELS AND HARBOR AGITATION

Özbay, Ali
M.Sc., Department of Civil Engineering
Supervisor : Prof. Dr. Ahmet Cevdet Yalçıner

June 2012, 112 pages

In this study, the evolution of the numerical water wave models with the theoretical background and the governing equations are briefly discussed and a numerical model MIKE21 BW which can be applied to wave problems in nearshore zone is presented. The numerical model is based on the numerical solution of the Boussinesq type equations formulated on time domain. Nonlinearity and frequency dispersion is included in the model. In order to make comparison between the results of nonlinear shallow water equations with Boussinesq terms, MIKE21 BW and NAMIDANCE are applied to the problem of wave propagation in the long distances and runup on simple and composite slopes. The numerical experiments are applied to Datça Marina and the results are compared to the results of the physical experiments on wave disturbance in Datça Marina. In these comparisons the reflection characteristics of different coastal boundaries in the harbor area are tested and the internal parameters in the model are calibrated accordingly. The numerical model MIKE21 BW is applied to İskenderun harbor as a case study. The input wave parameters are selected from the wave climate study for Iskenderun Harbor. The model is set up and the agitation inside the harbor is computed according to four different incoming wave scenarios. The disturbance maps inside the harbor for different incoming wave scenarios are obtained. The critical regions

of the harbor according to disturbance under different wave conditions are presented and discussed.

Keywords: Boussinesq Type Model, Numerical Water Wave Model, Harbor Disturbance, MIKE21 BW, NAMI DANCE

ÖZ

YAYILGAN VE YAYILGAN OLMAYAN SAYISAL UZUN DALGA MODELLERİ KARŞILAŞTIRMASI VE LİMANİÇİ ÇALKANTISI

Özbay, Ali
Yüksek Lisans, İnşaat Mühendisliği Bölümü
Tez Yöneticisi : Prof. Dr. Ahmet Cevdet Yalçıner

Haziran 2012, 112 sayfa

Bu çalışmada, sayısal su dalgası modellerinin gelişiminden, teorilerinden ve hakim denklemlerden kısaca bahsedilmiş ve yakın kıyı dalga problemlerine uygulanabilen MIKE21 BW sayısal modeli sunulmuştur. Sayısal model, zaman bazında formülleştirilen Boussinesq tipi denklemlerin sayısal çözümlerine dayanmaktadır. Doğrusalsızlık ve frekans dağılımı model tarafından kapsanmaktadır. Doğrusal olmayan sığ su denklemleri sonuçlarını Boussinesq denklemleri sonuçlarıyla karşılaştırabilmek için, MIKE21 BW ve NAMI DANCE uzun mesafelerde dalga ilerlemesi, basit ve kompozit eğimlerde tırmanma problemlerine uygulanmışlardır. Datça Marina'sına sayısal deneyler uygulanmış ve sonuçlar Datça Marinası fiziksel çalkantı modeli sonuçları ile karşılaştırılmıştır. Bu karşılaştırmalarda liman içerisindeki değişik kıyı sınırlarının yansıtıcı özellikleri test edilmiş modeldeki dahili parametreler kalibre edilmiştir. MIKE21 BW sayısal modeli durum çalışması olarak İskenderun Limanı'na uygulanmıştır. Dalga girdi parametreleri İskenderun Limanı için yapılmış olan dalga iklimi çalışmalarından alınmıştır. Model kurulmuş ve liman içerisindeki çalkantı dört farklı dalga koşuluna göre hesaplanmıştır. Limaniçi çalkantı haritaları her bir dalga koşulu için elde edilmiştir. Liman içerisinde değişik dalga koşullarına göre kritik olan bölgeler sunulmuştur.

Anahtar Kelimeler: Boussinesq Tipi Model, Sayısal Su Dalgası Modeli, Liman Çalkantısı, MIKE21 BW, NAMI DANCE

To All Who Suffered From War

and

To Peace

ACKNOWLEDGEMENTS

The author wishes to express his deepest gratitude to his supervisor Prof. Dr. Ahmet Cevdet Yalçıner and Mr. Okan Taktak for their invaluable guidance, advice, criticism, encouragements and insight throughout the research.

The author would like to thank Mr. Okan Taktak also for providing the necessary software license without which this study would not be possible.

The author is grateful to his beloved girlfriend Başak İpekci for her support and charming smile throughout the course of this study. If it wasn't for her, this study would weigh tons over the shoulders.

Both the spiritual and material support of the author's family is very well acknowledged. Their never ending faith has always been there to hold onto. Without them, this path would lead nowhere.

This study was supported by Derinsu Underwater Engineering.

TABLE OF CONTENTS

LIST OF TABLES

TABLES

LIST OF FIGURES

FIGURES

LIST OF SYMBOLS

a	local wave amplitude
B	dispersion coefficient
c	roller celerity
d	total water depth
f_δ	roller shape factor
g	gravitational acceleration
h	still water depth
H_m	mean wave height
H_σ	variance based wave height
m	bottom slope
P	depth integrated velocity in x direction (volume flux)
Q	depth integrated velocity in y direction (volume flux)
R	excess momentum term due to rollers
$t_{1/2}$	half-time for cut-off roller (transition between the two breakers)
Z_B	lower limit of porous region for moving shoreline
Z_L	physical seabed elevation for moving shoreline
β	shape factor for moving shoreline porosity transition function
γ	porosity
ε	minimum value of porosity for moving shoreline
λ_L	length scale
λ_T	time scale
φ	phase shift
δ	thickness of the surface roller

η	surface profile
τ	bottom friction term
ψ	dispersive boussinesq type terms
ω	angular frequency
ϕ_B	initial breaker angle
ϕ_0	terminal breaker angle

LIST OF ABBREVIATIONS

BW	boussinesq waves
DERINSU	Derinsu Underwater Engineering
DHI	Danish Hydraulic Institute
DP	deterministic parameters
FFT	fast fourier transform
Hs	significant wave height
LDW	leading depression wave
LEW	leading elevation wave
METU	Middle East Technical University
N	north
NNE	north northeast
OERC	Ocean Engineering Research Center
PAP	phase averaged parameters
SWL	still water level
TM	transverse mercator
Tp	peak period
Ts	significant period
UTM	universal transverse mercator
W	west
WD	wave direction
WDP	wave disturbance parameters
WGS-84	world geodetic system

CHAPTER 1

INTRODUCTION

There is a pleasure in the pathless woods
There is a rapture on the lonely shore
There is society, where none intrudes
By the deep sea, and music in its roar
I love not the man less, but nature more

Lord Byron

Such a vast mass; not so hard to feel it is alive; to feel its breath penetrating into you as a tranquil yet overwhelming breeze. One can think he can stare at it for eternity. Once seduced by its irresistible lullaby, none can say farewell to it; not to find peace elsewhere.

Ocean has attracted the mankind throughout the history. Not only in modern times, but also during the ancient times, man has exploited the blessings of it. He has fed from it, rejoiced in it, and through it, reached for distant realms leagues away. Battles have been fought on it; cities have been established on the coast of it. Empires rose by it and nations fought to dominate it. The big picture is the same today. The majority of the population lives within the 100 km of the coast. It is an undeniable fact that ocean is an invaluable resource for mankind. It is the biggest fish yet to be caught.

Due to this never-ending quest of man to conquer the ocean, the need to understand its dynamics better has emerged. Even though they were primitive, there are many ruins of ancient ports and harbors that were constructed thousands of years ago. Since then there is a continuous accumulation of knowledge, experience and observation about the ocean dynamics, especially in the coastal areas where the interaction of the mankind with the ocean is at the highest rate. So

it can be stated that the roots of coastal engineering stretches out to thousands of years ago. However, giant leaps in coastal engineering have been taken since the Second World War. The well-known D-Day is a milestone in the history of modern coastal engineering.

For coastal engineering applications, the most important parameters are the wave characteristics of the project area. During the design of all coastal structures, the main design criterion is the wave climate of the project area. The type, size, shape and orientation of the structures are planned by analyzing the effects of the ocean waves that the project area is exposed to. A good understanding of the nearshore wave field of the project area is vital not only to carry out structural designs but also to determine the change in the shoreline due to the change in the sediment transportation due to the planned coastal structures.

Throughout the history, long before computers were invented, engineers resorted to simple analytical methods and empirical formulas. After the invention of computers, research was concentrated on the computational methods. Since then, there is a continuous improvement in the development of numerical wave models which is a still on-going research field.

Today, there are a considerable number of different numerical wave models commercially available or developed for educational purposes by universities or institutes. These models can be grouped into categories according to the zone of the ocean they deal with. Some of them are developed to model the generation of wind waves, some to model the propagation of tsunami waves, some to model nearshore waves etc. In other words, it can be stated that each model has a specific zone of application. For practical reasons, unfortunately there is not, and also most probably will not be, a universal water wave model which can reproduce the combined effects of all types of wave phenomena. The practice is to analyze the problem and choose the modeling method which suits best or sometimes use two or more models in combination by using one's output as input to the other.

The modeling of waves in the coastal zone, from deep water limit to the shoreline has been a major field of study for researchers. The most interesting wave transformations take place in this zone where the utmost detail about the wave field is necessary for the sake of coastal structures or beaches. The modeling of the

highly nonlinear processes in this zone is one of the major problems to be tackled. Today, there are many numerical modeling softwares which can reproduce well the effects of wave transformation types such as shoaling, refraction, diffraction, reflection, breaking, runup as well as taking into account nonlinearity.

MIKE21 BW, which is a Boussinesq type numerical model developed by Danish Hydraulic Institute, is utilized in this thesis to study the wave agitation inside the harbor as the case studies. The model verification has already been done in numerous studies in the past. Its verification has also been performed in this thesis in order to make sure of reliability and applications. The model has several capabilities one of which is the determination of the safe operation time inside the harbors which is selected as the main objective of this thesis.

In Chapter 2, an overview of the evolution of the computational tools for the wave problems in relation to harbor disturbance are presented.

In Chapter 3, the general characteristics and capabilities of the numerical model MIKE21 BW is presented. Its verification is discussed by presenting the comparisons of the results of the previous laboratory experiments.

In Chapter 4, the regular shaped bathymetry with simple and composite slopes are used to compare the results of MIKE21 BW. The problem of runup of long waves is investigated in this chapter by comparing the results with the numerical model NAMI DANCE which uses similar equations without dispersion term.

In Chapter 5, the numerical model is tested and the internal parameters (reflections from coastal boundaries) are calibrated by applying to the wave disturbance problem of Datça Harbor for which a complete experimental study was performed and available.

In Chapter 6, the model is applied to Iskenderun bay for determination of the critical regions under critical wave conditions for the safe operation times. The results are compared and discussed.

In Chapter 7, the general discussions and main concluding remarks are presented.

CHAPTER 2

LITERATURE REVIEW

A model, in its simplest definition, is the representation of an original object or a physical process. As far as the ocean waves are concerned, models can be categorized into 4 main groups:

1. Analytical
2. Empirical
3. Physical
4. Numerical

Analytical models are expressed by partial differential equations or ordinary differential equations. Closed-form solutions can be obtained when the equations are solved analytically for a specific condition. Empirical models are obtained by summarizing a mathematical expression according to the field data of the prototype. They are easy tools to describe the prototype behavior by simple algebraic equations. Physical models are miniatures of prototypes with certain scales. The data gathered from physical models, can be extrapolated to estimate the parameters for the prototypes (Lin, 2008).

"A numerical wave model is the combination of the mathematical representation of a physical wave problem and the numerical approximation of the mathematical equations. Compared to theoretical modeling, the difference is only in the means of finding the solution of the governing equations for the wave problems. To model ocean waves numerically, we must start from some existing "wave equations" obtained from theoretical studies." (Lin, 2008).

In coastal engineering projects, the engineer has to know what sort of waves are going to be dealt with at the project area. However, such data may not always readily available. In such cases, the engineer can resort to utilizing numerical models to simulate the wave conditions at the project site by making use of the indirect measurement data collected at or near the project area. Thus, a cost-efficient way of predicting the design wave parameters is secured.

"Practical wave prediction applications involve a mixture of local wind generated sea and swell, spatially and temporally varying winds and irregular bathymetry and coastlines. Predicting waves in these demanding situations requires resorting to a model; however a comprehensive model which incorporates our full understanding of wind wave physics and is applicable in all situations would be prohibitively expensive. Instead, a variety of models have been proposed for applications in specific situations. In order to select the most appropriate model requires an understanding of the relative importance of the various physical processes active in each domain." (Young, 1999).

There are a number of numerical model types for water waves. These are;

1. Spectral Models
2. Mild-slope Equation Models
3. Shallow-water Equation Models
4. Quasi-three-dimensional hydrostatic pressure wave models
5. Boussinesq Equation Models

As seen in Table 2-1 (Battjes, 1994) has classified the wave domain into 4 categories according to the importance of the physical processes taking place.

Table 2-1: The relative importance of various physical mechanism in different domains: ⊗ - negligible; ○ - minor importance; ● - significant; ⬤ - dominant [after (Battjes, 1994)]

Physical Process	Deep Oceans	Shelf Areas	Shoaling Zone	Harbours
Diffraction	⊗	⊗	○	⬤
Depth refr./Shoaling	⊗	●	⬤	●
Current Refraction	⊗	○	●	⊗
Quad. Interactions	⬤	⬤	○	⊗
Triad Interactions	⊗	○	●	○
Atmospheric Input	⬤	⬤	○	⊗
White-Capping	⬤	⬤	○	⊗
Depth Breaking	⊗	○	⬤	⊗
Bottom Friction	⊗	⬤	●	⊗

Numerical models fall into 2 main categories: phase resolving models and phase averaging models. Phase resolving models estimate the height and the phase of each wave whereas the latter ones estimate spectral parameters such as H_s, T_p, etc. (Young, 1999).

Boussinesq type models are phase-resolving models which take into account shoaling, refraction, diffraction, reflection, wave-wave interaction and wave-current interaction. All these characteristics of Boussinesq type models make them powerful tools for studying wave conditions at coastal zones and inside harbors.

2.1 Overview of Boussinesq Type Models

"The irrotational motion of an incompressible homogeneous inviscid fluid is generally a three-dimensional problem. The main issue of Boussinesq-type equations is, however, to reduce the description to a two-dimensional one by introducing a polynomial approximation of the vertical distribution of the flow field into the integral conservation laws, while accounting for non-hydrostatic effects due to the vertical acceleration of water." (Madsen & Schäffer, 1998)

The original Boussinesq equations were introduced by J. V. Boussinesq in 1872. In (Boussinesq, 1872), depth-averaged velocities were used to express the original formulation. The most important aspects of the original formulation are that the depth was constant, the dispersion was weak and the nonlinearity was weak as well (Madsen & Fuhrman, 2010).

The original equations introduced by (Boussinesq, 1872) were improved by (Mei & Méhauté, 1966) and (Peregrine, 1967) for uneven bathymetry and also alternative horizontal velocity variables were used to express the equations. What are now referred to as "classical" Boussinesq equations were derived by Peregrine in 1967. The results of these studies also kick-started the first computer model simulations of solitary waves on beaches in (Peregrine, 1967) and (Madsen & Mei, 1969). (Madsen & Fuhrman, 2010)

Numerical stability and dispersive characteristics were improved by (Benjamin, et al., 1972). Shortly after, the first commercial modeling system, which was based on classical low-order Boussinesq equations, was introduced by (Abott, et al., 1978) (Madsen & Fuhrman, 2010). Short waves, either regular or irregular, were modeled on both irregular and regular bathymetry. The modeling system was cross-checked with the results of analytical results and physical models and it was observed that the model predicts the wave thrusts, radiation stresses and alongshore currents correctly (Abott, et al., 1978). The outputs of this study focused the researches on improving the shallow water dispersive limits and nonlinear characteristics of the Boussinesq models.

In (Witting, 1984), a milestone, which altered the future path of researches on Boussinesq type models, was discussed. The concept of Padé approximants within differential equations initiated a series of studies which led to the development of the modern Boussinesq equations which are still being continuously improved (Madsen & Fuhrman, 2010).

In (Madsen, et al., 1991) the linear dispersion characteristics of the Boussinesq equations in deeper water are improved by introducing a new set of lower-order equations. This study expanded the applicable range of the low-order Boussinesq equation by increasing the allowable depth limits from $kh \approx 1$ up to $kh \approx 3$. Yet, no significant improvements of the nonlinear properties of the Boussinesq formulation

were obtained as a result of this study. So far, the linear properties of the Boussinesq formulations yielded far more satisfactory results than the nonlinear characteristics did.

(Madsen & Schäffer, 1998) presented formulations, which they called fully nonlinear, of Boussinesq type equations of higher-order in dispersion and nonlinearity. Formulations of the enhanced equations, which put emphasis especially on linear dispersion, shoaling and nonlinear properties for large wave numbers, were introduced in terms of several velocity variables. In the end, although the linear dispersion accuracy was very good up to kh=6, the improvement in the accuracy of the nonlinear characteristics was not as great.

However, (Agnon, et al., 1999) finally succeeded to obtain considerably good results with respect to nonlinear characteristics. The linear characteristics of the formulations were perfect as well. In this new Boussinesq-type formulation, the solution is divided into two parts: the linear part and the nonlinear part. The linear part, which corresponds to shoaling and dispersion, is solved by satisfying the Laplace problem and the kinematic bottom condition by an infinite power series expansion of the velocity field from the still water level. The nonlinear part was treated by expressing and time-stepping the dynamic and kinematic surface boundary conditions in terms of velocity variables defined directly on the free surface (Madsen & Fuhrman, 2010).

After this point, the research was focused more on improving the vertical distribution of the velocity field which yielded poor results for wave numbers as small as $kh \approx 1.7$. In (Madsen, et al., 2002) and (Madsen, et al., 2003), accurate linear and nonlinear properties were obtained up to $kh \approx 25$ while achieving accurate results for interior velocity field up to $kh \approx 12$. In these studies the bathymetry was restricted to mildly sloping ones whereas in (Madsen, et al., 2006) this restriction was removed to extend the formulation for rapidly varying bathymetries (Madsen & Fuhrman, 2010).

2.2 MIKE21 Boussinesq Wave Module

MIKE21 BW includes two modules which are based on the numerical solution of the time domain formulations of Boussinesq type equations. Both nonlinearity and frequency dispersion is included in the Boussinesq equations. By including the effect of vertical accelerations on the pressure distribution, the frequency dispersion is enabled. A flux formulation with improved linear dispersion characteristics is used in both modules to solve the Boussinesq type equations. Propagation of directional wave trains travelling from deep to shallow water can be simulated in both modules by means of the enhanced Boussinesq type equations which are originally derived by (Madsen, et al., 1991) and (Madsen & Sørensen, 1992).The depth limitation in the modules is $h/L_0 \approx 0.5$ (or $kh \approx 3.1$) where h is water depth, L_0 is deep water wave length an kh is the relative wave number. Instead of the enhanced equations, the classical Boussinesq equations derived by (Peregrine, 1967) are also available. But in that case the depth limitation becomes $h/L_0 \approx 0.22$ (or $kh \approx 1.4$). (Madsen, et al., 1997) and (Madsen, et al., 1997) revised the equations in the model to simulate the wave breaking and moving shoreline (DHI, 2010).

The two modules of MIKE21 BW version is as follows:

- 1DH Boussinesq Wave Module
- 2DH Boussinesq Wave Module

"The 1DH Module (one horizontal space coordinate) solves the enhanced Boussinesq equations by a standard Galerkin finite element method with mixed interpolation for variables defined on an unstructured (or a structured) grid. Surf zone dynamics and swash zone oscillations can be simulated for any coastal profile in this module." (DHI, 2010)

"The 2DH Module (two horizontal space coordinates) solves the enhanced Boussinesq equations by an implicit finite difference technique with variables defined on a space staggered rectangular grid. The module is capable of reproducing the combined effects of most wave phenomena of interest in port, harbor and coastal engineering" (DHI, 2010). These include:

- Shoaling
- Refraction
- Diffraction
- Wave Breaking
- Bottom Friction
- Moving Shoreline
- Partial Reflection and Transmission
- Non-linear Wave-Wave Interaction
- Frequency Spreading
- Directional Spreading

"Phenomena, such as wave grouping, surf beats, generation of bound sub-harmonics and super-harmonics and near-resonant triad interactions, can also be modeled using MIKE21 BW. Thus details like generation and release of low-frequency oscillations due to primary wave transformation are well described in the model. This is of significant importance for harbor resonance, seiching and coastal processes" (DHI, 2010).

"Wave breaking is implemented on basis of the surface roller concept for spilling breakers. The effect on the wave motion is modeled by introduction of additional convective terms, and the determination of the surface rollers is based on a geometric approach. The roller is considered as a passive bulk of water isolated from the rest of the wave motion, while being transported with the wave celerity. The wave breaking is assumed initiated if the slope of the local water surface roller is determined" (DHI, 2010).

"The incorporation of a moving shoreline is based on the following approach: the computation domain is extended artificially by replacing the solid beach by a permeable beach characterized by a very small porosity. Near the moving shoreline the water surface will intersect with the seabed and continue into the porous beach. Hence the instantaneous position of the shoreline is simply determined by this intersection" (DHI, 2010).

"MIKE21 BW also includes porosity for the simulation of partial reflection from and transmission through piers and breakwaters. Sponge layers are applied when full absorption of wave energy is required. Internal generation of waves is also included" (DHI, 2010).

2.3 Other Boussinesq Type Models

In the literature, there are a number of different numerical models based on the solution of Boussinesq type equations which have been continuously enhanced by different researchers in order to reproduce the effects of shoaling, refraction, diffraction, reflection, breaking, wave-wave interaction and runup better on bathymetries as deep as the deep water limits.

In (Kennedy, et al., 2000) and (Chen, et al., 2000), the extension of a fully nonlinear Boussinesq type model is introduced. The model is based on the extension of the fully nonlinear equations of (Wei, et al., 1995) and (Nwogu, 1993) to include wave-breaking and runup. Both 1D and 2D models are tested and verified for breaking and runup. The model results show generally good agreement when compared to experimental test results.

In (Nwogu & Demirbilek, 2001), a Boussinesq type numerical model, BOUSS-2D, is described in detail. The equations in the model basically originate from (Peregrine, 1967). In (Nwogu, 1993) the "classical" equations were improved to increase the range of applicability from shallow water to deep water. Then in (Wei, et al., 1995), these equations were further improved to obtain a fully nonlinear form. Finally in (Nwogu, 1996), the fully nonlinear form of Boussinesq equations were extended to the surf zone to include important phenomena such as bottom friction, breaking and runup. The model is validated by comparing to a number of analytical, laboratory and field experiments. The results of the comparisons are most satisfactory and the model is proved to be applicable to many coastal and harbor wave transformation studies.

CHAPTER 3

MODEL VERIFICATION

In this chapter, the comparison of the model outputs and a number of physical model tests from previous studies are presented. The model is tested for the basic wave transformations such as shoaling, refraction and diffraction. In all cases, the model yields very good results compared to the physical model outputs.

3.1 Linear Shoaling

In (Madsen & Sørensen, 1992), the linear shoaling properties of the model are verified and compared to the first order Stokes theory results. In the test, the model bathymetry is slowly varying from deep to shallow water. All the non-linear terms are turned off and the dispersion coefficient B is set equal to 1/15 in order to enable the deep water solution of the wave field.

Two tests are carried out with the wave characteristics presented in Table 3-1.

Table 3-1: Wave Characteristics for Shoaling Test

	Experiment 1	Experiment 2
T (sec)	4	8
h/L_0	0.52-0.008	0.13-0.002

Experiment 1 is a deep water to shallow water example whereas Experiment 2 is a typical intermediate to shallow water example. The comparisons of the results are given in Figure 3-1 & Figure 3-2.

In both experiments, the results are in good agreement with the first order Stokes theory.

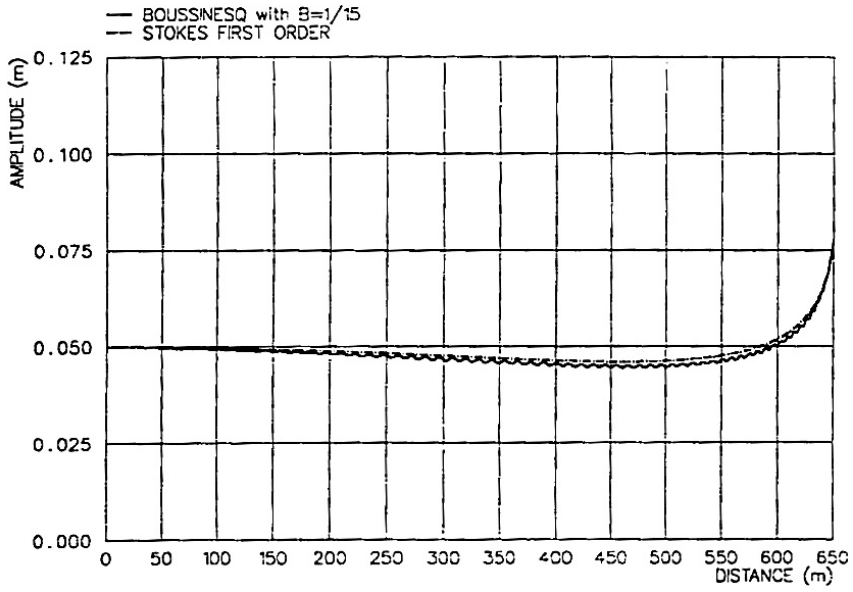

Figure 3-1: Results of Experiment 1. Wave Period = 4.0s, water depth=13-0.2m, B=1/15. Maximum elevations compared to Stokes first order theory (Madsen & Sørensen, 1992)

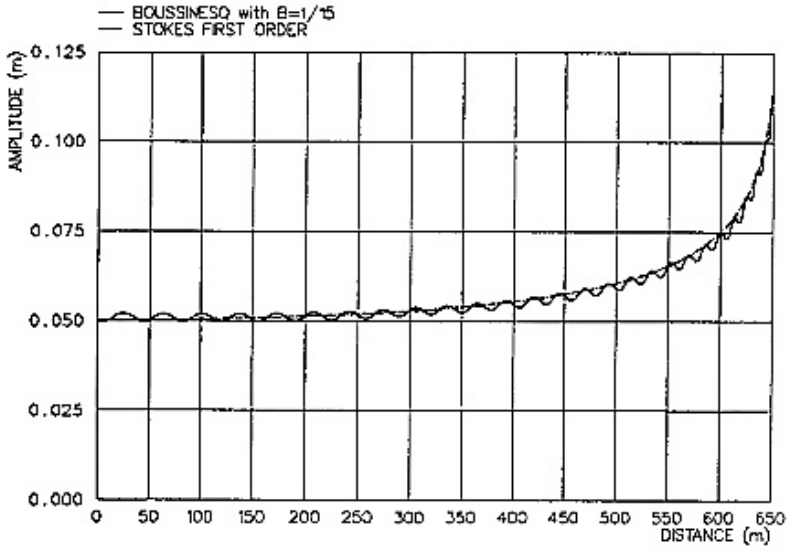

Figure 3-2: Results of Experiment 2. Wave Period = 8.0s, water depth=13-0.2m, B=1/15. Maximum elevations compared to Stokes first order theory (Madsen & Sørensen, 1992)

3.2 Shoaling and Breaking of Regular Waves

In (Madsen, et al., 1997), the numerical model is verified for shoaling and breaking of regular waves on gently sloping plane beaches. The research was focused on shoaling of unidirectional waves which break as either spilling or plunging. The model outputs are compared to several different physical model test results, each of which has different wave characteristics.

In the first case, the model is compared to the results of (Stive, 1980) for the breaking of monochromatic waves on a plane slope. The breaker is a spilling type and a second order Stokes wave is used as input in the numerical model.

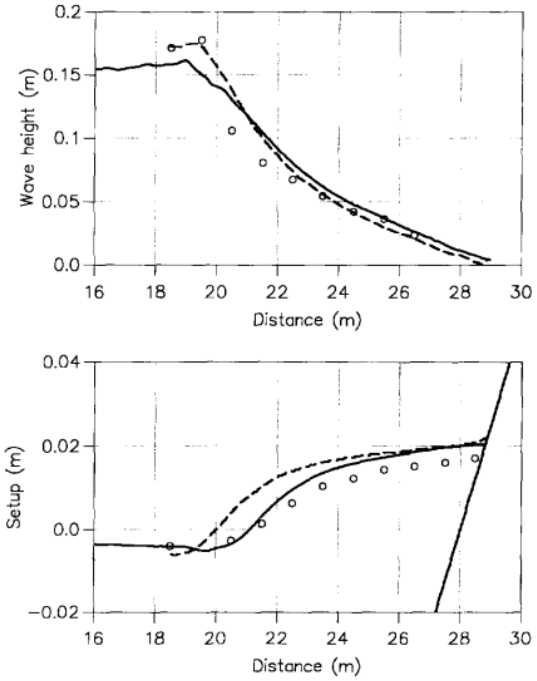

Figure 3-3: Spatial variation of the wave height setup for the test of (Stive, 1980). Present model (————); numerical solution by (Kobayashi, et al., 1989) (− − −); experimental data (○). (Madsen, et al., 1997)

As seen in Figure 3-3, the overall performance of the model is acceptable while shoaling is slightly underestimated just before breaking and the wave height decay after breaking is milder than the experiment results. (Madsen, et al., 1997)

In the second case, the model is compared with the results of a flume test carried out by (Hansen & Svendsen, 1984). The breaker in this case is a spilling one in

shallow water. The comparison of the experimental results and the Boussinesq model results are shown in Figure 3-4.

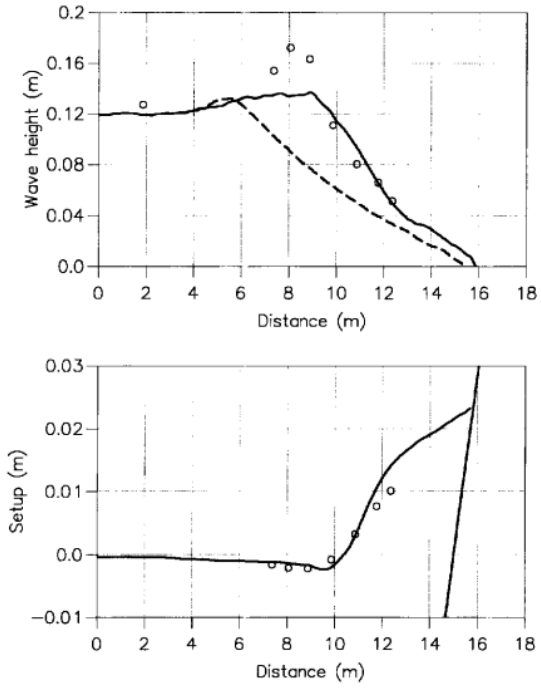

Figure 3-4: Spatial variation of wave height and setup for the test of (Hansen & Svendsen, 1984). Present model (————); numerical solution by (Kobayashi, et al., 1989) (– – –); experimental data (○). (Madsen, et al., 1997)

As seen in Figure 3-4, although the shoaling up to the breaking point is not reproduced perfectly by the model, the position of the breaking point and the wave parameters in the surf zone such as wave height and setup are predicted very well. (Madsen, et al., 1997).

In the third case, the model outputs are compared to the experimental data obtained by (Ting & Kirby, 1994). In this case, instead of the spilling breakers as in the previous two cases, the breaker type is plunging. Although the model is not designed to handle plunging breakers, by altering the breaker parameters, the plunging breakers are represented fairly well. (Madsen, et al., 1997).

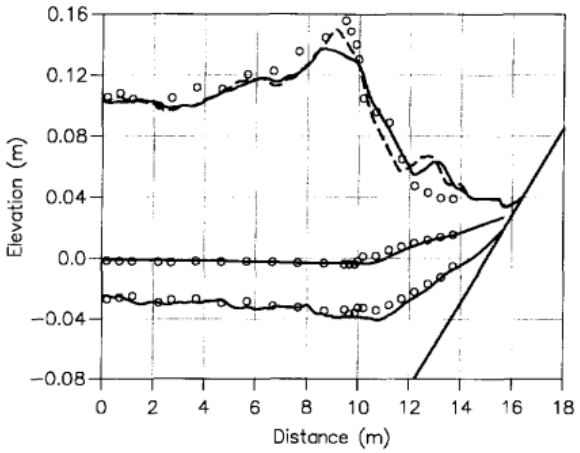

Figure 3-5: Spatial variation of the crest elevation, wave trough elevation and mean water level for the test of (Ting & Kirby, 1994) with plunging breakers (T=5 s). Present model with default parameters (————); present model with calibrated parameters (ϕ_B=25 deg and $t_{1/2}$ =T/10) (− − −); experimental data (○). (Madsen, et al., 1997)

As observed in Figure 3-5, the trough elevation and the mean water level are presented well in the model, while the predicted crest elevations are relatively less accurate. It should also be noted that the second peak in the crest elevation outputs of the numerical model appears due to the limitations of the model. (Madsen, et al., 1997).

3.3 Variation of Surface Elevations and Shoreline Motion

In (Madsen, et al., 1997), the numerical model is tested for the breaking and runup of irregular waves. The research is focused on the surface elevations and the shoreline motion. The outputs of the numerical model are compared to the experimental results obtained by (Mase, 1994) and (Mase, 1995). The sketch of the wave flume is given in Figure 3-6.

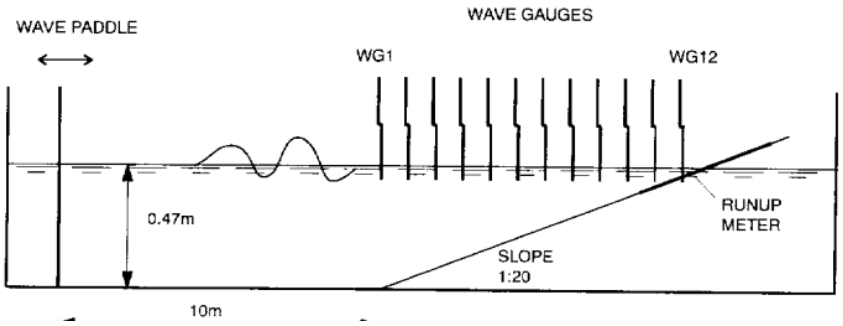

Figure 3-6: Sketch of physical wave flume (Mase, 1994)

The waves created by the wave paddle in the experiment are bi-chromatic. In the numerical model, in order to avoid errors introduced during the generation of the planned surface profile by the paddle, the model boundary is placed at the first wave gauge and the wave input is selected as the surface profile recorded by the first wave gauge (WG1). "The measured signal at WG1 is analyzed by FFT, the low frequency motion is removed and the remaining signal is converted into a flux boundary condition using the linear theory. At the position of WG1 the waves are generated internally and re-reflection from this boundary is prevented by using a 1m wide sponge layer offshore from the line of generation." (Madsen, et al., 1997).

For the purpose of illustration, the comparison figures of only one wave input scenario is given

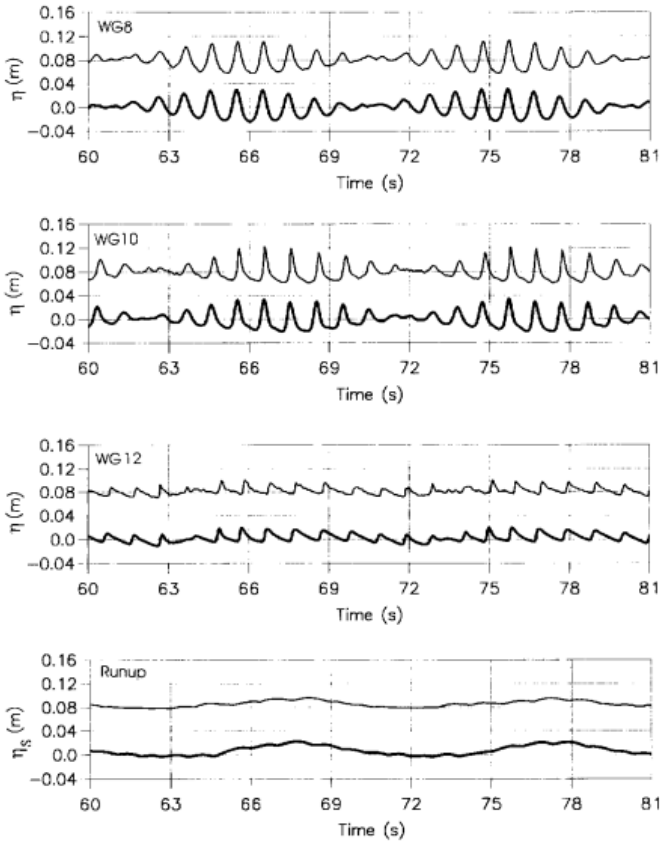

Figure 3-7: Surface elevation (η) and swash oscillation(η_s, vertical displacement). Case: WP2, f_m=1.0 Hz i.e. f_1=1.05 Hz and f_2=0.95 Hz.(——) Present model. (——) Experimental data by (Mase, 1994), shifted relative to computed results by 0.08. (Madsen, et al., 1997)

In Figure 3-7, the results of the physical model test are shifted 0.08m for the making comparison easier. By comparing all cases in (Mase, 1994) with the numerical model outputs, it is observed that, although the wave conditions vary considerably, the surface profiles and runup records of the numerical model agree well with the physical model results. The breakers in the experiment vary as spilling and plunging. Dispersion, wave-wave interaction and dissipation due-to breaking are predicted well by the numerical model.

3.4 Wave Induced Currents In A Rip Channel

(Sørensen, et al., 1998) tested the numerical model for the case of the wave induced currents on a plane sloping beach with a rip channel in the middle. The numerical model bathymetry and wave inputs are identical to the laboratory experiments carried out by (Hamm, 1992). The contour plot and the profile view of the bathymetry are presented in Figure 3-8.

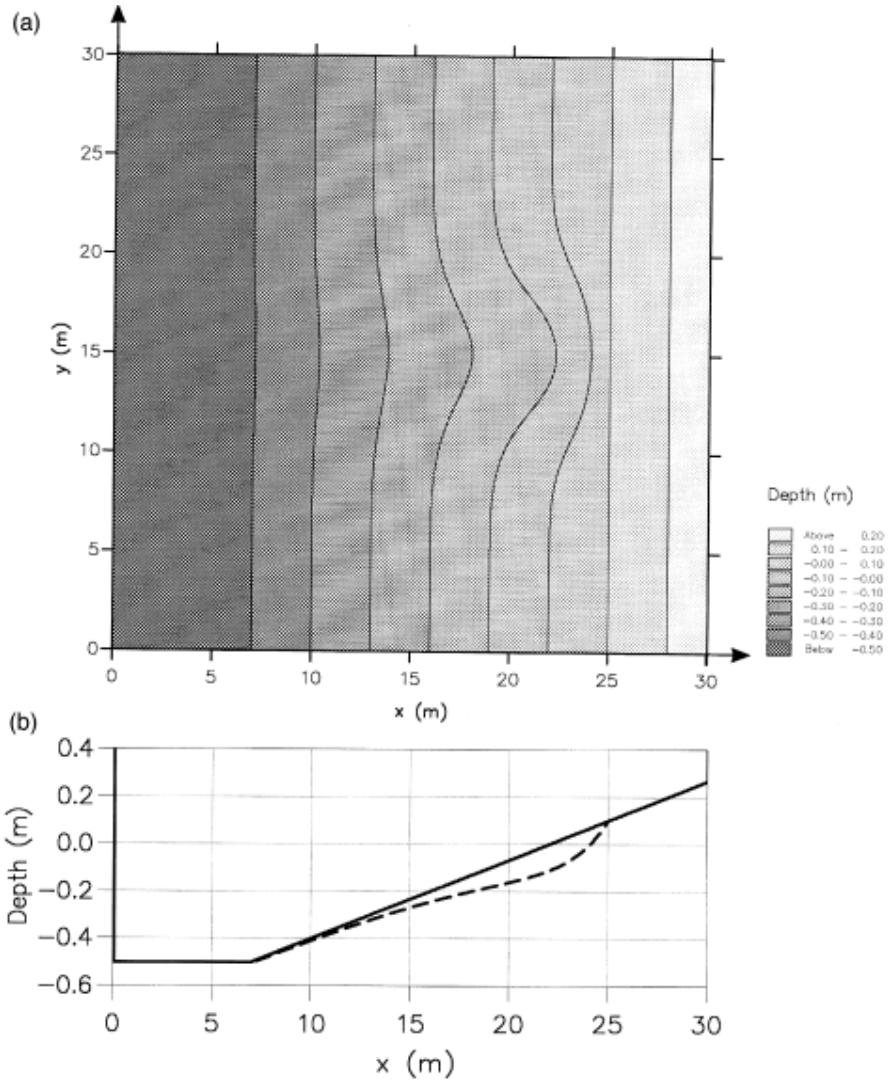

Figure 3-8: The wave basin for the model setup. (a) Contour plot of the bathymetry and (b) beach profiles. (————) along the plane beach section, (− − −) along the rip channel. (Sørensen, et al., 1998)

The wave input for the test is selected as a unidirectional and regular waves with T=1.25 s and H=0.07 m at the offshore boundary. In the numerical model, the bathymetry was split in half by a reflective boundary along the center line of symmetry.

The breaking occurs closer to the shoreline along the centerline due to the increased depth and the refraction due to the bathymetry of the rip channel which results in a smaller setup along the centerline compared to the plane beach section of the domain. The difference in the water level due to different setup values causes a flow into the rip channel from both directions. These flows from both sides are

combined to form a rip current in the offshore direction. The depth-averaged velocity field in the domain is illustrated in Figure 3-9.

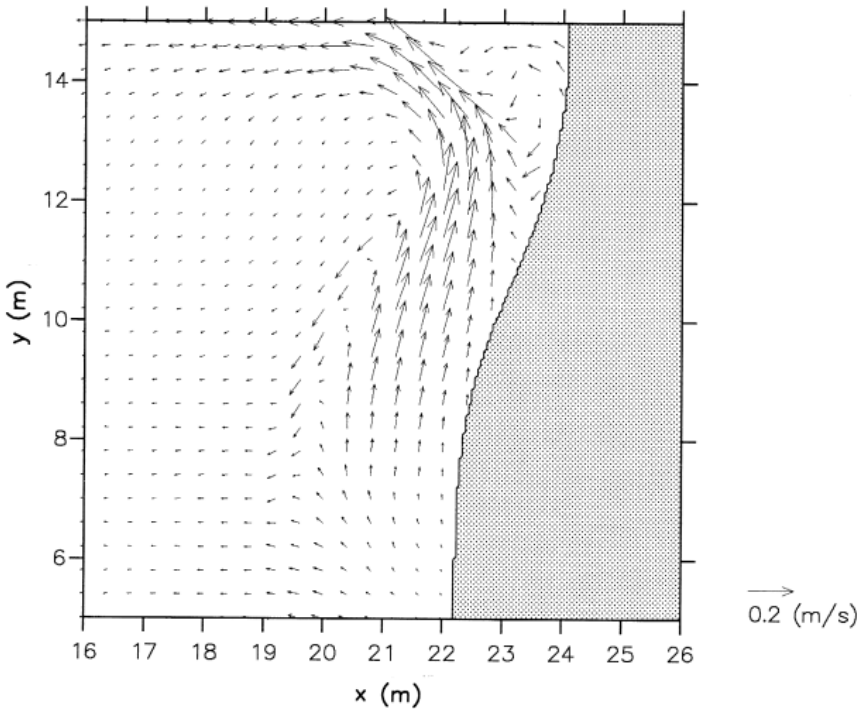

Figure 3-9: Depth-averaged velocity over the domain. The centerline of the rip channel is at the top (y=15 m) and the shoreline is to the right. (Sørensen, et al., 1998)

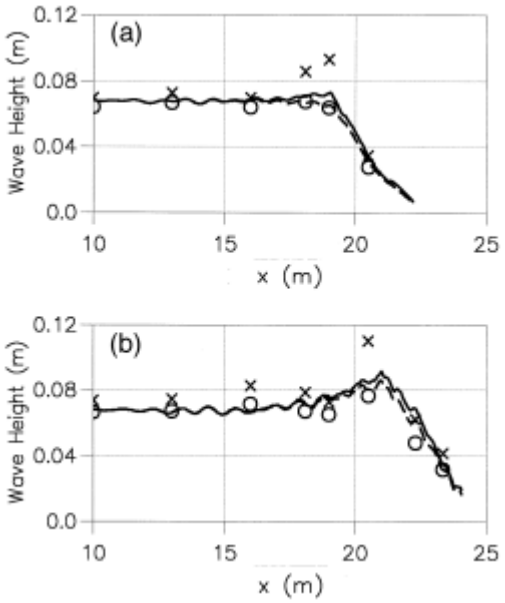

Figure 3-10: Comparison between the laboratory experiments and the numerical model outputs. (a) Along a plane beach section and (b) along the rip channel. (————) Mean wave height, H_m, present model; (− − −) Variance-based wave height, $H_\sigma/\sqrt{2}$, present model: (x) Significant wave height $H_{1/3}$, experimental data by (Hamm, 1992); (○) Variance-based wave height $H_\sigma/\sqrt{2}$ experimental data by (Hamm, 1992). (Sørensen, et al., 1998)

In Figure 3-10, it is observed that the model results are in good agreement with the laboratory experiments. In (Sørensen, et al., 1998), it is also noted that the current speeds along the rip channel also is represented well in the numerical model.

3.5 Diffraction and Wave Induced Currents Around A Detached Breakwater

In (Sørensen, et al., 1998), simulations were run to compare the results of the Boussinesq type numerical model to the results of the laboratory experiments reported by (Mory & Hamm, 1997) and (Hamm, et al., 1995). The model setup is presented in Figure 3-11.

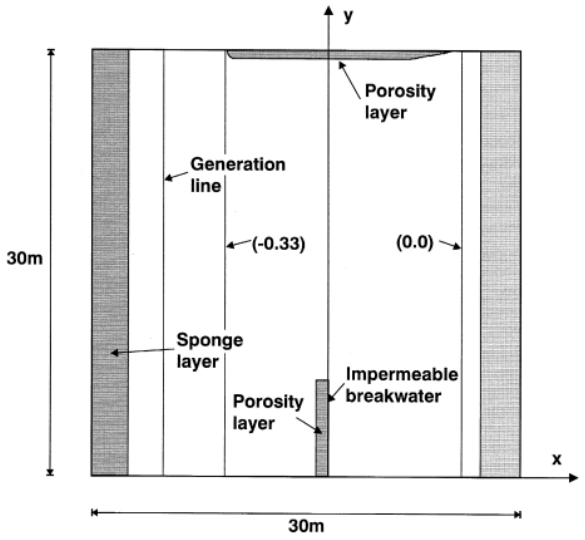

Figure 3-11: Model setup for the detached breakwater experiment (Sørensen, et al., 1998)

In the numerical model setup, the wave generation line is placed on the left. A sponge layer is placed behind the generation line in order to absorb the waves propagating to the left offshore boundary. If not absorbed by the sponge layer, these waves will be reflected from the closed offshore boundary and will be re-sent into the model domain. A detached breakwater with a porosity layer on the offshore side is placed approximately in the center. Normal incident regular unidirectional waves are generated in the model.

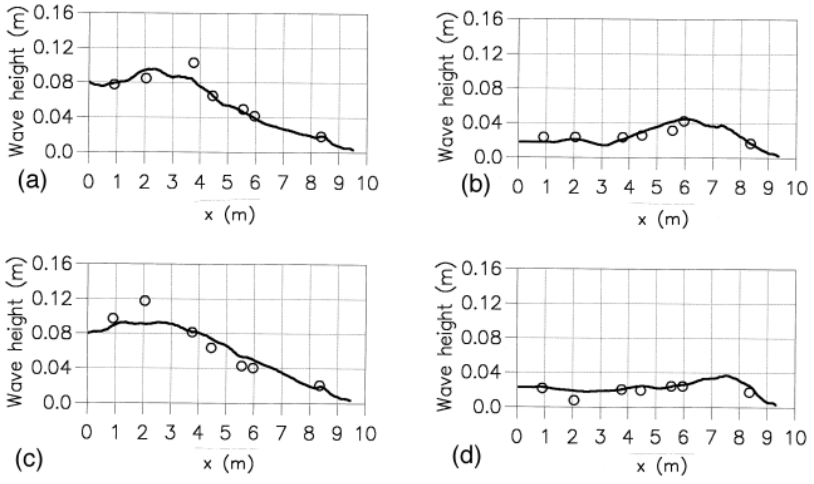

Figure 3-12: Cross-shore variation of the mean wave height, H_m. (a) y=16 m, (b) y=9 m, (c) y=5 m, (d) y=1 m. (———) Present model; (○) Experimental data by (Hamm, et al., 1995). (Sørensen, et al., 1998)

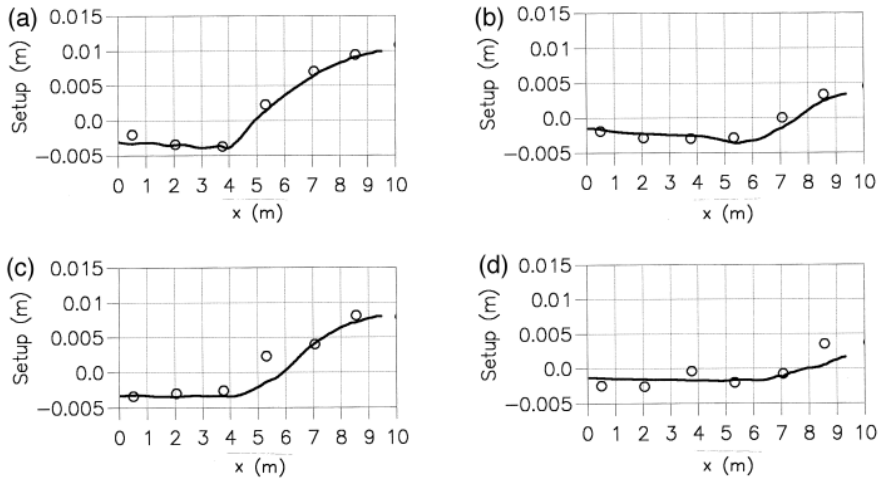

Figure 3-13: Cross-shore variation of the setup. (a) y=16 m, (b) y=9.39 m, (c) y=6.29 m, (d) y=3.19 m. (———) Present model; (◌) Experimental data by (Hamm, et al., 1995). (Sørensen, et al., 1998)

In Figure 3-12 & Figure 3-13, it is observed that the numerical model outputs are in good agreement with the experimental results. The wave height and the setup values at various sections are represented well in the numerical model.

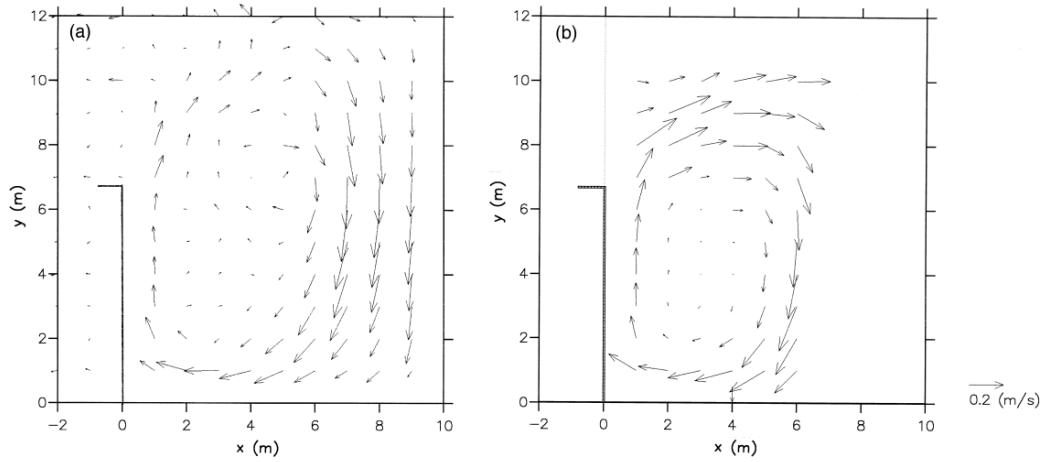

Figure 3-14: Circulation cell behind the detached breakwater. (a) Numerical model outputs; (b) Experimental data by (Hamm, et al., 1995). (Sørensen, et al., 1998)

The comparison of (a) & (b) in Figure 3-14 shows that the current pattern around the detached breakwater due to normal incident regular unidirectional waves are very similar in both the numerical model outputs and the laboratory experiment results. The major difference in two cases is that the current is strongly pointed towards the shore at the tip of the breakwater in the laboratory experiment results while in the numerical model results, the current is not curved so sharply towards

the shore. This indicates that the current in the numerical model is strongly dominated by convection. (Sørensen, et al., 1998)

CHAPTER 4

COMPARISON OF LONG WAVE PROPAGATION AND RUNUP BY DIFFERENT NUMERICAL MODELS

In this chapter MIKE21 BW, which solves Boussinesq type long wave equations and NAMI-DANCE which uses nonlinear form of shallow water equations are applied to the same bathymetry conditions with different (plane or stepwise) slope conditions. In order to eliminate the vertical coordinates from the equations, in Boussinesq theory, the horizontal velocity distribution is assumed to increase linearly from zero at the bottom to the maximum at the surface while in nonlinear shallow water equations, it is assumed to be constant from the bottom to the surface. There are also dispersive terms in the Boussinesq type equations while dispersion effect is not included in the nonlinear shallow water equations. The dispersion mainly refers to the phenomena that waves with different lengths propagate with different phase speeds.

The propagation, climbing and the deformation of the wave on the slope are computed by two different models. The maximum water surface elevations computed on land, the inundation distances and the surface profiles at certain gauge locations are compared. In the plane slope case, 10 different sinusoidal wave conditions are applied to 4 different slope conditions.

In Section 4.2, 4 different sinusoidal wave conditions are simulated for 1 bathymetry. The propagation and the transformation of the waves until the shoreline are compared at certain gauges.

More information and theoretical background of NAMI-DANCE is given at (Anon., 2010) and (Imamuira, et al., n.d.).

4.1 Dispersion Effect on the Plane Sloping Beach

The basic input parameters of the two models are bathymetry and input wave conditions. In the applications same bathymetry and initial wave are used for both models. The breaking effect is enabled in MIKE21 BW while breaking is not taken into account by NAMI-DANCE.

4 different plane sloping bathymetries are determined for applications. The maximum water depth in the basin is selected 50m at the toe of the slope. The plane slope is selected to be 1/10, 1/15, 1/20 and 1/25 for different cases. A cross section of a sample profile of the bathymetry and the gauge location is given in Figure 4-1. The spatial grid spacing is selected as 5 meters in both numerical models.

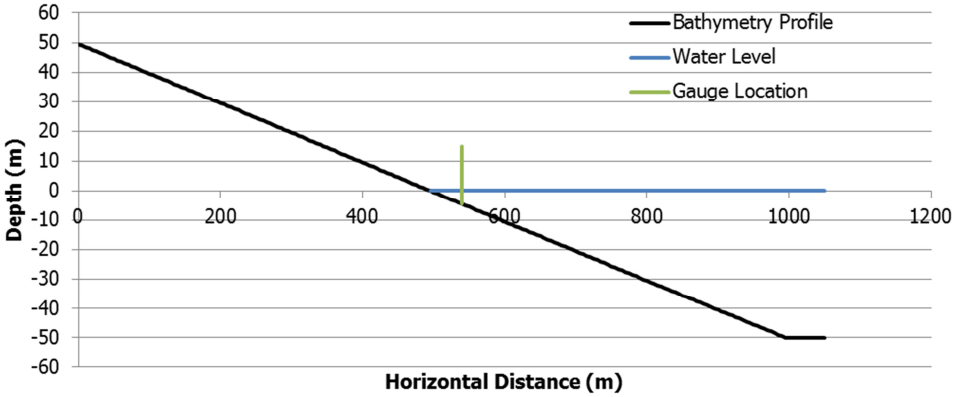

Figure 4-1: Bathymetry Profile and Gauge Location for 1/10 Slope

The simulation duration is selected as 5 minutes to simulate the wave runup properly. This duration is sufficiently long to simulate the approach, climbing and runup of the wave on the slope. The time steps for both models however are different because of different equation sets. The time step is 0.1 seconds for NAMI-DANCE and it is 0.01 for MIKE21 BW. Time step in MIKE21 BW is smaller due to the additional terms in the Boussinesq type equations that MIKE21 BW solves.

10 different sinusoidal waves are used as input from the sufficient distance from the toe of the slope. A single sinusoidal wave is used in each simulation. The wave period is selected as 180 seconds with the wave heights of 0.5m, 1.0m, 1.5m, 2.0m and 2.5m. All the wave conditions are simulated two times as i) leading elevation and ii) leading depression wave conditions. The wave properties are given in Table 4-1.

Table 4-1: Input Wave Properties

	H (m)	T (sec)
Leading Elevation Wave	0.5	180
	1	180
	1.5	180
	2	180
	2.5	180
Leading Depression Wave	0.5	180
	1	180
	1.5	180
	2	180
	2.5	180

In both models, the waves are generated along the same location from the toe with the perpendicular direction of the wave towards the shore. The generation line is located at the end of the slope. The wave propagates normal to the shore.

4.1.1 Simulation Results

40 simulations are done both in MIKE21 BW and NAMI-DANCE. The runup and inundation distances are given in Table 4-2 and Table 4-3. The definition of inundation distance and runup is given in Figure 4-2.

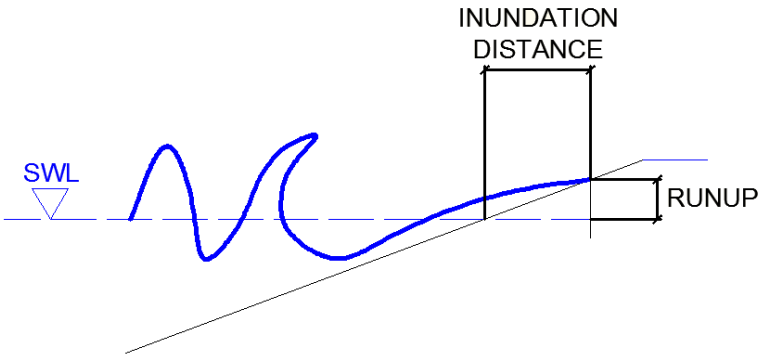

Figure 4-2: Inundation Distance and Runup

Table 4-2: Run-up and Inundation Distance Results for LDW

			Run-up (m)		Inundation Distance (m)	
		H_i	MIKE21	NAMI-DANCE	MIKE21	NAMIDANCE
Bottom Slope	1/10	0.5 m	0.68	0.90	5.00	5.00
		1.0 m	1.36	1.63	10.00	15.00
		1.5 m	2.06	2.28	20.00	20.00
		2.0 m	2.73	3.06	25.00	30.00
		2.5 m	3.41	3.70	30.00	35.00
	1/15	0.5 m	0.91	1.08	10.00	15.00
		1.0 m	1.81	2.06	25.00	30.00
		1.5 m	2.65	2.86	35.00	40.00
		2.0 m	3.50	3.60	50.00	50.00
		2.5 m	4.36	4.32	65.00	60.00
	1/20	0.5 m	1.04	1.11	20.00	20.00
		1.0 m	2.01	1.98	40.00	35.00
		1.5 m	2.94	2.73	55.00	50.00
		2.0 m	3.77	3.42	75.00	65.00
		2.5 m	4.60	4.05	90.00	75.00
	1/25	0.5 m	1.13	1.13	25.00	25.00
		1.0 m	2.12	1.98	50.00	45.00
		1.5 m	2.99	2.66	70.00	55.00
		2.0 m	3.80	3.29	90.00	80.00
		2.5 m	4.55	3.90	110.00	85.00

Table 4-3: Run-up and Inundation Distance Results for LEW

			Run-up (m)		Inundation Distance (m)	
		H_i	MIKE21	NAMI-DANCE	MIKE21	NAMI-DANCE
Bottom Slope	1/10	0.5 m	0.70	0.72	5.00	5.00
		1.0 m	1.39	1.44	10.00	10.00
		1.5 m	2.02	2.10	20.00	20.00
		2.0 m	2.65	2.67	25.00	25.00
		2.5 m	3.35	3.23	30.00	30.00
	1/15	0.5 m	0.81	0.81	10.00	10.00
		1.0 m	1.58	1.55	20.00	20.00
		1.5 m	2.29	2.19	30.00	30.00
		2.0 m	3.03	2.79	40.00	40.00
		2.5 m	3.80	3.30	55.00	45.00
	1/20	0.5 m	0.90	0.89	15.00	15.00
		1.0 m	1.73	1.61	30.00	30.00
		1.5 m	2.52	2.19	50.00	40.00
		2.0 m	3.26	2.73	65.00	50.00
		2.5 m	3.98	3.22	75.00	60.00
	1/25	0.5 m	0.95	0.91	20.00	15.00
		1.0 m	1.79	1.57	40.00	35.00
		1.5 m	2.58	2.17	60.00	50.00
		2.0 m	3.30	2.66	80.00	60.00
		2.5 m	3.98	3.03	95.00	75.00

In the leading depression wave cases, the inundation distances are in fairly well agreement. On the 1/25 bottom slope case, the runup results of both models are in agreement for small wave heights. As the bottom slope gets steeper, the runup results for the small wave heights begin to diverge whereas the difference between the runup for the larger wave heights begins to decrease.

In the leading elevation wave cases, the results of the numerical models are very close to each other for smaller wave heights. But as the wave height increases, the difference between the results of the models increase as well both for runup and inundation distance.

For the leading elevation waves, the best overall match is obtained for the 1/10 slope. In almost all the simulations for LEW case, MIKE21 BW yields higher results for both run-up and inundation distances.

The run-up results of two models are given in Figure 4-3, Figure 4-4,Figure 4-5 and Figure 4-6. The results of both the LDW and LEW simulations are plotted together with a 1:1 reference line.

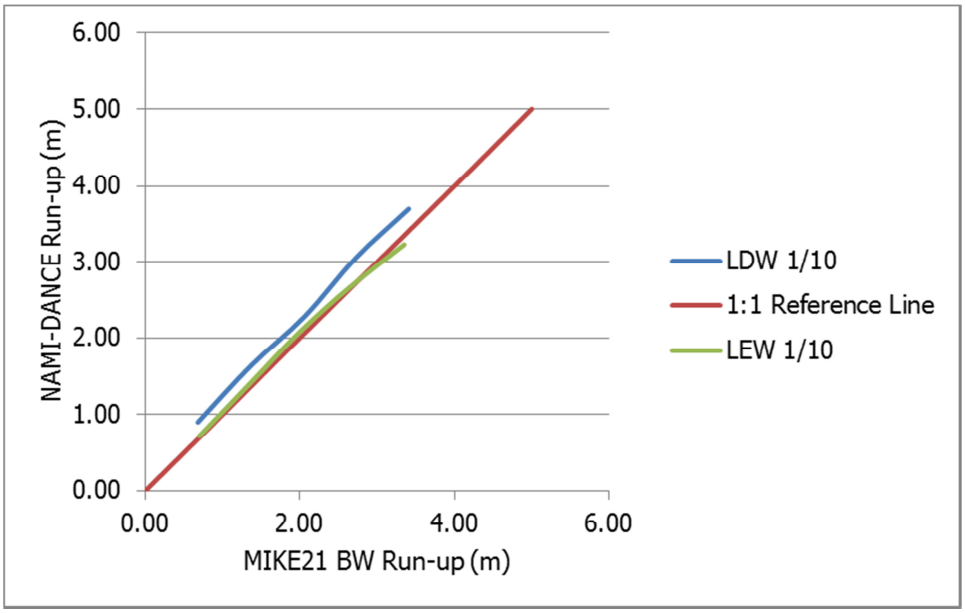

Figure 4-3: Comparison of Run-up for 1/10 Sloping Bathymetry

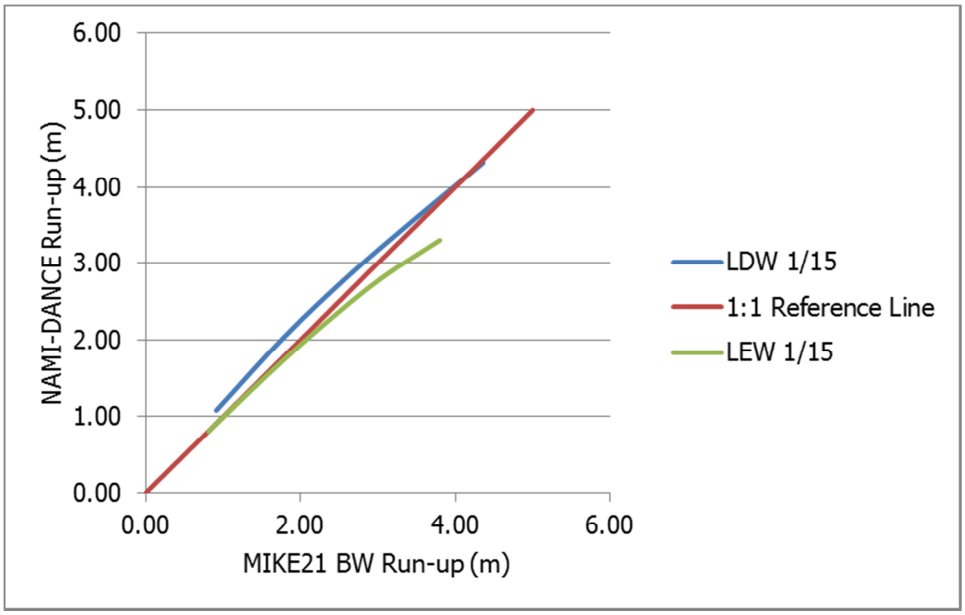

Figure 4-4: Comparison of Run-up for 1/15 Sloping Bathymetry

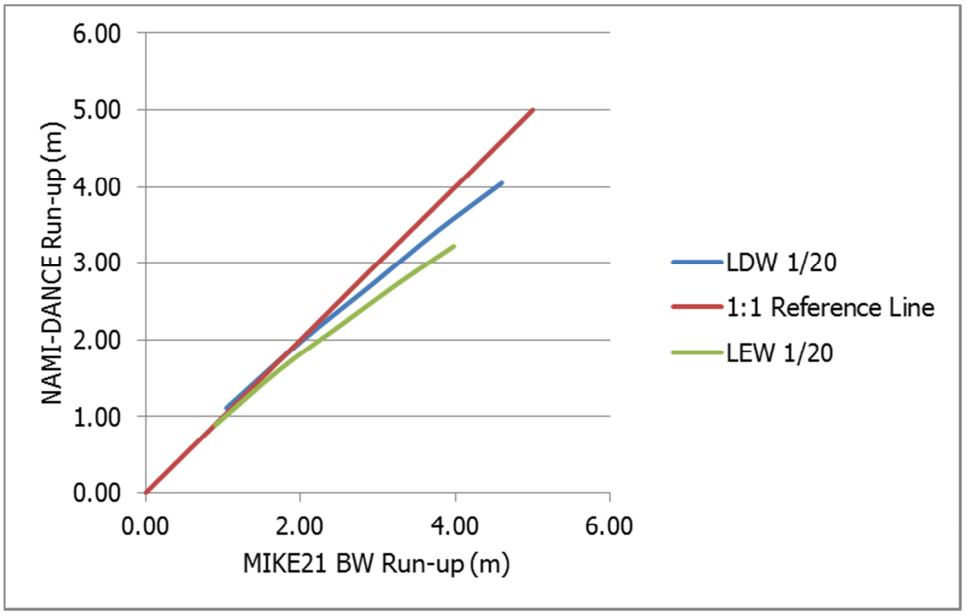

Figure 4-5: Comparison of Run-up for 1/20 Sloping Bathymetry

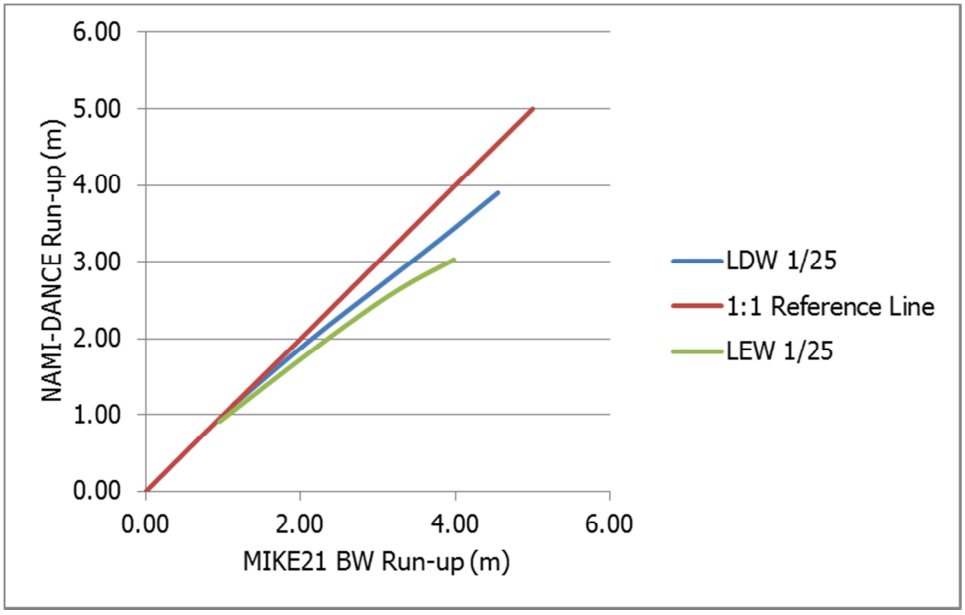

Figure 4-6: Comparison of Run-up for 1/25 Sloping Bathymetry

From Figure 4-3 to Figure 4-6, it is observed that both model results are in fairly well agreement. LEW results of the models are closest to each other in the 1/10 sloping bathymetry while the LDW results are closest to each other in the 1/15 sloping bathymetry.

It is also observed that, in all the simulations, for the small wave heights, two models yield very close results for both LDW and LEW.

4.1.1.1 Comparison of Water Surface Fluctuations at Gauges

The surface profile with respect to time has been recorded in both models at gauge points. The deformation of the wave on the slope at these gauge points can be seen on the plots.

The gauge locations in both models are fixed, i.e. the depth at which a specific gauge is placed varies with respect to the bathymetry (Figure 4-1). The depth of the gauges are -4.5m, -3.0m, -4.75m and -3.8m for the bottom slopes of 1/10, 1/15, 1/20 and 1/25 respectively. The input wave heights chosen for the comparison of the wave shape at the gauges are 1.0 m and 2.0 m.

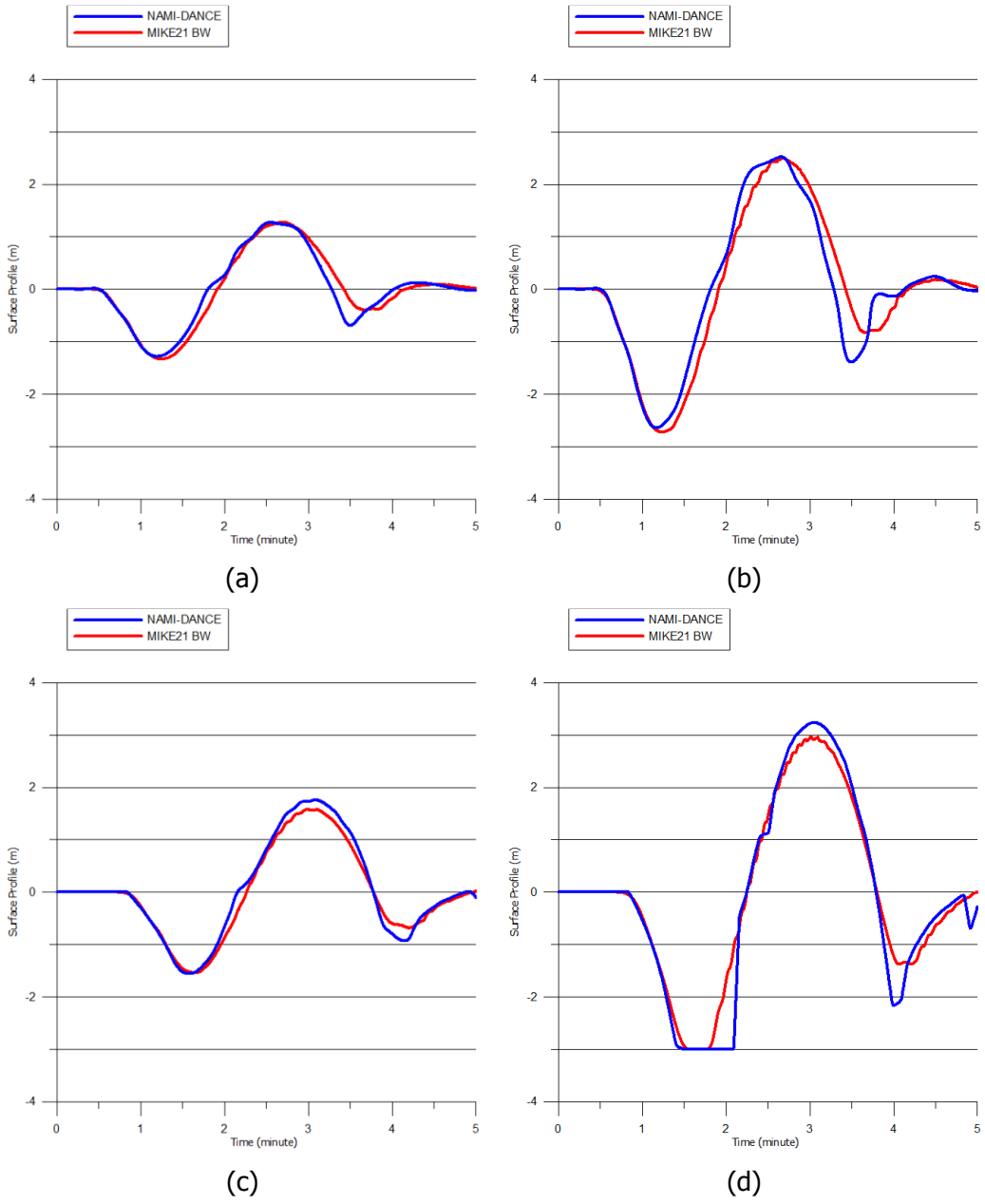

Figure 4-7: Gauge Comparison for Leading Depression Wave. (a) m=1/10, H_i=1.0m, at d=4.5m; (b) m=1/10, H_i=2.0m, at d=4.5m; (c) m=1/15, H_i=1.0m, at d=3.0m; (d) m=1/15, H_i=2.0m, at d=3.0m

In Figure 4-7, it is observed that both model results are in fairly well agreement. The positive peak values in MIKE21 BW are slightly larger than NAMI-DANCE while the leading depression values are almost the same with an insignificant phase shift.

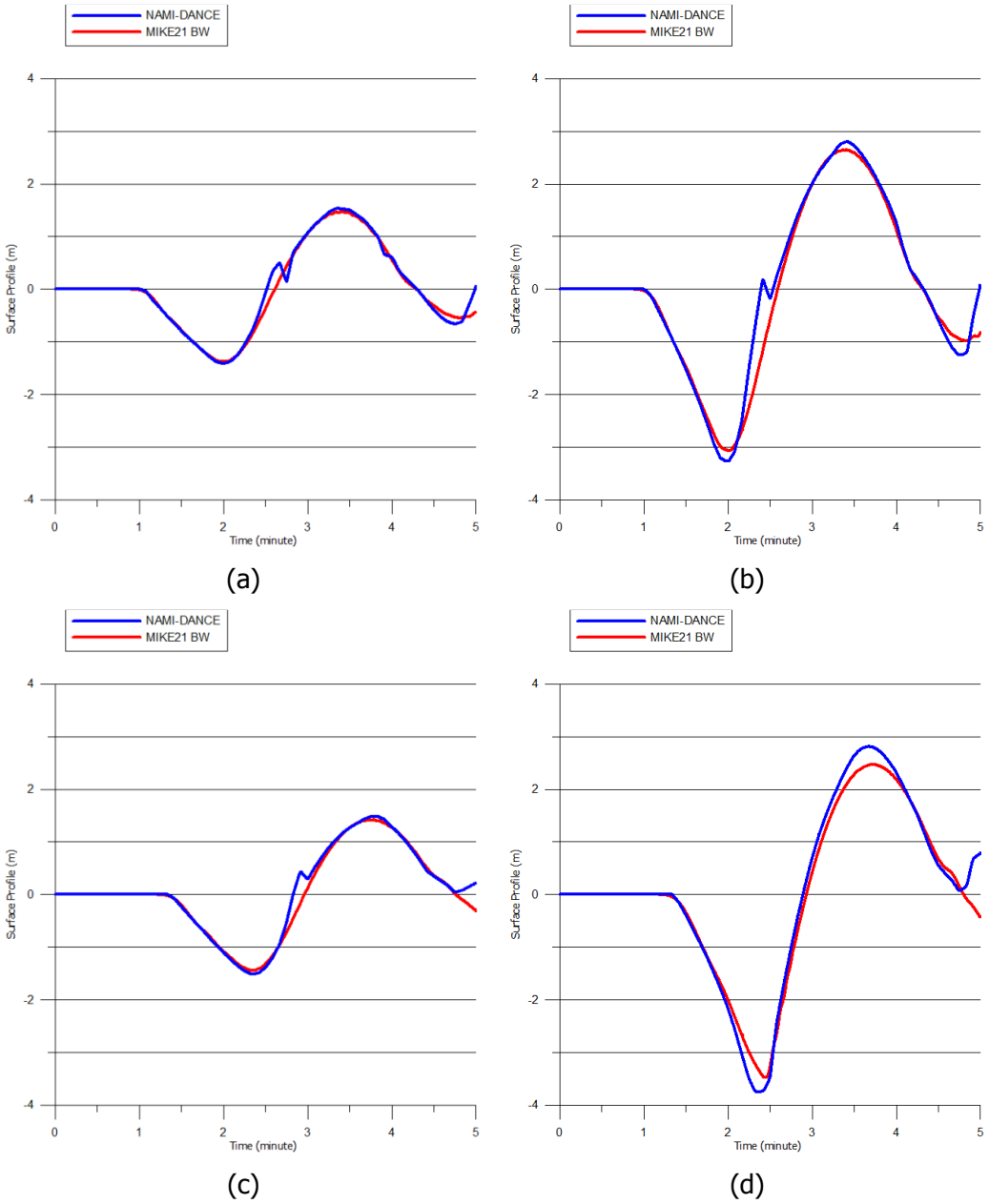

Figure 4-8: Gauge Comparison for Leading Depression Wave. (a) m=1/20, H_i=1.0m, at d=4.75m; (b) m=1/20, H_i=2.0m, at d=4.75m; (c) m=1/25, H_i=1.0m, at d=3.80m; (d) m=1/25, H_i=2.0m, at d=3.80m

In Figure 4-8, the results of both models are very close to each other except for the spike between 2.5 and 3rd minutes which is caused by reflection from the bottom slope as explained in section 4.1.2.1. Although the surface profile lines overlap reasonably the little differences in the positive and negative peak values may be due to the dispersive terms in MIKE21 BW.

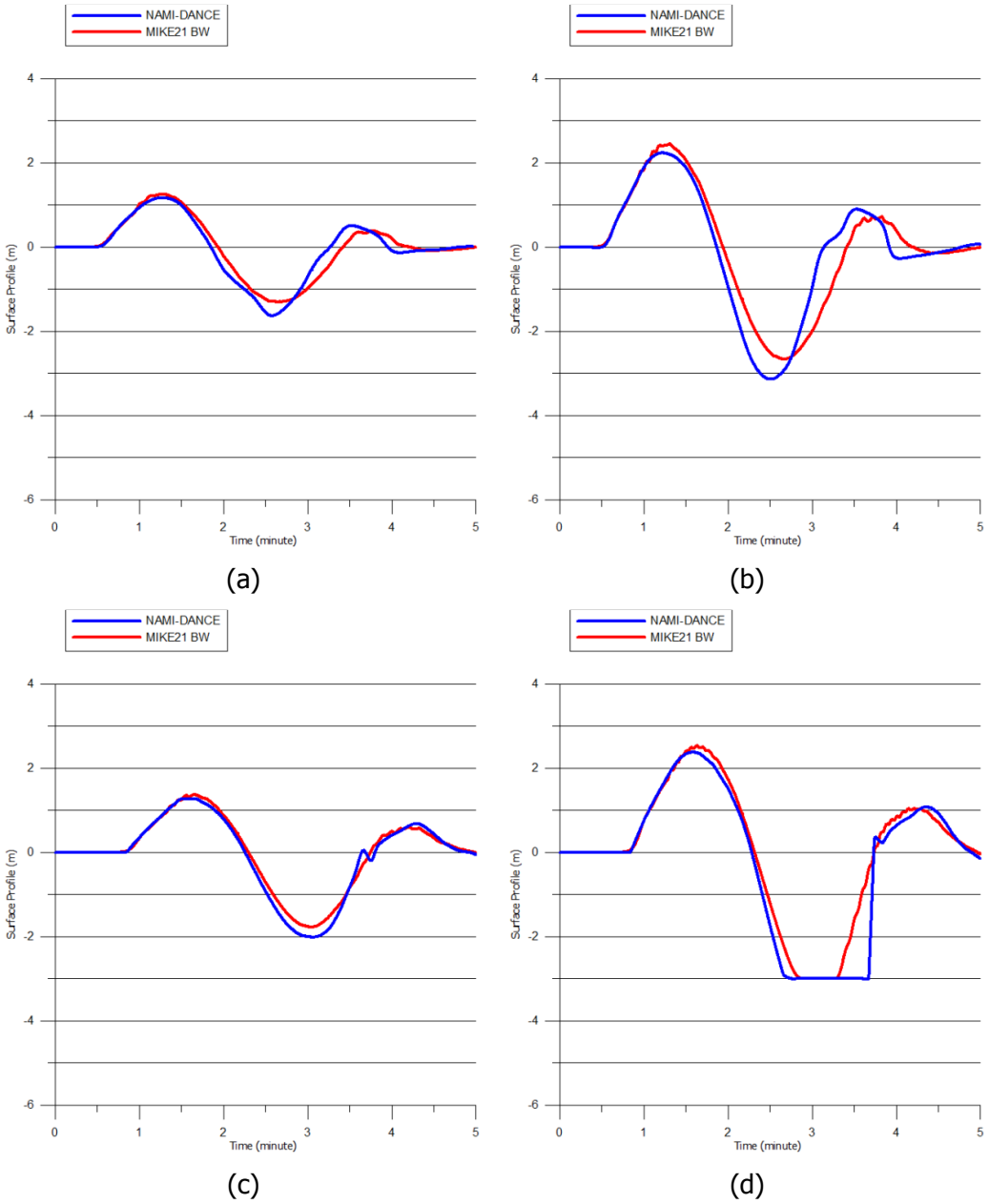

Figure 4-9: Gauge Comparison for Leading Elevation Wave. (a) m=1/10, H_i=1.0m, at d=4.5m (b) m=1/10, H_i=2.0m; at d=4.5m (c) m=1/15, H_i=1.0m, at d=3.0m; (d) m=1/15, H_i=2.0m, at d=3.0m

In Figure 4-9, the differences between the wave profiles computed from two models are presented. The wave amplitude at the steeper slopes is higher when dispersion is enabled.

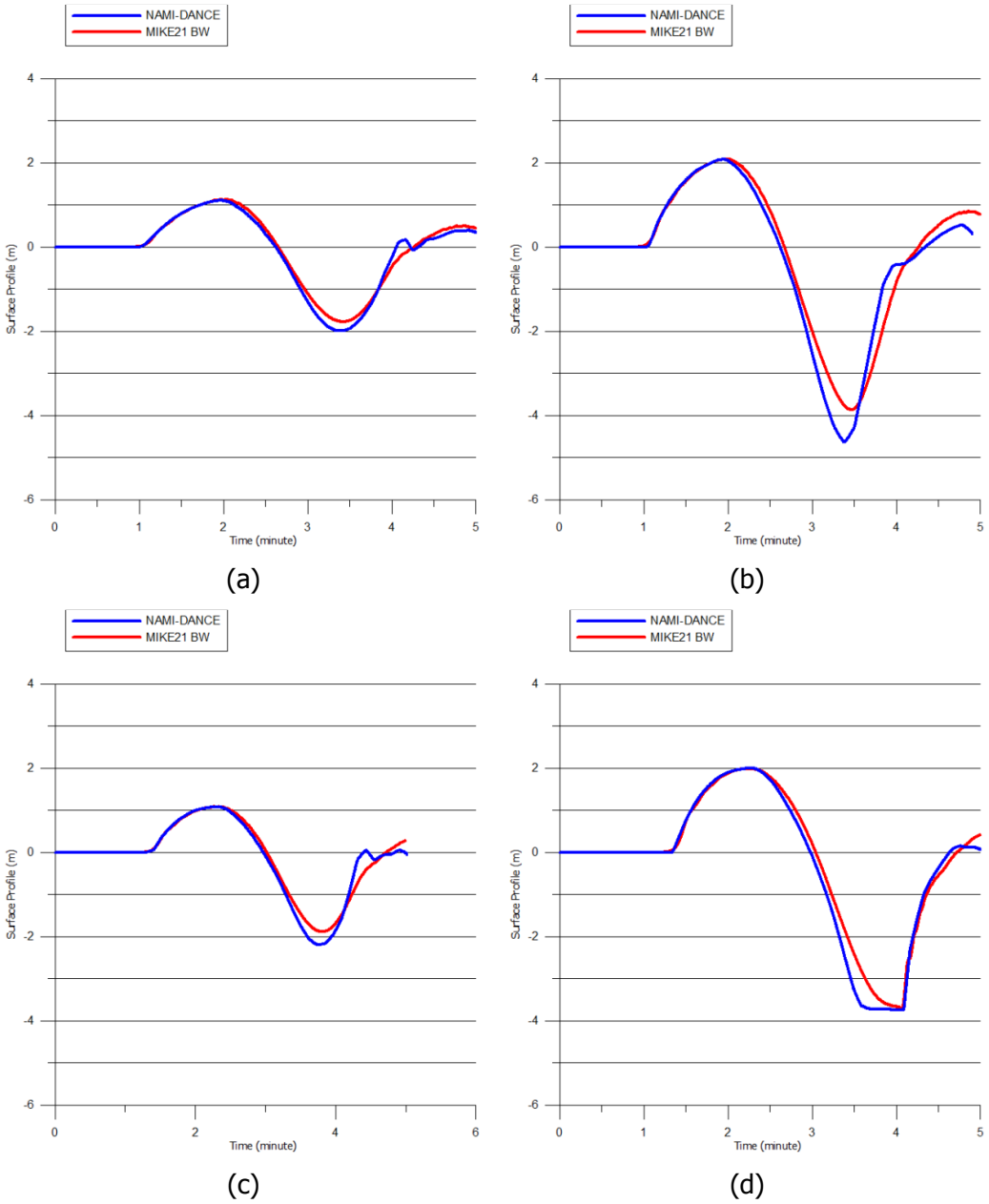

Figure 4-10: Gauge Comparison for Leading Elevation Wave. (a) m=1/20, H_i=1.0m, at d=4.75m; (b) m=1/20, H_i=2.0m, at d=4.75m; (c) m=1/25, H_i=1.0m, at d=3.80m; (d) m=1/25, H_i=2.0m, at d=3.80m

The major differences are observed in the wave profiles on the slope at the trough of the wave where the equations without dispersion computes lower value of the wave trough. The maximum elevation and the phase of the two results are similar.

4.1.2 General Discussion of the Comparisons

The two numerical models reproduce the effects of the transformation of the input waves by solving different set of equations. MIKE21 BW solves Boussinesq type equations while NAMI-DANCE solves shallow water equations. Each model is expected to perform well in reproducing the transformation of waves in shallow water.

The input waves are sinusoidal waves with a period of 180 seconds and the maximum water depth is 50 meters which is in the range of shallow water interval for a 180 second period sinusoidal wave. The wave is generated just at the toe of the slope in every bathymetry. So the input wave immediately begins shoaling. Since the wave propagates normal to the shore, no refraction is enforced. The wave deformation, runup and inundation distances are compared and discussed in the following sections.

4.1.2.1 Leading Depression Wave Conditions

The run-up values obtained in both models vary with respect to different bathymetries. As the bottom slope changes, so do both the run-up values and the relative difference between the two model results. The run-up values given in Table 4-2 show that, for each bottom slope, there is a different relation between the two model results.

In the leading depression wave cases, the absolute percent difference varies with respect to input wave height and the bottom slope. For the bottom slopes of 1/10 and 1/15, it can be stated that the absolute percent difference decreases as the input wave height increases. On the other hand, for bottom slopes of 1/20 and 1/25, the opposite applies, i.e. as the wave height increases the absolute percent difference increases as well. In other words, run-up of steeper waves is fairly well predicted by the two models with respect to each other for more steeply sloping bathymetries. In addition, as the steepness of the waves decreases, the run-up is predicted fairly well by the models with respect to each other for mildly sloping bathymetries.

The inundation distances are also in fairly well agreement in the results of the two models. Although the relative %difference in inundation distances for small run-up cases may be high, it should be noted that the grid size is 5 meters in both models.

For more steeply sloping bathymetries, the inundation distances in NAMI-DANCE are slightly higher than in MIKE21 BW. But as the bottom slope decreases, the inundation distances in MIKE21 BW become greater than the values in NAMI-DANCE.

When the graphs of gauge readings from Figure 4-7 and Figure 4-8 are considered, it is observed that the disturbance in the surface profile at the gauge locations begins at the same time steps for each case. The surface elevation at the gauge location continues to decrease at exactly the same rate in both model results until the trough of the leading depression approaches. As the trough passes, a slight difference in the results is observed. For the 1/10 bottom slope case, MIKE21 BW predicts a slightly lower trough elevation at the gauge point while in the rest of the bathymetries, the trough elevation in both model results is either equal to each other or is predicted slightly less by NAMI-DANCE. Once the trough passes by, the surface profile may be affected from reflection from shore and the amount of reflection may vary between the two models. But the rest of the surface profile in two models exhibits a fairly well agreement.

In order to understand the reason of the spikes in Figure 4-8 (a), (b) & (c), the surface profiles recorded at gauges which are at near 10m depth (greater than the depths of gauges in section 4.1.1) are plotted as shown in Figure 4-11. In Figure 4-11, it is seen that the spikes are recorded at greater time steps than they are recorded at the gauges at shallower depths. This shows that the spikes are caused by the reflection from the bottom slope since they are recorded at later time steps at the deeper gauges meaning that they are propagating away from the shore.

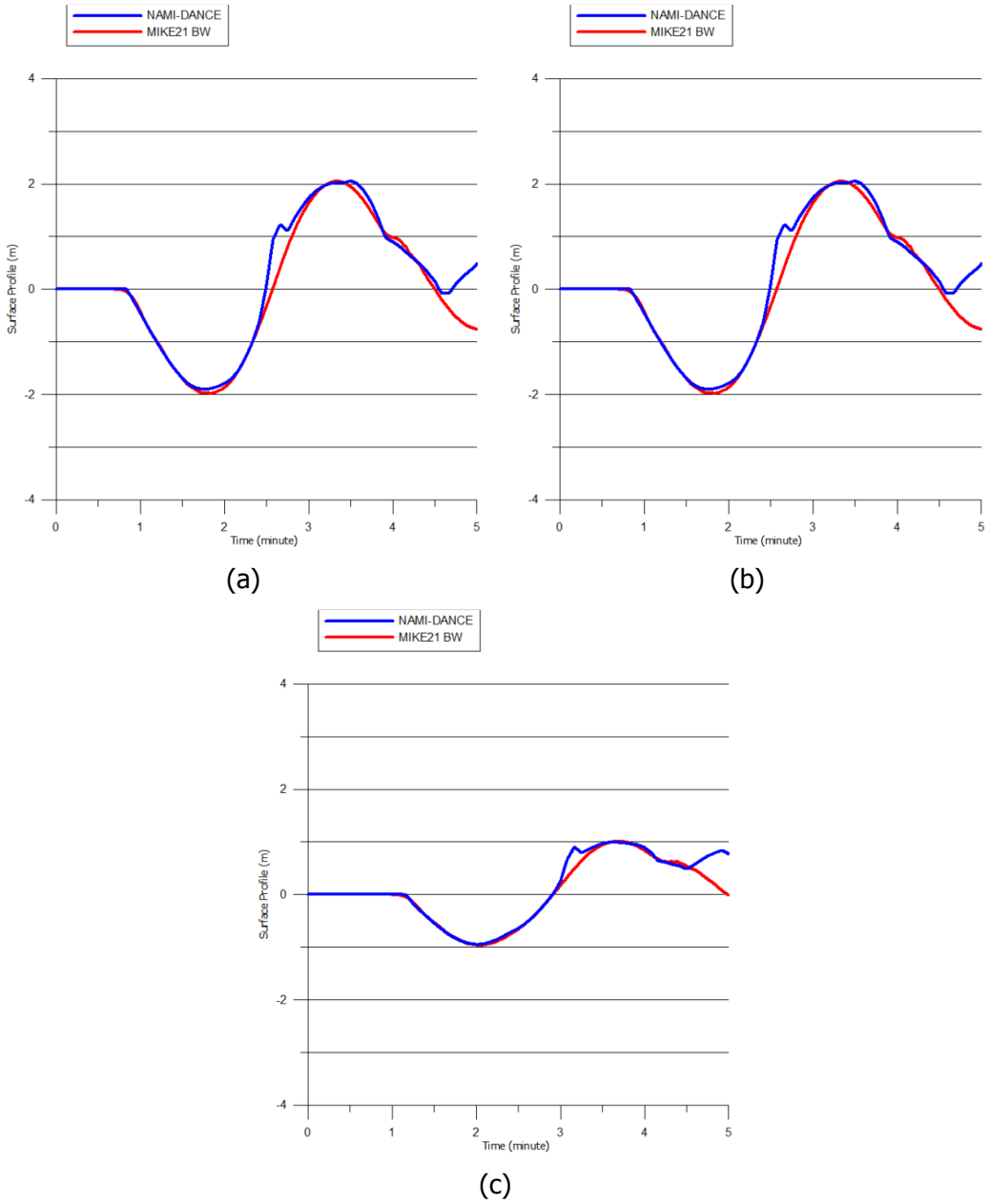

Figure 4-11: Gauge Comparison for Leading Depression Wave. (a) m=1/20, H_i=1.0m, at d=9.75m; (b) m=1/20, H_i=2.0m, at d=9.75m; (c) m=1/25, H_i=1.0m, at d=7.80m

4.1.2.2 Leading Elevation Waves

The similarity in run-up values obtained for leading elevation waves show a different pattern with respect to leading depression wave cases. In leading elevation wave cases, contrary to the leading depression wave cases, the trend is similar for all bottom slopes.

For the leading elevation wave cases, it is clearly observed that the relative absolute difference for small wave heights is very small for all bottom slope cases. As the wave steepness increases, the relative absolute difference increases as well. On the other hand, the relative absolute difference in steeper slopes is small compared to the mildly sloping bathymetries.

The inundation distances given in Table 4-3 show that, the predictions match well with each other. The results of the two models for less steep waves are very close to each other. As the wave steepness increases, the relative difference increases similar to the cases in leading depression waves.

When the gauge readings for leading elevation waves in Figure 4-9 and Figure 4-10 are examined, similar observations as in the leading depression cases are made. The leading elevation of the incoming wave approaches the gauge and begins altering the surface profile at the same time step in both models. The surface elevation increases at the same rate in both models until the crest of the wave approaches. This is similar to the cases of leading depression. In the leading elevation cases, the crest of the wave causes a slightly higher surface elevation for the steeper bottom slopes. But as the bottom slope gets milder, the surface profiles recorded at the gauges in the two models begin to overlap more and more from the beginning of the simulation to the arrival of the crest. After the crest passes by the gauge, the trough of the wave is recorded to drag the surface profile to lower elevations in NAMI-DANCE compared to MIKE21 BW.

Considering all these observations it can be stated that the gauge readings in both models are close to each other. But there are minor differences in the wave profiles, especially the maximum positive and negative amplitudes.

4.2 Dispersion Effect on the Long Distance Propagation of Long Waves

The basic input parameters such as the bathymetry and the wave properties are same in both models. Four simulations are run in both models. The only varying parameter in the simulations is the input wave properties.

The model domain is a 750km*300km rectangular area. The grid size is 1km in both x and y directions. The profile view of the bathymetry is given in Figure 4-12. The waves are generated at the left side of the bathymetry at 1000 meter water depth. The properties of the bathymetry are given in Table 4-4. From left to right, the bathymetry starts with 1000 meter depth. Next there is a shelf at top of which there is a plateau with 50 meter depth. And finally there is a slope which extends beyond the shore up to 50 meters height on land.

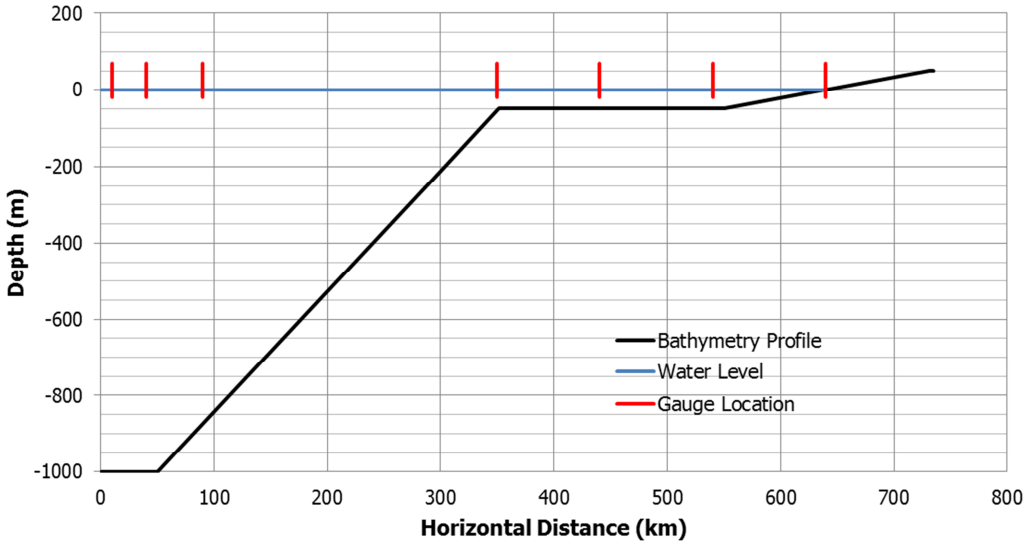

Figure 4-12: Bathymetry Profile and the Gauge Locations

Table 4-4: Properties of the Bathymetry

Horizontal Distance (km)	Bottom Slope
0-50	0
51-350	1/315
351-550	0
551-730	1/1800
731-750	0

The simulation duration in both models is 5.5 hours which is sufficient to observe the wave propagation and deformation along the basin to the shoreline. Since only the transformations of the waves until the shoreline are compared, the simulation is

ended at 5.5 hours. The time step is chosen as 0.5 seconds in MIKE21 BW and 5 seconds in NAMI-DANCE. The input wave characteristics are given in Table 4-4.

Table 4-5: Input Wave Characteristics

Wave Type	Wave Height (m)	Wave Period (min)	Number of Waves
LEW, Sinusoidal	4	12	1
LEW, Sinusoidal	4	12	2
LEW, Sinusoidal	4	60	1
LEW, Sinusoidal	4	60	2

The general layout of the test basin is given in Figure 4-13.

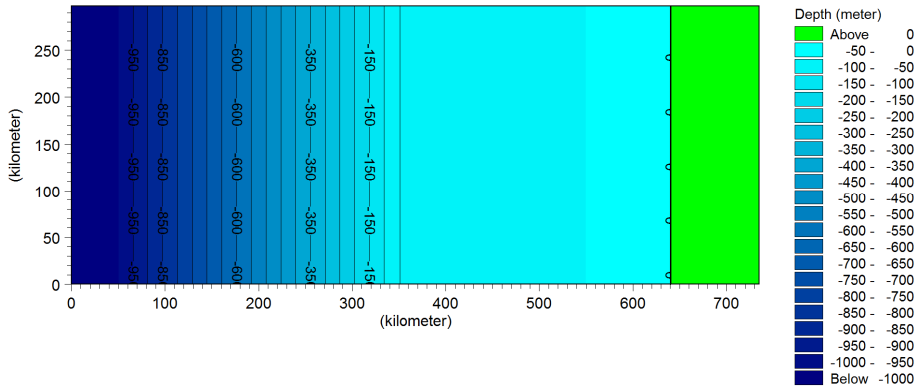

Figure 4-13: General Layout of the Test Basin

4.2.1 Simulation Results

Several gauges are placed along the centerline of bathymetry of the model domain along the wave propagation line. Among those, 7 gauge locations are selected to plot the wave profiles. The selected gauge locations are given in Table 4-6.

Table 4-6: Locations of the Gauges

Gauge Number	Horizontal Distance (km)	Depth (m)
1	10	1000
2	40	1000
3	90	553
4	350	50
5	440	50
6	540	50
7	640	5

The computed wave profiles (time histories of water surface fluctuations) at the gauges are given in Figure 4-14 to Figure 4-21.

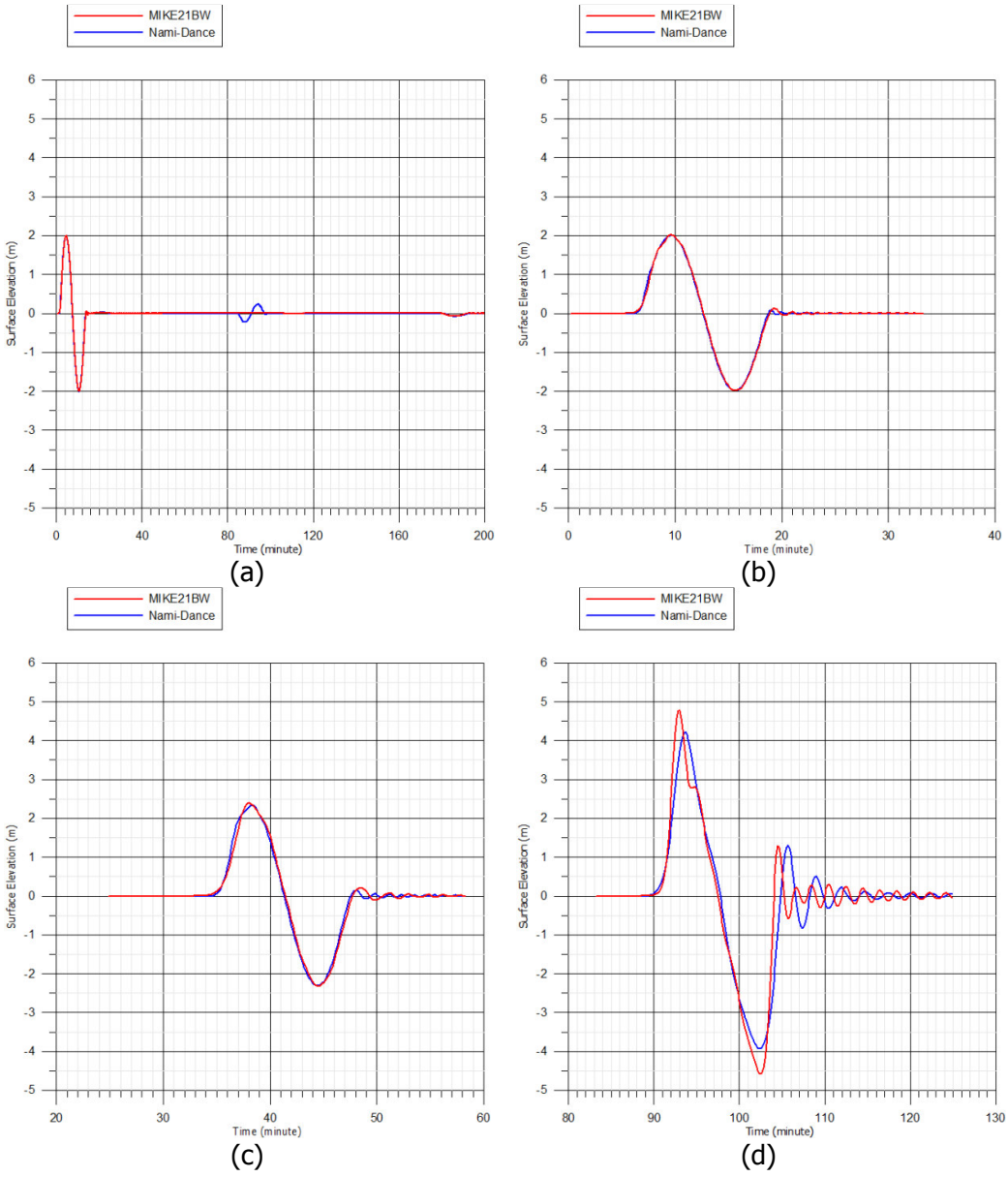

Figure 4-14: The Computed Wave Profiles at Different Gauges for the Input of Leading Elevation Wave (One wave with H=4m & T=12 min) (a) Gauge 1, d=1000m; (b) Gauge 2, d=1000m; (c) Gauge 3, d=553m; (d) Gauge 4, d=50m

The small wave in Figure 4-14 (a) is the reflected wave from the shelf which is computed by NAMI-DANCE.

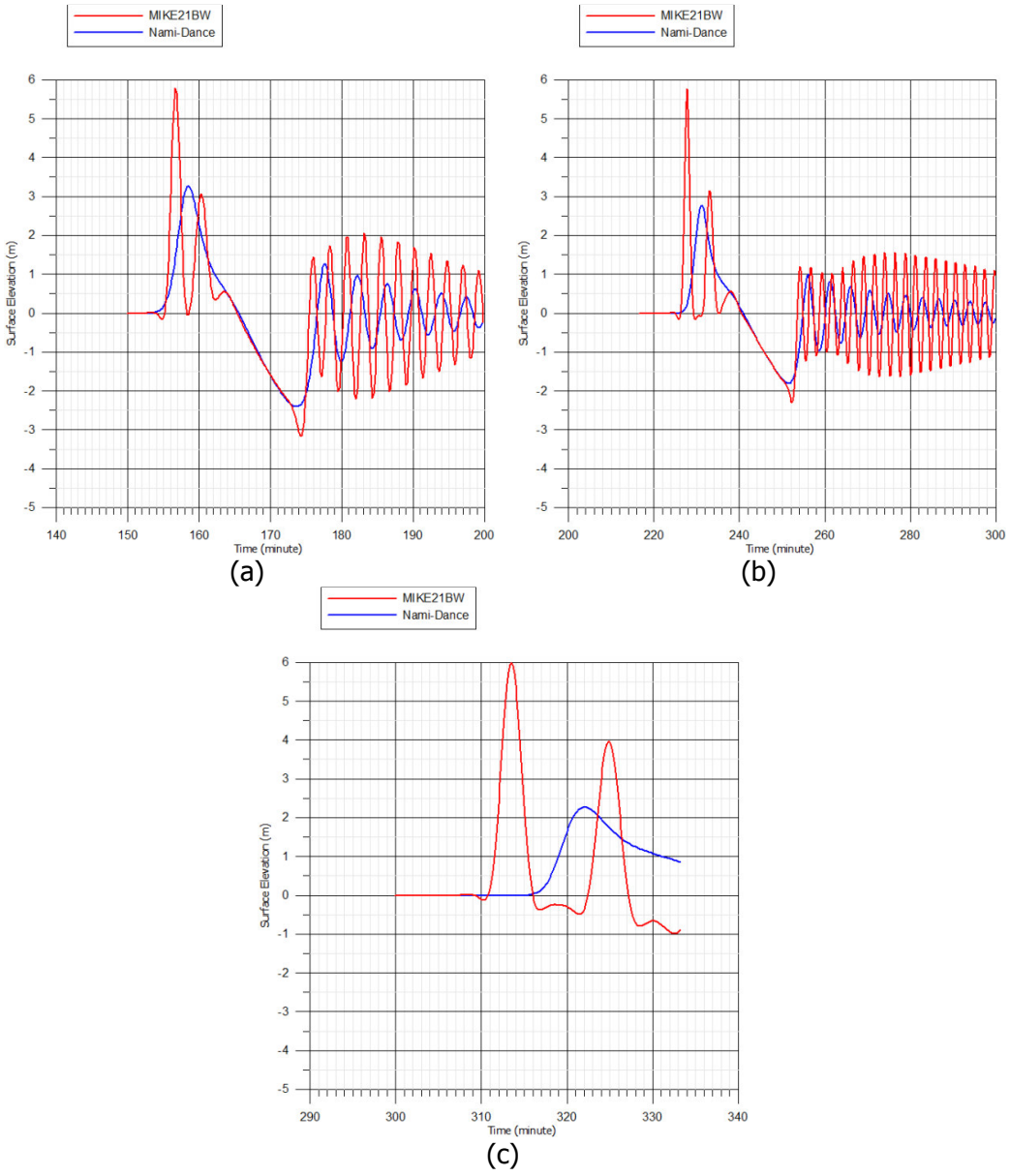

Figure 4-15: The Computed Wave Profiles at Different Gauges for the Input of Leading Elevation Wave (One wave with H=4m & T=12 min) (a) Gauge 5, d=50m; (b) Gauge 6, d=50m; (c) Gauge 7, d=5m

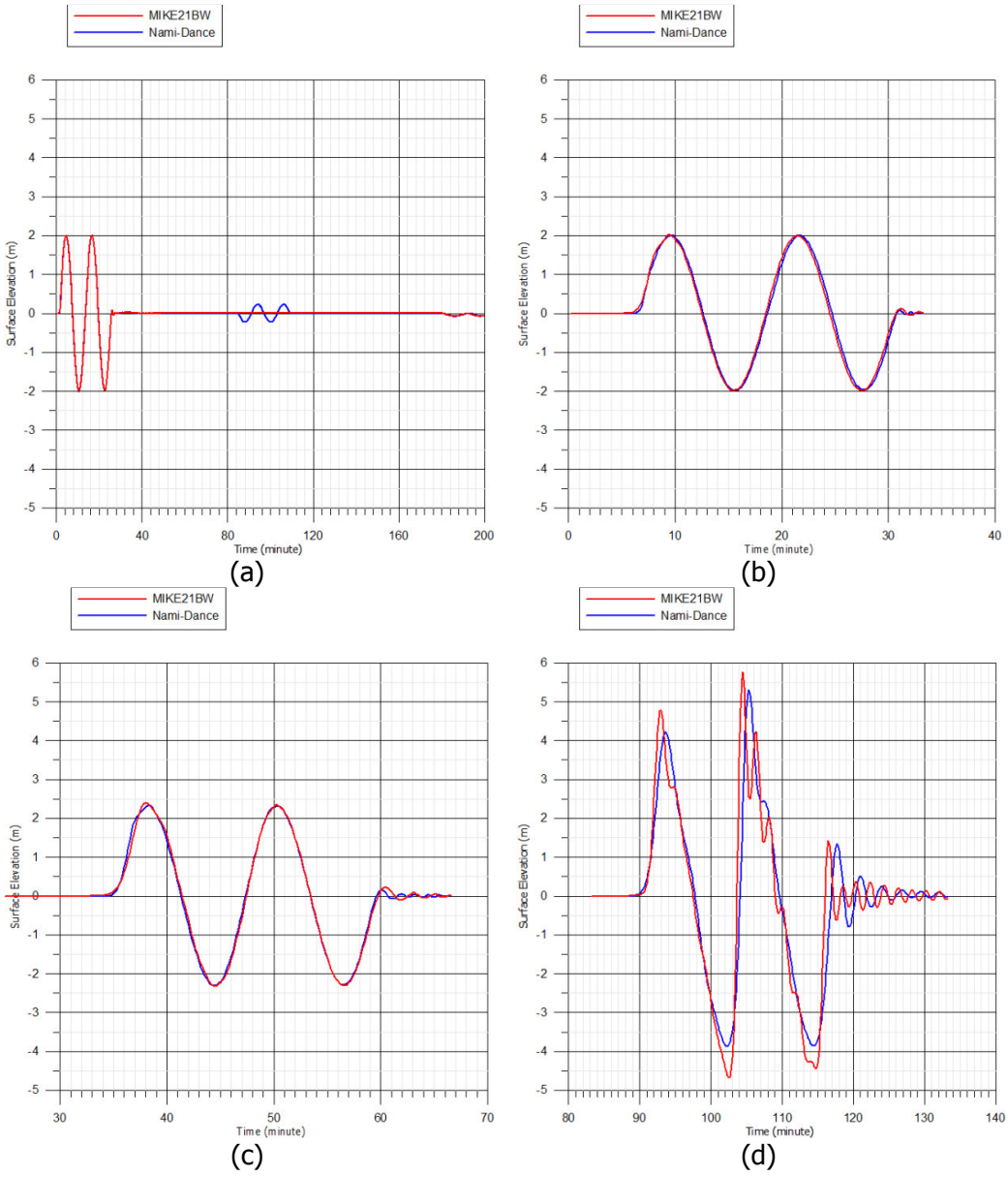

Figure 4-16: The Computed Wave Profiles at Different Gauges for the Input of Leading Elevation Wave (Two waves with H=4m & T=12 min) (a) Gauge 1, d=1000m; (b) Gauge 2, d=1000m; (c) Gauge 3, d=553m; (d) Gauge 4, d=50m

The small wave in Figure 4-16 (a) is the reflected wave from the shelf which is computed by NAMI-DANCE.

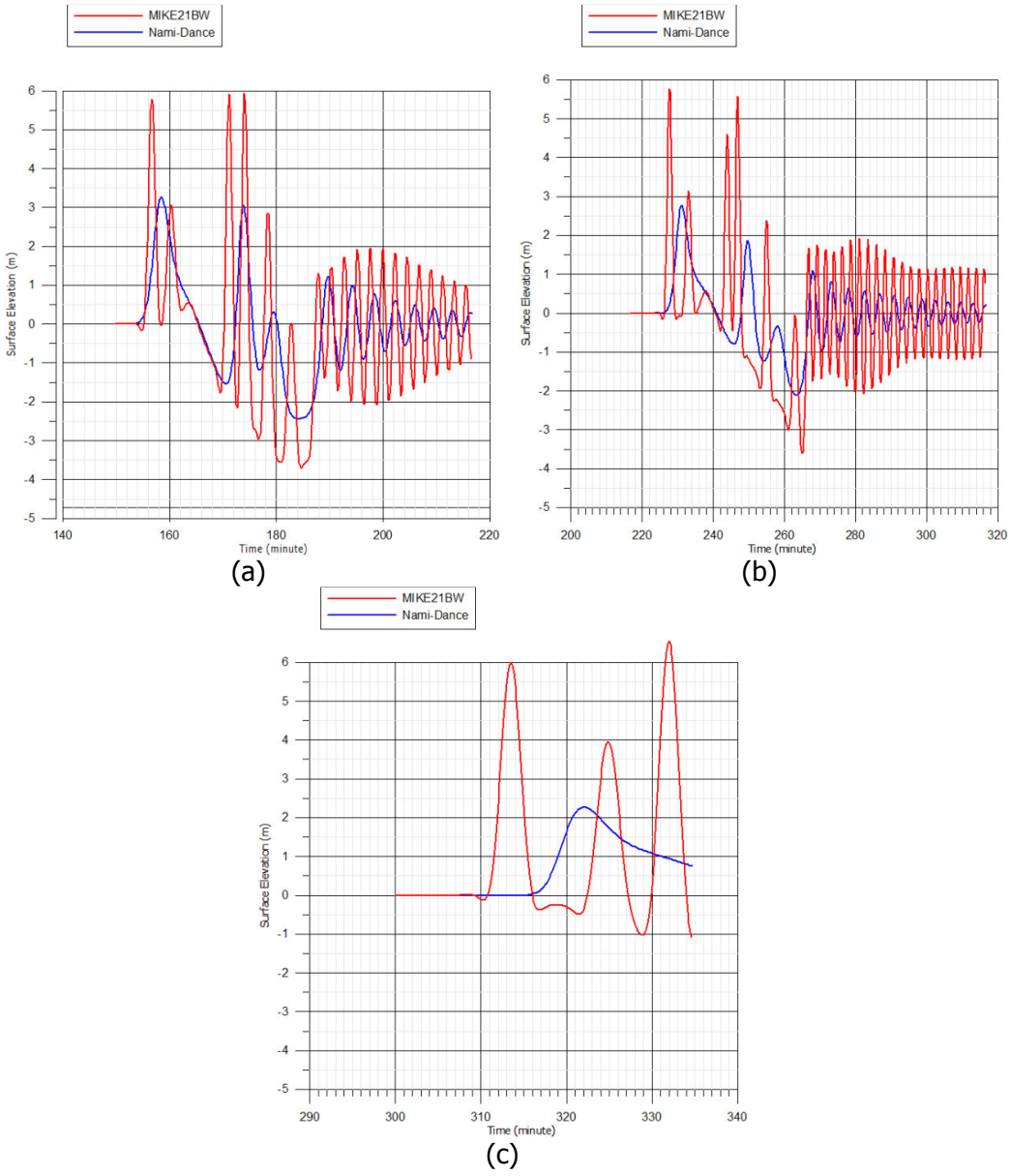

Figure 4-17: The Computed Wave Profiles at Different Gauges for the Input of Leading Elevation Wave (Two waves with H=4m & T=12 min) (a) Gauge 5, d=50m; (b) Gauge 6, d=50m; (c) Gauge 7, d=5m

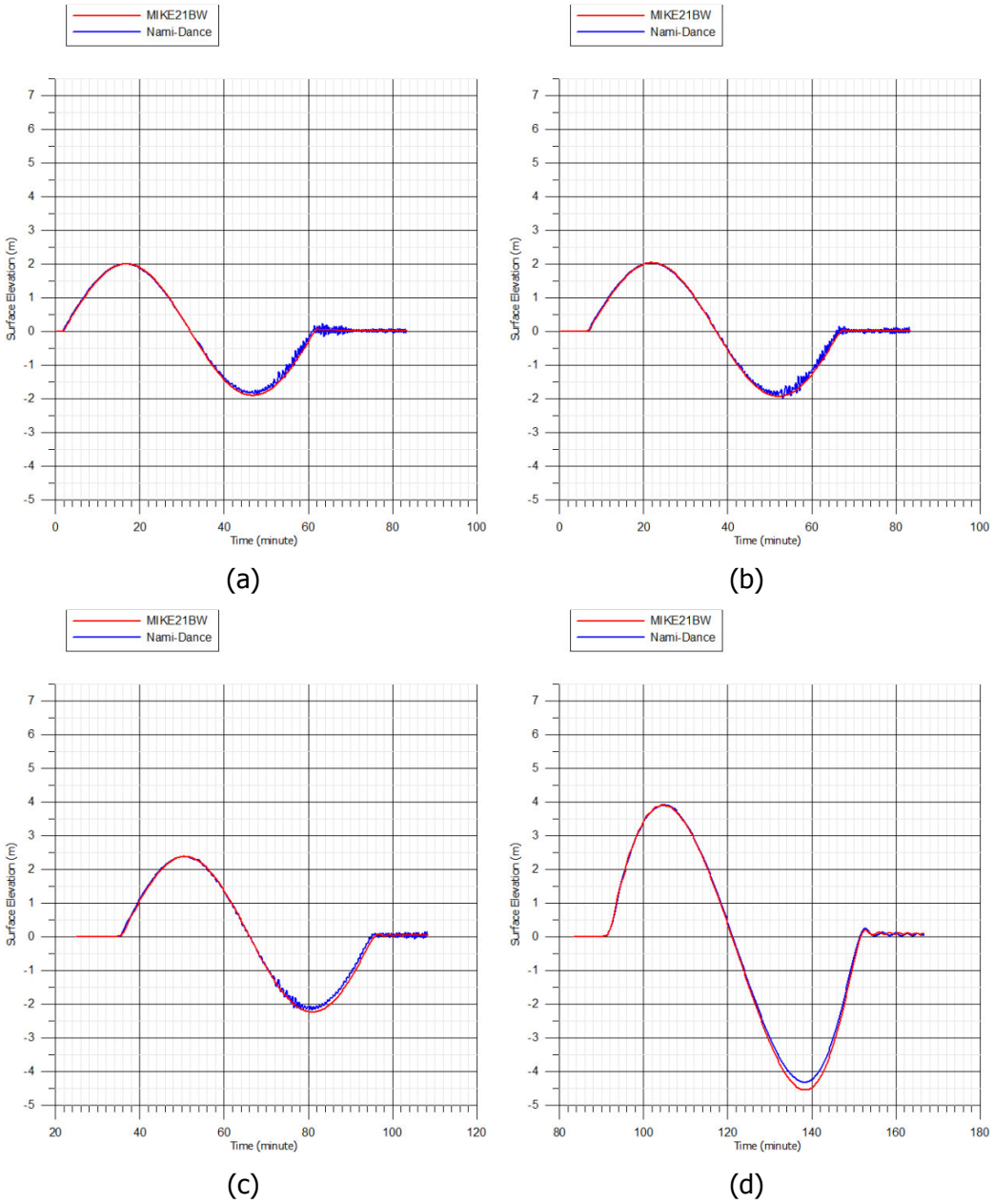

Figure 4-18: The Computed Wave Profiles at Different Gauges for the Input of Leading Elevation Wave (One wave with H=4m & T=60 min) (a) Gauge 1, d=1000m; (b) Gauge 2, d=1000m; (c) Gauge 3, d=553m; (d) Gauge 4, d=50m

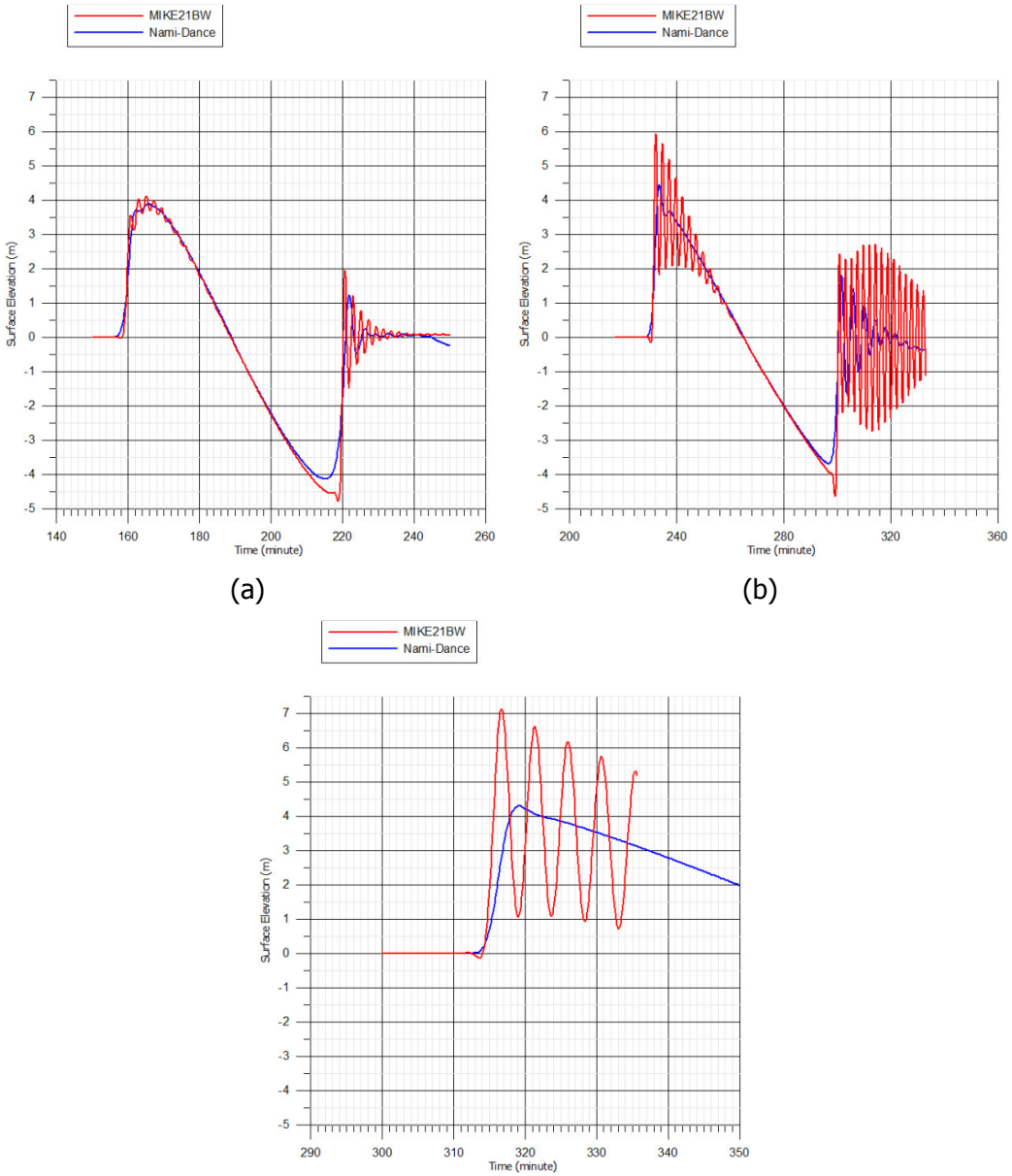

Figure 4-19: The Computed Wave Profiles at Different Gauges for the Input of Leading Elevation Wave (One wave with H=4m & T=60 min) (a) Gauge 5, d=50m; (b) Gauge 6, d=50m; (c) Gauge 7, d=5m

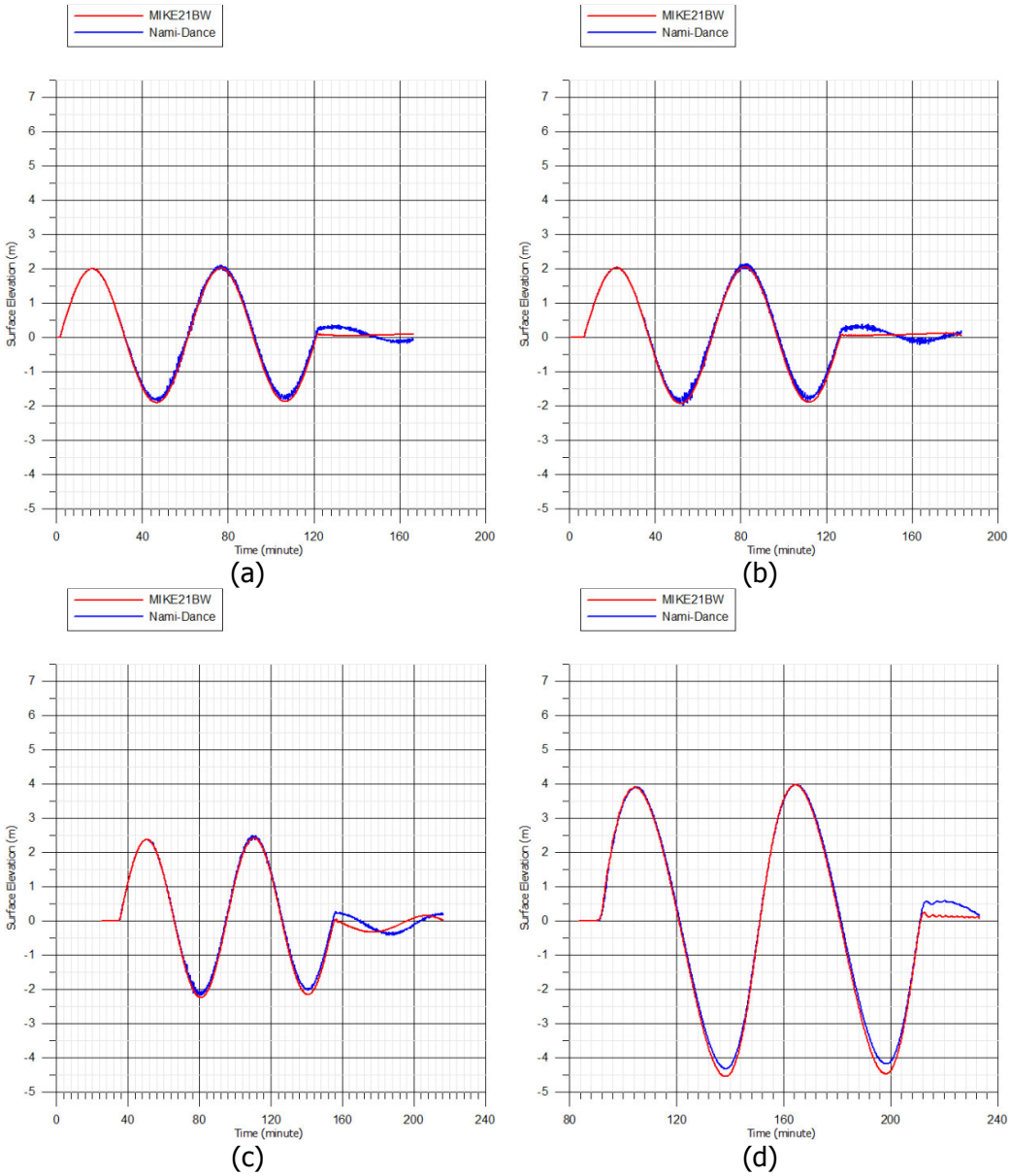

Figure 4-20: The Computed Wave Profiles at Different Gauges for the Input of Leading Elevation Wave (Two waves with H=4m & T=60 min) (a) Gauge 1, d=1000m; (b) Gauge 2, d=1000m; (c) Gauge 3, d=553m; (d) Gauge 4, d=50m

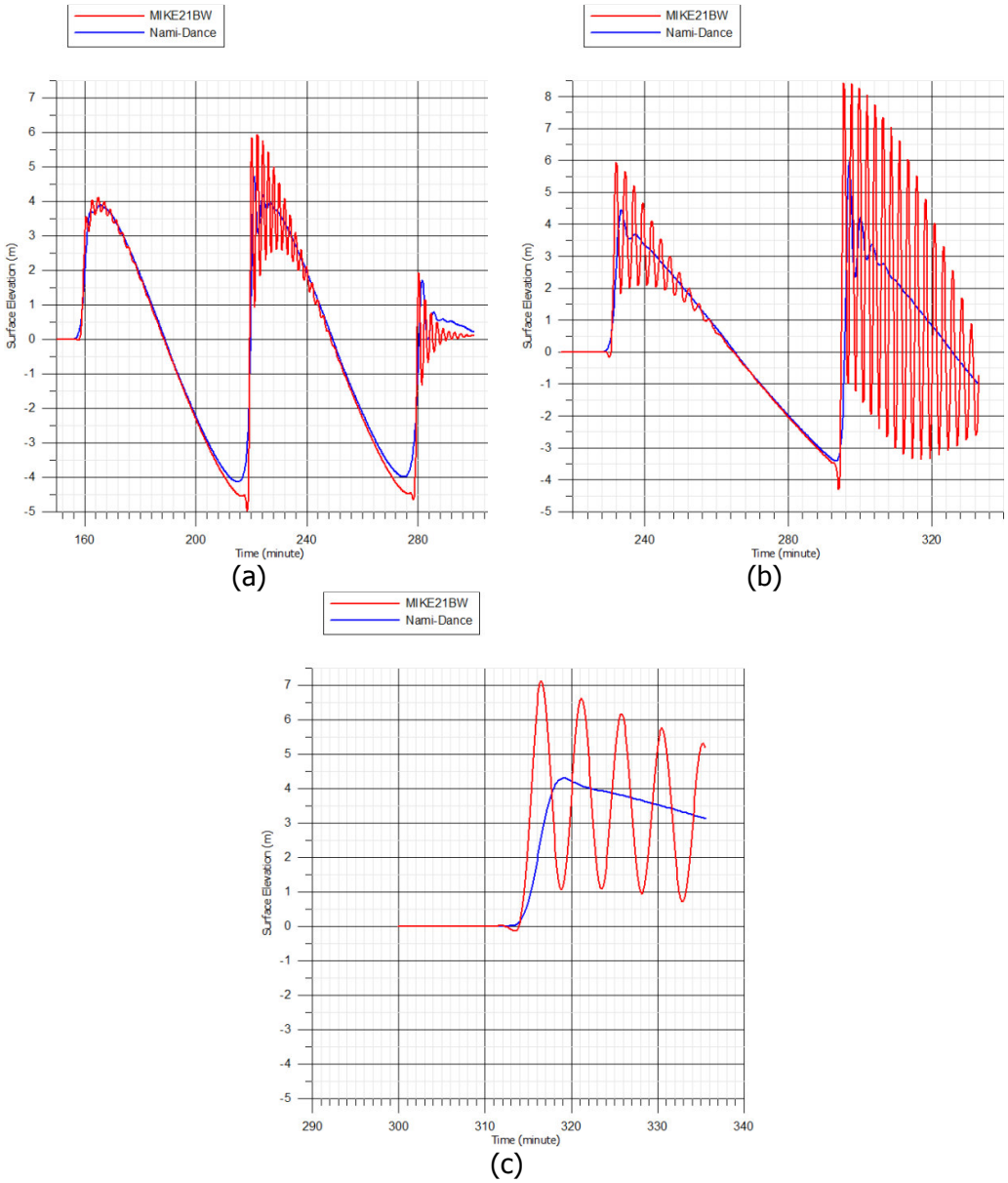

Figure 4-21: The Computed Wave Profiles at Different Gauges for the Input of Leading Elevation Wave (Two waves with H=4m & T=60 min) (a) Gauge 5, d=50m; (b) Gauge 6, d=50m; (c) Gauge 7, d=5m

4.2.2 Overview of Results

The wave profiles computed at the gauges at 1000m depth are very close to each other in both models. When the waves reach the shelf, differences between wave profiles (with and without dispersion) become larger which indicates that dispersion term becomes effective at the shelf.

In MIKE21 BW (with dispersion), the leading elevation type, 12 minute wave is split into 2 waves when it enters and propagates over the shallow region while in NAMI-DANCE DANCE (without dispersion) the wave keeps its initial form. As for the 60 minute wave, the both models reproduce similar results while MIKE21 BW results have high frequency fluctuations which might be noise. The effect of dispersion can be seen more clearly in the results of the simulations with two successive waves.

Reflection due to the slope is computed by both models. However, in Figure 4-14 (a) and Figure 4-16 (a) it is clearly seen that NAMI-DANCE computes a reflection which is not computed by MIKE21 BW.

CHAPTER 5

COMPARISON WITH PHYSICAL MODEL EXPERIMENTS

In this chapter, the numerical model (MIKE21 BW) results are compared to the results of the physical experiment of Datça Yacht Harbor whose experiments were performed in METU Civil Engineering Department Ocean Engineering Research Center (Özhan, et al., 1999). The comparisons are in the following sections. The project area Datça Town is located in Muğla province at the south west coast of Turkey. The satellite image of the model area is given in Figure 5-1.

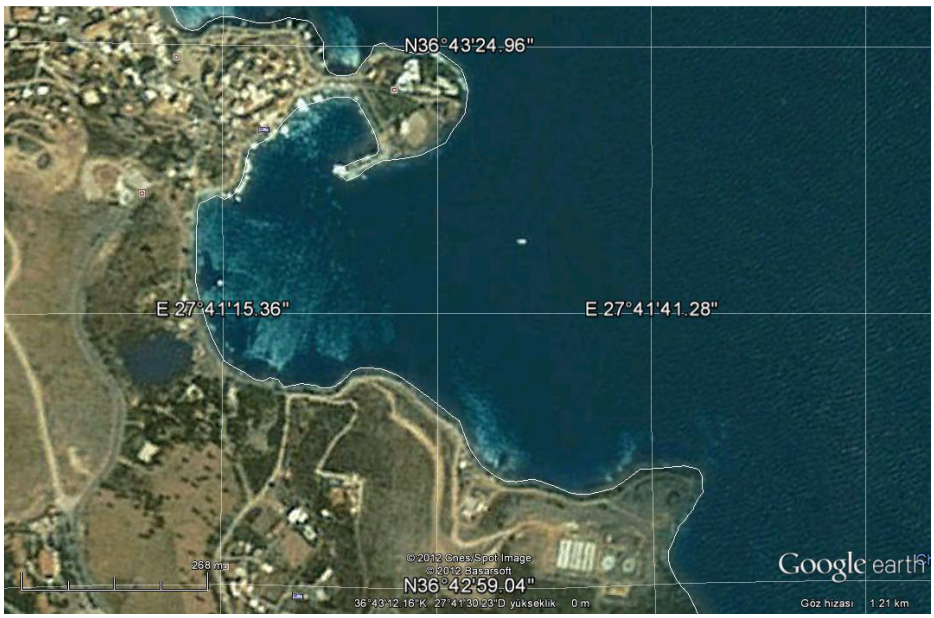

Figure 5-1: Project Area (Google Earth, 2012)

In the model experiment different harbor layouts are tested. The general layout of the proposed marina and the bathymetric contours are given in Figure 5-2. The

main breakwater of the proposed marina is planned to be rubble mound and located at the southern part of the Datça bay with a length of about 430 meters.

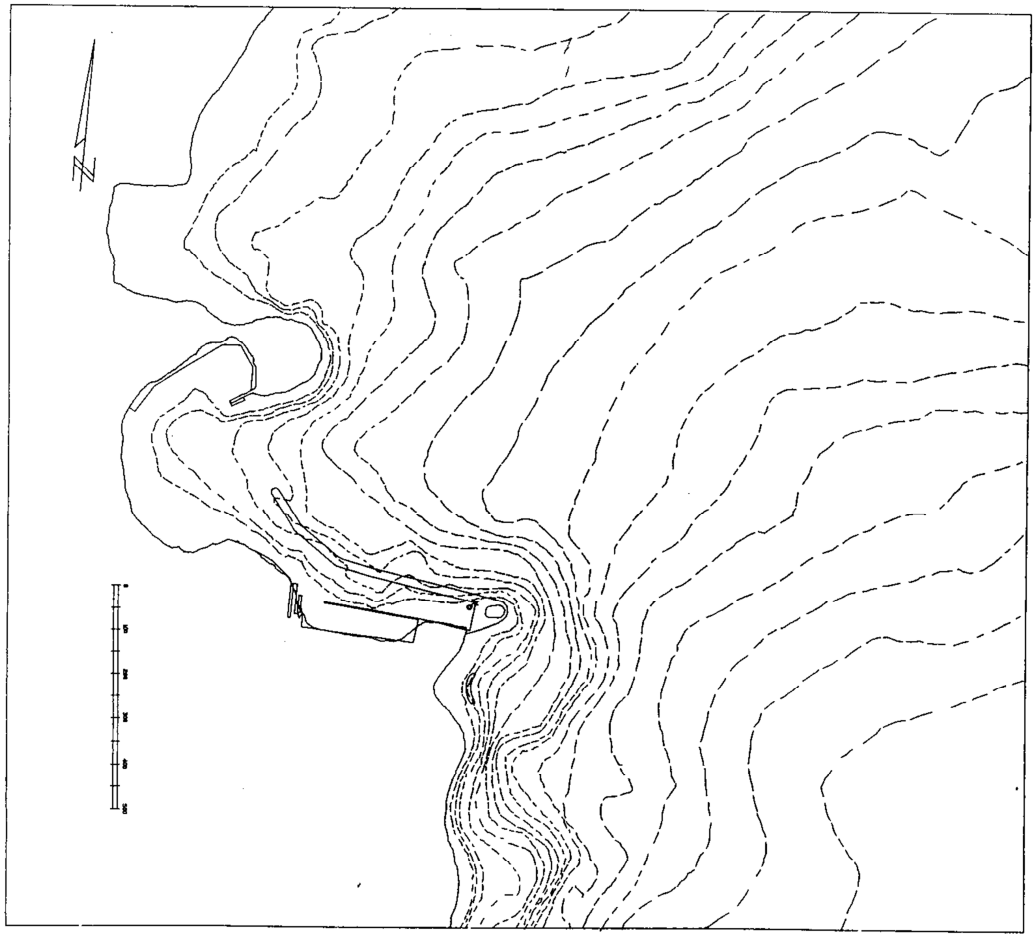

Figure 5-2: Proposed Layout of the Marina (Özhan, et al., 1999)

In (Özhan, et al., 1999), extensive studies were conducted in order to determine the wind and wave climate which were going to be the decisive factors in the design of the main breakwater and the marina layout. Many different layout and wave conditions were modeled. One layout case and one wave condition case is selected for comparison with the numerical model. The layout case (named "Case A" in the report) is used for comparisons with the sinusoidal wave input approaching from East with H=1m T=6sec and no directional spreading.

The wave data presented in the results of the physical model tests includes only the disturbance coefficients measured at 10 gauges which are spread over the sheltered

zone of the proposed marina. So the comparison is made between the physical and numerical model results at these 10 gauge points (Figure 5-3).

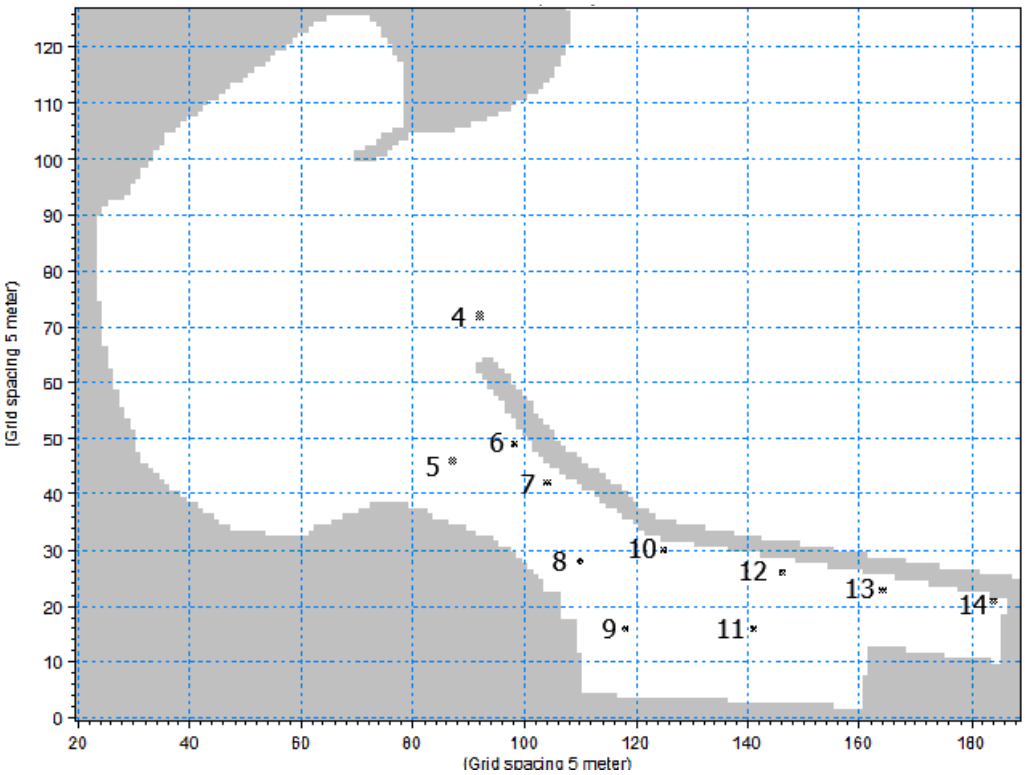

Figure 5-3: Gauge Locations

5.1 Numerical Model Inputs

The basic inputs of the numerical model are bathymetry, simulation duration, internal wave generation, porosity layers at the coastline and sponge layers at the boundaries.

The numerical model domain is divided into 236x148 grid nodes equally spaced with 5 meters of grid spacing in both x and y directions. It covers a total area of 1180x740 square meters. The layout of the proposed marina is given Figure 5-4.

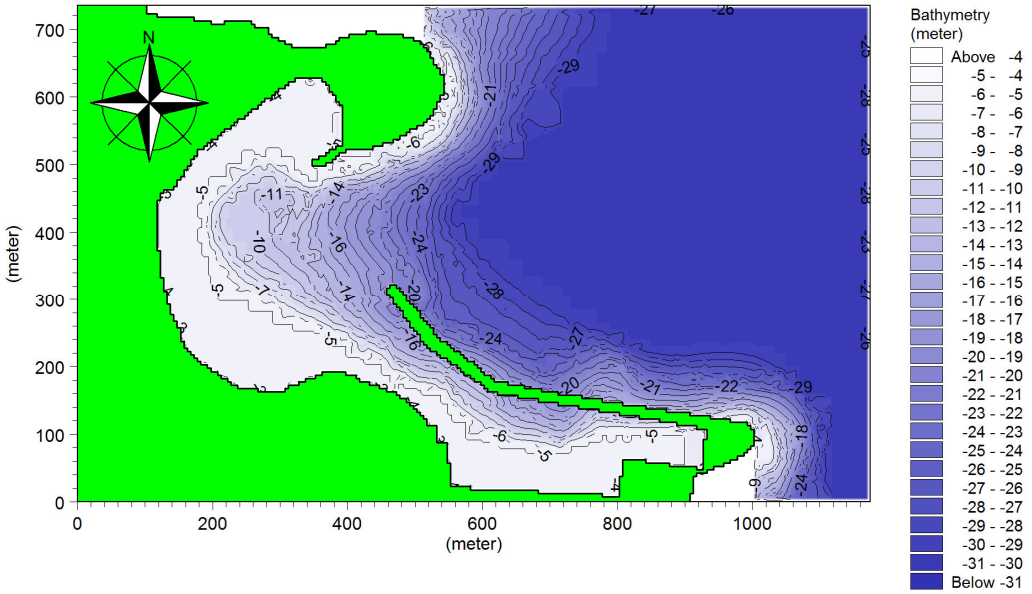

Figure 5-4: Numerical Model Domain

The bathymetry of the model domain is obtained by digitizing the bathymetry map given in Figure 5-2. The maximum depth in the prototype is 30 meters which satisfies deep water conditions of 6 second period waves. So in the numerical model, the maximum depth is set to 30 meters which is the allowable depth limit for a proper simulation of a 6 second period wave in MIKE21 BW. The minimum depth inside the model domain is set to 5 meters.

The simulation duration is 30 minutes in the numerical model. 30 minutes is more than enough to let the agitation inside the marina fully build up. The agitation inside the marina is mainly caused by the diffraction of the waves around the breakwater head and the reflection from the northern shore inside the Datça bay. The simulation duration is chosen considering these conditions.

Bottom friction is not included in the model. The effects of bottom friction are relatively unimportant in simulation of short wave propagation in ports and harbors. Since the model domain is small, there is not a sufficient distance for the bottom friction to cause any significant effect on short wave propagation. So the bottom friction can usually be excluded without any further detailed evaluations.

Eddy viscosity is excluded in the model. Eddy viscosity is mainly introduced in MIKE21 BW for modeling of wave-current interaction, where sub grid effects in the current field are not resolved.

Wave breaking is excluded in the model. This is mainly due to the fact that the waves of interest are inside the harbor and there is no significant wave-breaking effect inside the harbor. In addition, since the maximum depth inside the model domain is set to 4 meters, no breaking will take place with the selected input wave conditions.

In MIKE21 BW the waves are generated inside the model domain along a line defined by the user. In this simulation, the internal wave generation line is placed near the eastern boundary of the model domain. The internally generated wave is a regular sinusoidal wave with H=1m and T=6sec. The waves approach exactly from East with no directional spreading. By setting the wave generation parameters as such, the same conditions as in the physical model are simulated.

In both the numerical model and the physical model, the waves are released into the model domain at 30 meter water depth which is approximately the deep water limit for the 6 second period wave. The location of the internal wave generation line is given in Figure 5-5. Internal generation of waves is performed by adding the discharge of the incident wave field along the specified generation line. The discharge values are obtained as time series by means of the tools of MIKE21 BW.

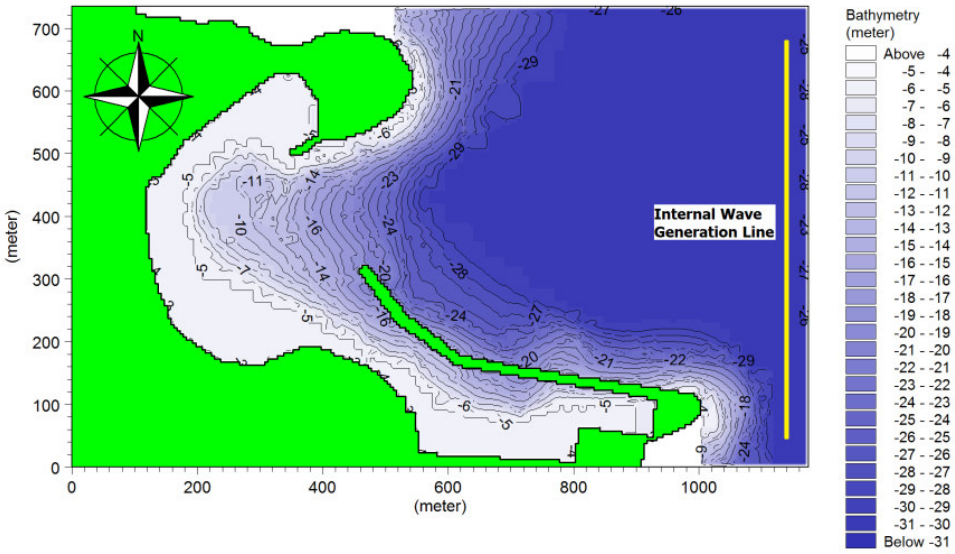

Figure 5-5: Position of the Internal Wave Generation Line

Porosity layers are used to model either partial reflection and/or transmission through structures. If porosity values are backed up by land, partial reflection will take place. In addition, partial transmission will also take place if the porosity values are not backed up by land points.

Inside the model domain, there are mainly 3 different coastal structures whose reflection rates are expected to be different from each other. These structures are the rubblemound breakwater, the vertical walls along the piers and the rocky shoreline.

Inside the model domain, porosity layers are placed in front of these structures which all together constitute the boundary between the land and the water grids. The reflection characteristics of the porosity layers for each structure are given in Table 5-1.

The porosity values defined in MIKE21 BW correspond to different transmission and reflection properties for varying incoming wave height and period in front of the coastal structure. In order to obtain the correct porosity values for the desired reflection and transmission rates, an estimate wave height distribution should be available for all coastal structures in the model domain. To obtain an initial estimate of the wave height distribution inside the harbor, diffraction diagrams can be used as well as running a rough model in MIKE21 BW. In this case, a rough model simulation is carried out to obtain the approximate wave parameters near the coast line inside the domain. According to the initial estimate of these values, MIKE21 BW tools were utilized to obtain the porosity values corresponding to the desired reflection and transmission rates.

Table 5-1: Reflection Coefficients of the Coastal Structures

Structure	Porosity Value	Number of Porosity Layers	Reflection Coefficient
Rubble Mound BW	0.58	3	0.40
Rocky Shoreline	0.48	3	0.60
Vertical Wall Piers	0.99	1	0.99

The porosity map is also given in Figure 5-6. The numbers from 1 to 3 correspond to rubblemound breakwater, rocky shore and the vertical wall piers.

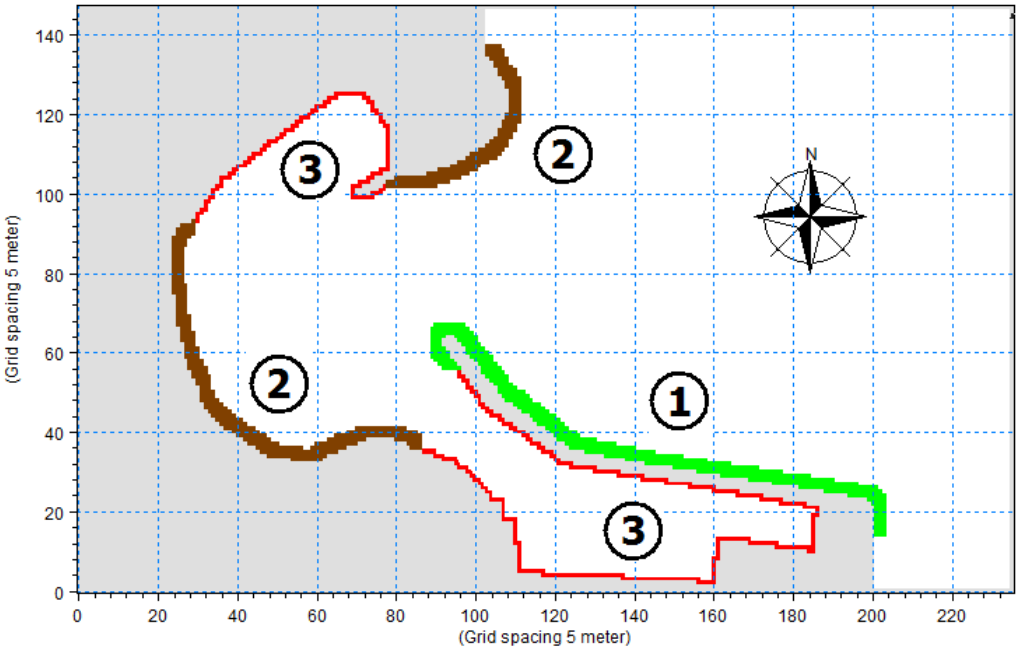

Figure 5-6: Porosity Map

Note that for varying water depth and incoming wave characteristics, the same porosity value results in different reflection coefficients. So in order to determine the correct porosity values to get the desired reflection rates, first an initial simulation was run with no porosity in order to have an idea about the wave characteristics around each coastal structure. Then using these wave characteristics as input, the correct porosity values are obtained for each structure by means of the porosity value calculator tool in MIKE21 BW.

In MIKE21 BW the waves are generated internally. During the wave generation two identical waves which propagate to opposite directions are generated. One wave is sent into the model domain from the generation line and the other wave is sent to the opposite direction. If the energy of these mirrored waves is not absorbed somehow, this wave energy will be fully reflected back into the model domain by the closed boundaries which are fully reflective. So sponge layers are placed between the generation lines and the closed boundaries of the model.

In the numerical simulation domain, sponge layers are placed not only behind the generation line on the east side of the domain, but also along the northern and southern closed boundaries as well. The positions of the sponge layers inside the

numerical model domain can be observed in Figure 5-7. The blue grids represent the sponge layers.

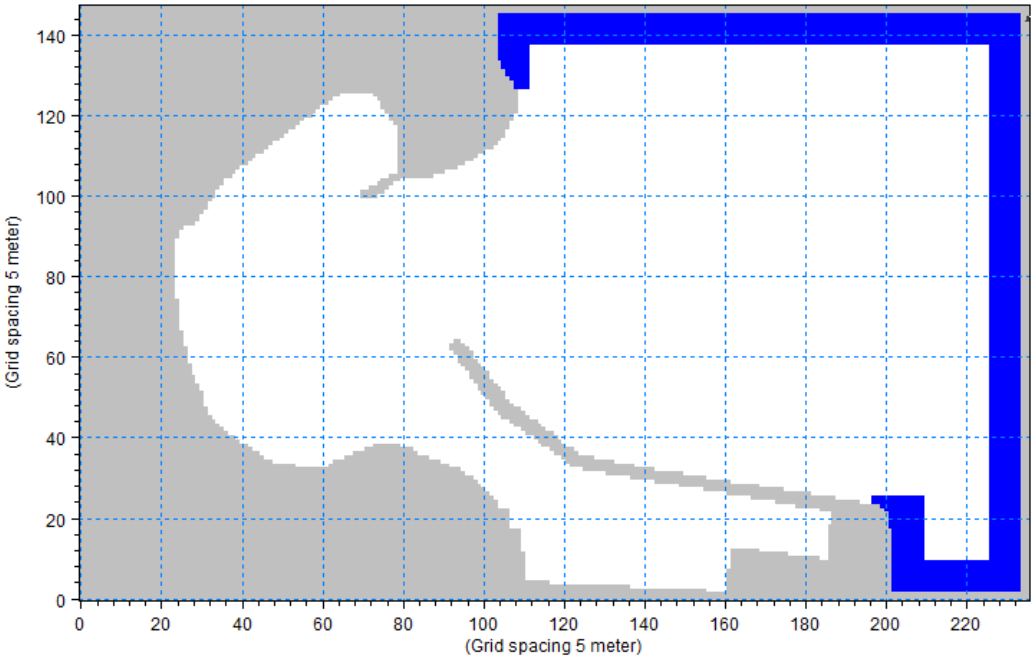

Figure 5-7: Sponge Layers Inside the Numerical Model Domain (Blue Grids)

5.2 Overview of Results

The numerical simulation was set up as explained in the previous section and it was run to cover a 30 minute period. The model yields 3 categories of outputs. These are deterministic parameters, phase averaged parameters and wave disturbance parameters. In deterministic parameters, time series of different values such as the surface elevation and flux density are recorded at either the whole domain and/or at certain predefined grids whereas by phase averaged parameters and wave disturbance parameters, statistical values corresponding to the whole or a predefined interval of the simulation are obtained. Some example parameters for these two parameters are significant wave height, maximum wave height, maximum surface elevation, mean flux densities, mean surface elevation and disturbance coefficients.

Since the only output wave parameters in (Özhan, et al., 1999) are the wave disturbance coefficients at 10 gauges, the calibration of the numerical model was carried out by comparing the disturbance coefficients at these gauges. After a few runs, the gauge readings of the numerical model were in fairly well agreement with

the gauge readings of the physical model. To obtain a better match between the physical experiment and numerical model results, different porosity values were tried. This cause different reflection rates along the coastline. In order to visualize the overall wave propagation inside the domain of the numerical model, the plan view of the sea state (surface elevations) at different time steps are shown in Figure 5-8 and Figure 5-9.

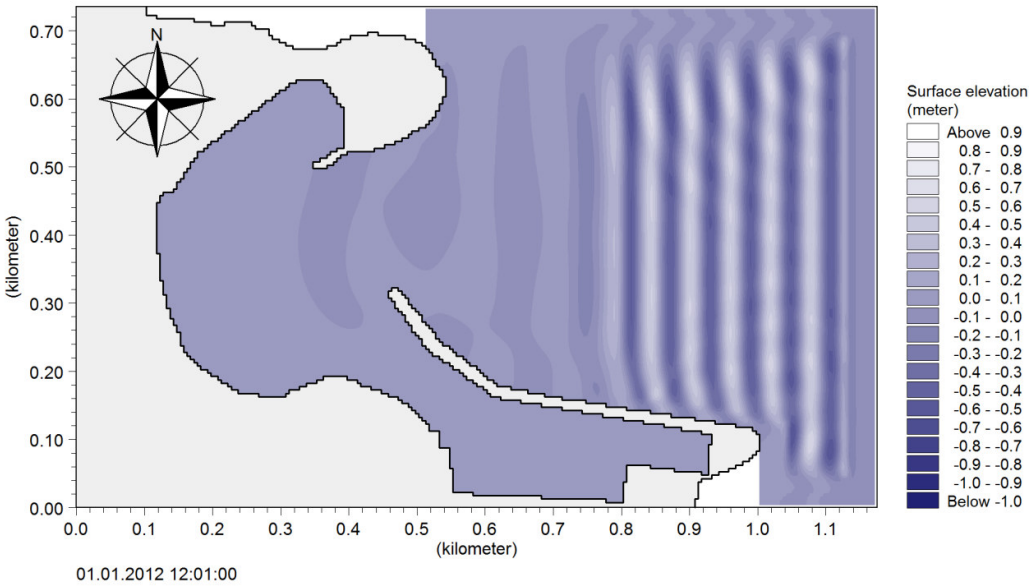

Figure 5-8: Instantaneous Surface Elevations at 1 Minute After Start

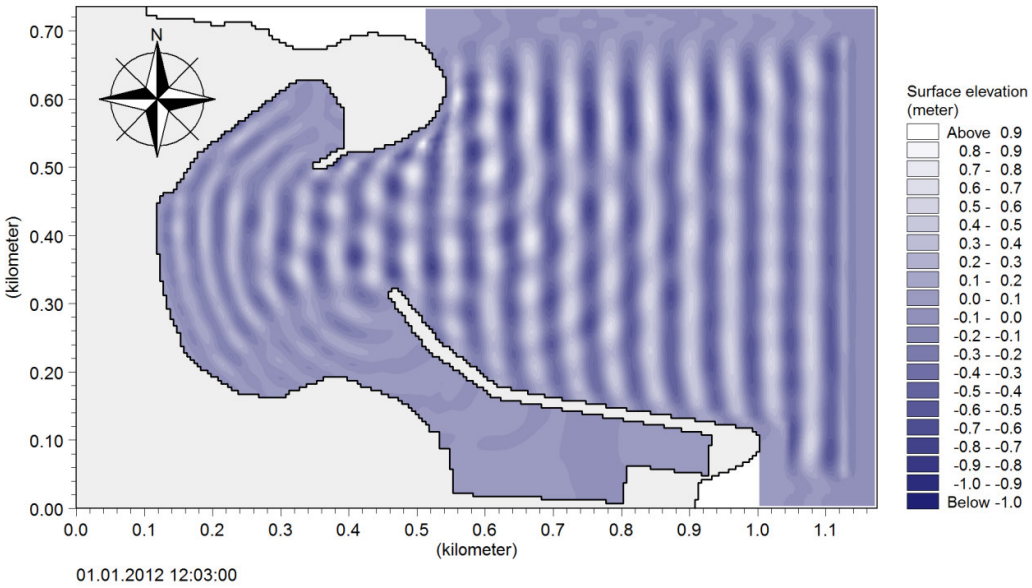

Figure 5-9: Instantaneous Surface Elevations at 3 Minutes After Start

Many wave transformation types can be observed in Figure 5-9. The reflection of the waves off the headland in the north, diffraction of the waves around the existing (northern) and the proposed (southern) breakwater heads, refraction of the waves which have penetrated directly through the gap and the shoaling of the same waves are some of the visible patterns in Figure 5-9.

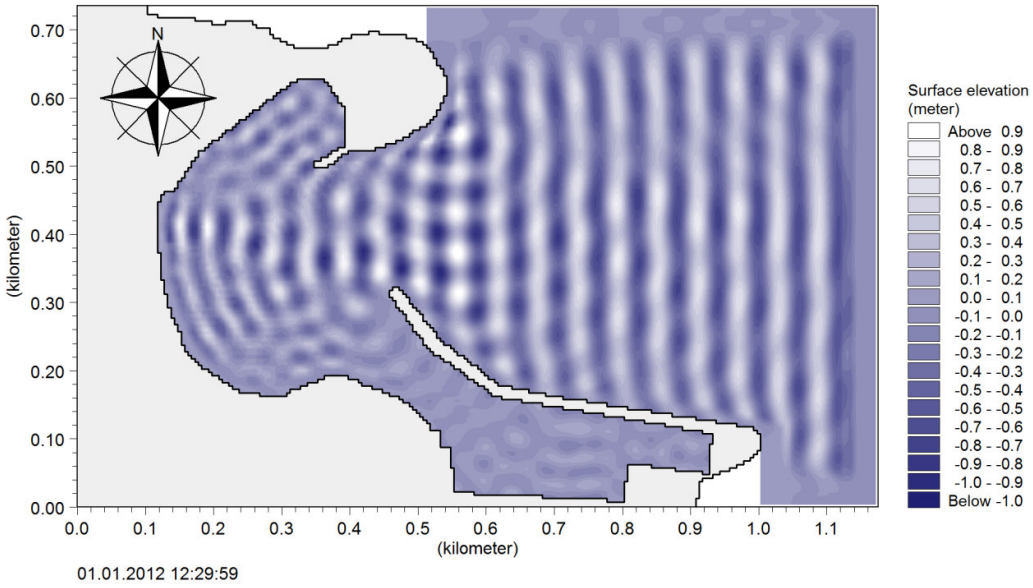

Figure 5-10: Instantaneous Surface Elevations at 30 Minutes After Start (Last Time Step)

The sea state at the end of the simulation (last time step) is shown in Figure 5-10. As seen in this snapshot, the agitation inside the proposed marina is fully built up. The reflection from every surface has taken place and the simulation has reached a steady state before the 30th minute.

In (Özhan, et al., 1999) a Froude model with λ_L=1:100 is tested. So the period of the waves generated in the physical experiment is 0.6 seconds (which corresponds to 6 seconds period of waves in prototype). The approximate distance between head of the breakwater and the wave paddles is 15 meters (in the model). The time required for the first generated waves to be re-reflected from the paddles and arrive at the entrance of the marina can be found by using the group velocity.

Average depth between paddles and the head of the breakwater, d_{avg}:

$$d_{avg} = \frac{0.3 + 0.2}{2} = 0.25m$$

Deep water wave length for 0.6 period waves, L_0:

$$L_0 = 1.56 \times T^2 = 0.56m$$

$$\frac{d_{avg}}{L_0} = \frac{0.25}{0.56} = 0.45$$

Since $0.0157 < \frac{d_{avg}}{L_0} < 0.5$, the waves propagate at intermediate depth. So the group velocity, C_g:

$$C_g = C \times n$$

$$n = \frac{1}{2}\left(1 + \frac{4\pi d/L}{Sinh 4\pi d/L}\right)$$

From Gravity Wave Table (Lyngby, 1974);

for $\frac{d}{L_0} = \frac{0.25}{0.56} = 0.45$

$$\frac{4\pi d/L}{Sinh 4\pi d/L} = 0.038$$

$$\frac{d}{L} = 0.453$$

$$L = 0.55m$$

Then C_g becomes:

$$C_g = \frac{L}{T} \times \frac{1}{2}\left(1 + \frac{4\pi d/L}{Sinh 4\pi d/L}\right)$$

$$C_g = \frac{0.55}{0.6} \times \frac{1}{2}(1 + 0.038)$$

$$C_g = 0.48\ m/s$$

Maximum allowable time in the physical experiment, t_{max}:

$$t_{max} = \frac{15m}{0.48\,m/s}$$

$$t_{max} = 31.25\,s$$

When t_{max} is multiplied by λ_T, the maximum unscaled time, $t_{max,u}$ becomes

$$t_{max,u} = 5.2\ minutes$$

In the physical model experiments, the waves re-reflected from the paddle arrives the harbor area in 31.25 seconds which corresponds to 5.2 minutes in the prototype

The disturbance coefficients at the gauges inside the harbor were calculated by taking the ratio of the wave height at the gauges inside the harbor to the wave height at the gauge located near the entrance of the harbor. The positions and the numbering of the gauges are presented in Figure 5-3.

Table 5-2: Average Disturbance Coefficients at Gauges

Gauge Number	Kd (MIKE21 BW)	Kd (Physical Model)
4	1.00	1.00
5	0.57	0.55
6	0.26	0.29
7	0.14	0.13
8	0.11	0.11
9	0.09	0.09
10	0.05	0.04
11	0.10	0.10
12	0.05	0.03
13	0.03	0.04
14	0.04	0.04

The same procedure is followed in the numerical model. Disturbance coefficient at gauge 4 is taken as unity and the disturbance coefficients at the rest of the gauges are calculated accordingly.

As seen in Table 5-2, the results of the numerical and the physical model are in fairly well agreement. The maximum difference between the disturbance coefficients of the numerical model and the physical model is seen as 0.03 at gauge 6. This was achieved by running the simulation for a number of different porosity values of the coastline. The best agreement was obtained by using the parameters given in Table 5-1.

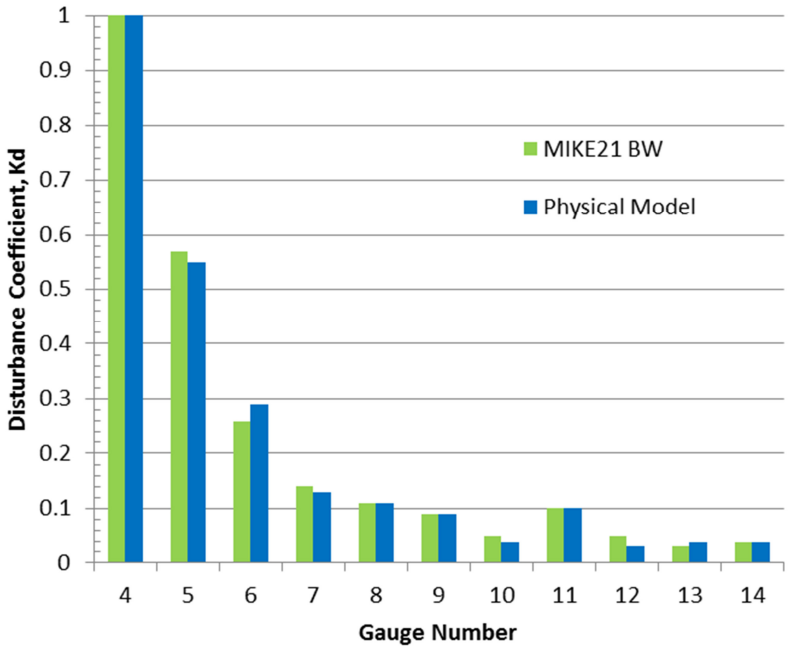

Figure 5-11: Comparison of Disturbance Coefficients

The results can also be observed in Figure 5-11. As seen in the bar chart, the physical model and numerical model results are very close to each other.

According to the above given comparisons, the disturbance coefficients obtained from the physical and numerical experiments are in fairly well agreement.

CHAPTER 6

A CASE STUDY: ISKENDERUN PORT

In this chapter, the results of a case study are presented. A numerical model is created for the purpose of calculating wave agitation inside the Iskenderun Port. The model experiments are carried out for irregular directional and regular unidirectional waves. The wave disturbance map of the inner port for the critical wave directions is obtained as an end result. This chapter is also a part of the report DERIN-LIMAK-REP-001 which was prepared for Limak Investments.

This case study covers the methodology and results of the numerical MIKE21 BW model for wave agitation calculations inside Iskenderun Port (Figure 6-1).

The required data (bathymetry, general layout and the wind-wave climate of the project area) were collected prior to the numerical modeling studies. Long-term wave climate of the project area was determined by a thorough analysis of the past wind and wave records covering more than 30 years. After all data were analyzed and processed by METU-OERC, the outputs of these studies were used as input for the numerical MIKE21 BW model.

The numerical modeling study covers the current layout case with 4 different critical wave conditions. The model is run for both regular and irregular waves, approaching from 2 different directions separately. The parametric properties of the wave conditions and the case scenarios are given in Table 6-1. The port is analyzed with respect to four critical wave conditions whose probability of exceedance is 10 hours in a year.

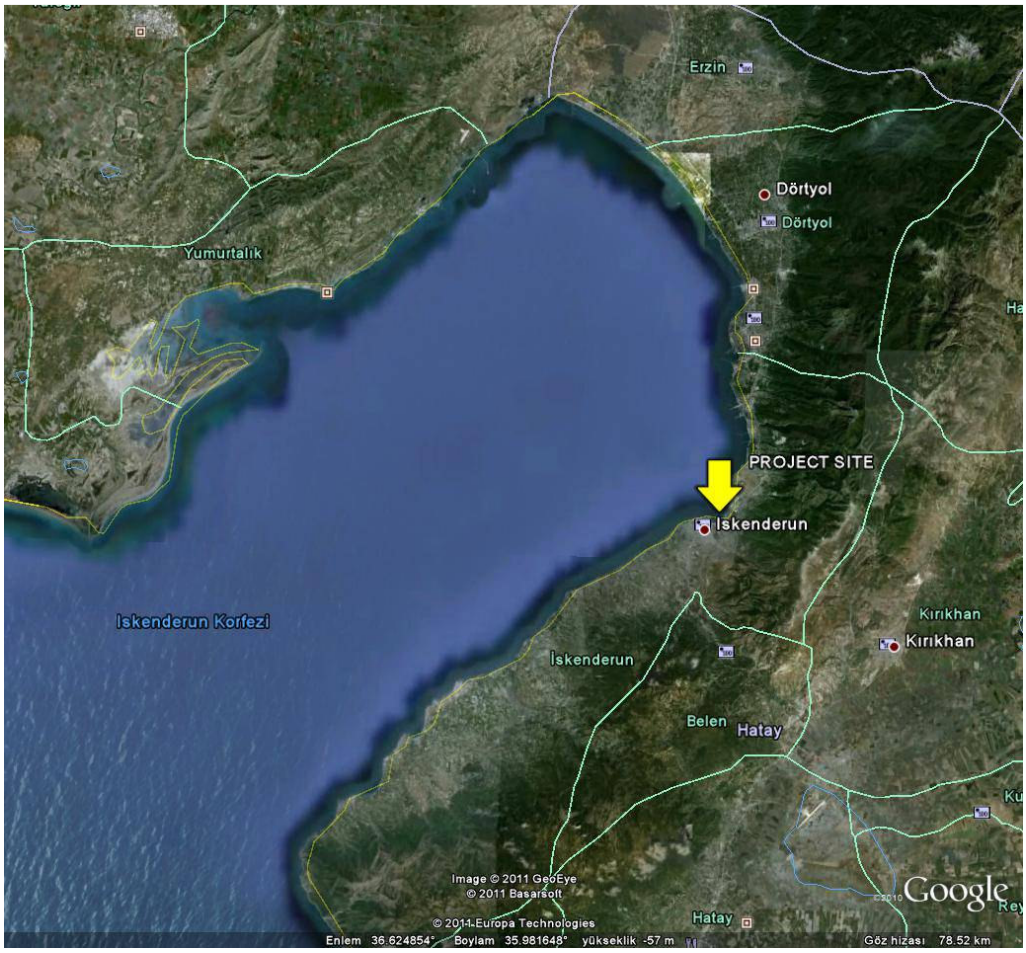

Figure 6-1: Project Site in Iskenderun Bay (Google Earth)

Table 6-1: Wave Conditions (Ergin, et al., 2011)

	Wave 1	**Wave 2**	**Wave 3**	**Wave 4**
Wave Direction	NNE	NNE	W	W
Hs (m, at 20m water depth)	1.19	1.19	1.99	1.99
Tp (seconds)	5.22	5.22	5.75	5.75
Approach Angle* (degrees)	2.8	2.8	279.6	279.6
Wave Regularity	Irregular	Regular	Irregular	Regular

*: Approach angle is measured clockwise from north direction.

Port of İskenderun is located in the north eastern part of Mediterranean Sea. It serves to South and South East Anatolia Region, as well as the transit traffic to the Middle East Countries. Thus, port of İskenderun is an important transit port. The port has a breakwater length of 1400m which provides shelter against the westerly waves and the depth at the entrance is about 12m. Port of İskenderun, which is a multi-purpose port, has connections to both rail and highway networks and serves customers to handle bulk, general cargos and Ro-Ro's.

Figure 6-2: Project Area (Google Earth)

6.1 Site Data

The bathymetry and the general layout of the project area had been previously determined by a field study by DERINSU Survey Department (Figure 6-3). A high resolution multibeam echosounder was utilized during the bathymetric survey. As seen in Figure 6-3, the bathymetry data includes many details such as the previously dredged areas and spreading of the main breakwater armor stones which may indicate damage received during past storms.

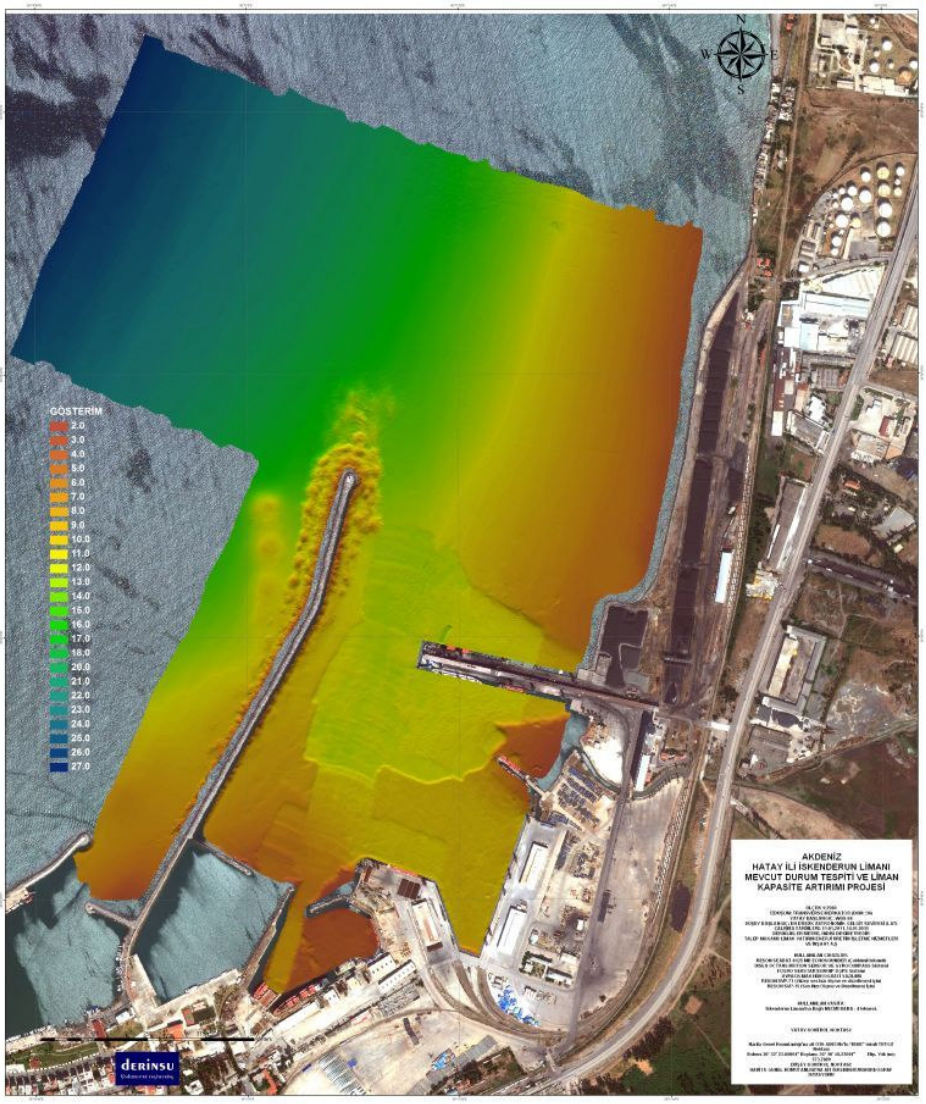

Figure 6-3: Bathymetry and the Satellite View of the Project Site (DERINSU)

The piers and other structures inside the harbor are labeled as shown in Figure 6-4.

Figure 6-4: Structures Inside The Harbor (Google Earth)

Table 6-2: Structure Names and Types

Structure Name	Structure Type
MBW (Main Breakwater)	Rubblemound
P1 (Pier 1)	Piled Pier Backed-up by Sheet-pile
P2 (Pier 2)	Piled Pier Backed-up by Sheet-pile
P3 (Pier 3)	Piled Pier Backed-up by Sheet-pile
P4 (Pier 4)	Piled Pier Backed-up by Sheet-pile
P5 (Pier 5)	Piled Pier
P6 (Pier 6)	Piled Pier
P7 (Pier 7)	Piled Pier
P8 (Pier 8)	Piled Pier
P9 (Pier 9)	Piled Pier
P10 (Pier 10)	Piled Pier
RM	Rubblemound
PP-SP	Piled Pier Backed-up by Sheet-pile

6.2 Numerical Model Inputs

Several different inputs such as domain, simulation period, calibration factors, internal wave generation, porosity layers and sponge layers are entered into the model as input.

The model consists of a 600x900 grid system where each grid size is 3x3 meters. This corresponds to an area of 1800x2700 meters in x and y directions respectively. In Figure 6-5, it can be observed that the numerical model domain is defined to cover an area larger than the present layout of the port. The computational domain is defined as such in order to make easier comparisons between the present and the future design case layouts.

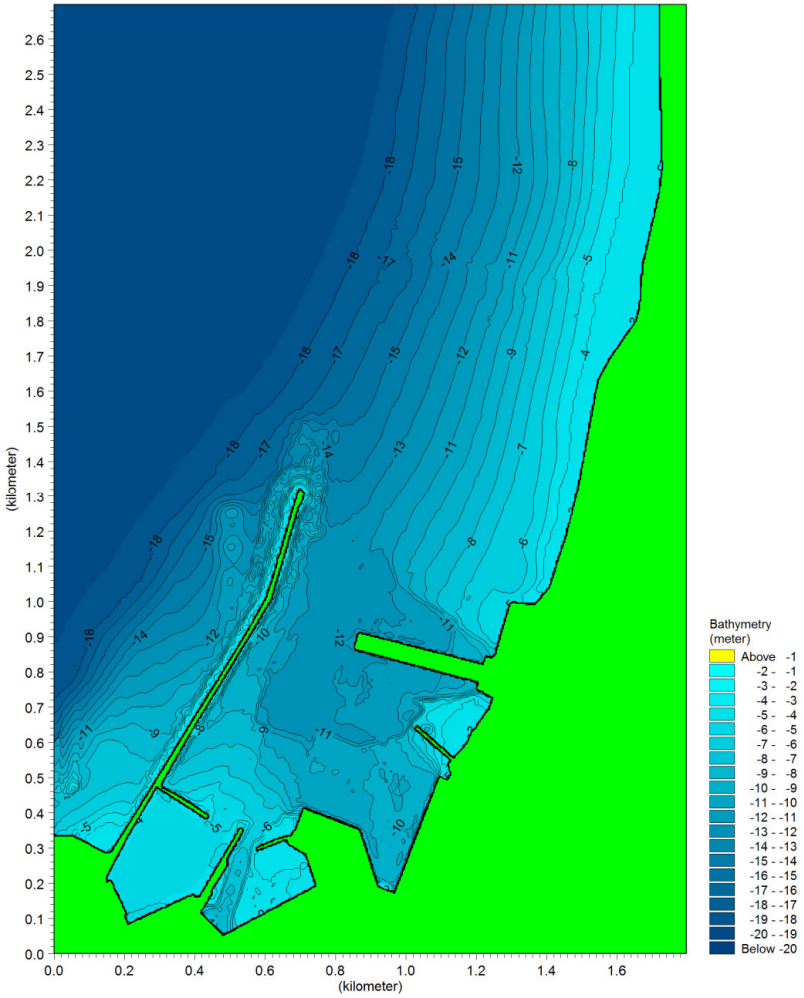

Figure 6-5: Present Layout and the Bathymetry

The simulation is run for 30 minutes. A period of 30 minutes allows for the wave agitation inside the harbor to fully develop. The minimum time required is less than about 20 minutes. An extra 10 minutes is added in order to ensure a fully developed sea-state inside the harbor. The time step used in the simulations is 0.1 seconds.

Bottom friction, eddy viscosity and wave breaking are not included in the model. The reasons for excluding these terms are explained in Section 5.1.

In order to be able to send waves from North-Northeast and West directions, wave generation lines are placed at the northern and western boundary of the domain (Figure 6-6)

The design wave conditions for the project area are given in Table 6-1. Both waves are caused by the wind blowing over the fetch zone in Iskenderun Bay. So, directional irregular waves with certain directional spreading as well as regular waves are generated in the model.

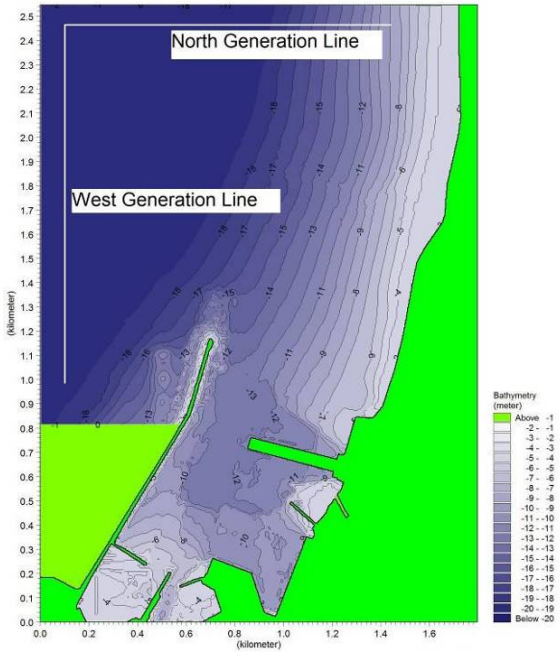

Figure 6-6: Internal Wave Generation Lines

The frequency spectrum, from which the directional frequency spectrum is generated, is specified in one of the following ways:

- A Pierson-Moskowitz Spectrum
- A JONSWAP Spectrum
- A TMA Spectrum
- Monochromatic Spectrum
- Time Series of Surface Elevation

In this project, both Regular Waves and Irregular Waves (JONSWAP Spectrum) are used to generate the wave conditions. The JONSWAP spectrum is specified through the following parameters:

- Significant Wave Height, Hs
- Peak Wave Period, Tp
- Shape Parameters, σ_a, σ_b, γ

The smallest wave period is specified as 4.94 seconds which correspond to the minimum allowable value for this model. The smallest wave period is limited by the maximum water depth in the computational domain. In this case, the maximum water depth is 19 meters which sets a limit of 4.94 seconds for the minimum wave period value. Since the high frequency (low period) part ($f>f_{cut-off}$) of the original spectrum is removed, the resulting integral parameters such as the significant wave height and mean wave periods are altered relative to the input specifications. In order to maintain the significant wave height as specified, the spectrum is re-scaled. Thus, the total energy in the truncated spectrum is the same as in the original specified spectrum Figure 6-7.

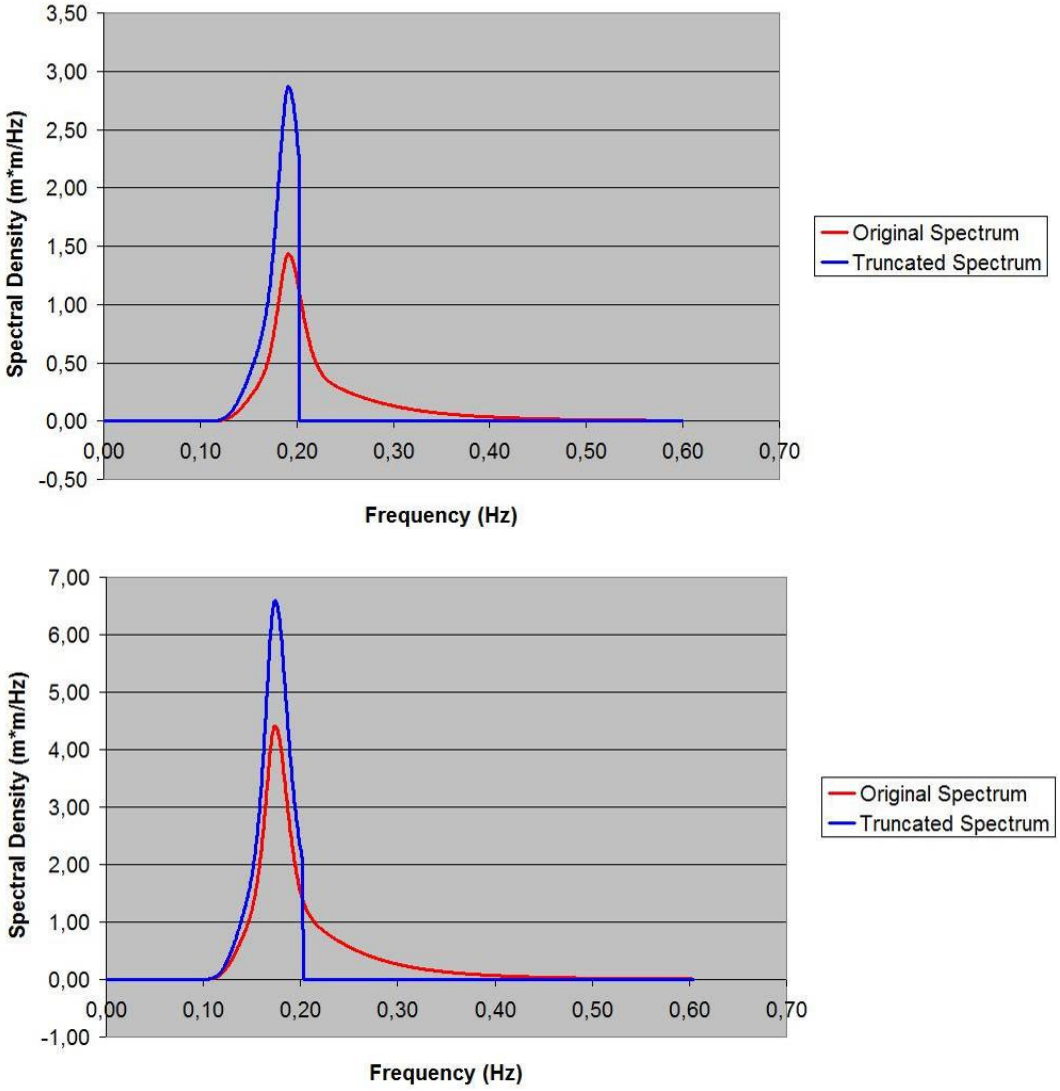

Figure 6-7: Original and Truncated Spectrums for NNE and W waves

In the model, all the piers, breakwaters, rubble mound shores and beaches, except piers 5-6-7-8-9-10, are defined as land points in front of which there are porosity layers. Piers 5-6-7-8-9-10 are directly defined as porosity layers which are not backed up by land. Thus, partial transmission is obtained at these piers as well as partial reflection. As an example, the porosity layer map for the present layout of the port is given in Figure 6-8.

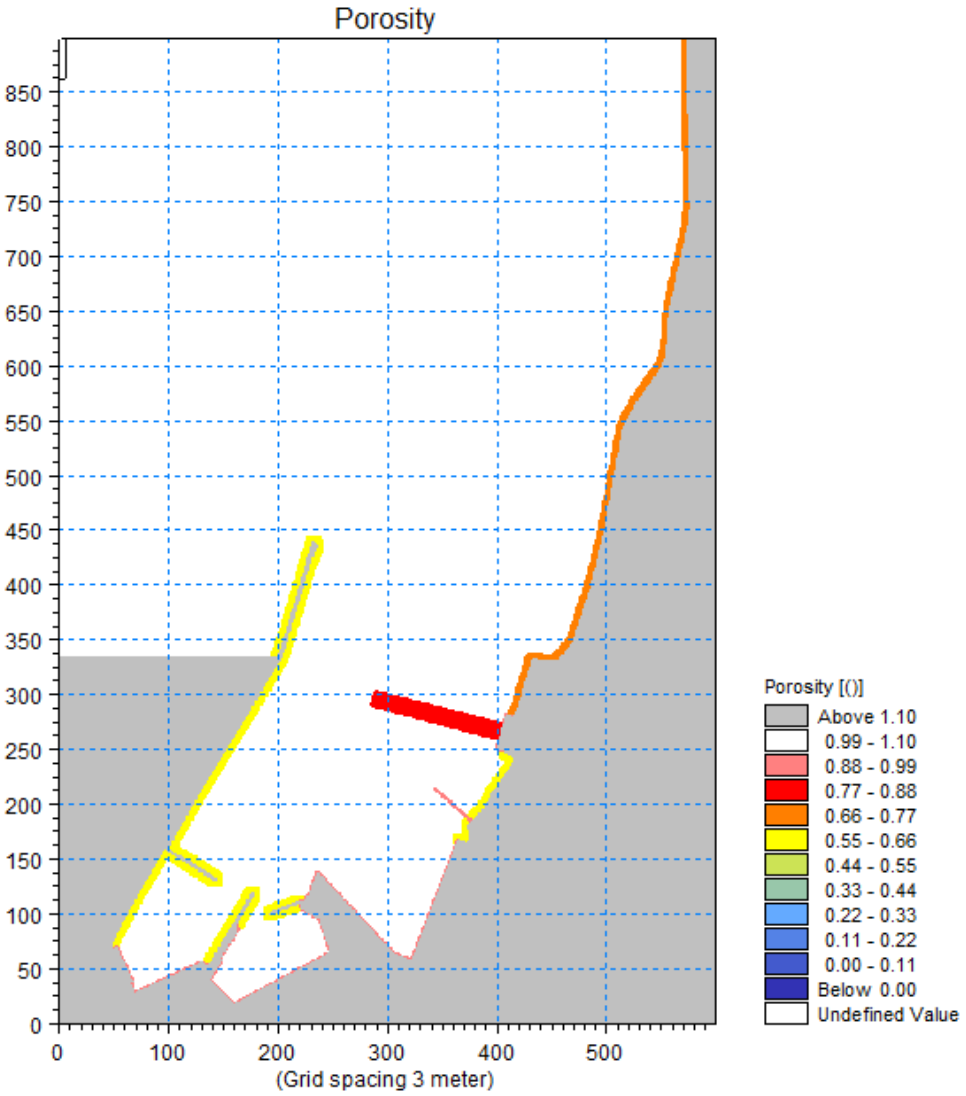

Figure 6-8: Porosity Layer Map for Present Layout Case

The relations between porosity-reflection-transmission of coastal structures are illustrated as an example in Figure A-1 to Figure A-7 in Appendix A.

The reflection and transmission (if available) rates of the piers and breakwaters in the project area is given in Table 6-3.

Table 6-3: Reflection & Transmission Values of Coastal Structures in the Project Area

Coastal Structure	Structure Type	Reflection Ratio	Transmission Ratio
Pier 1-2-3-4	Piled Pier Backed Up by Sheetpile	1	-
Pier 5-6	Piled Pier	0.10	0.90
Pier 7-8-9-10	Piled Pier	0.10	0.44
Main Breakwater	Rubble Mound	0.40	-
Rubble Mound Inside Military Zone	Rubble Mound	0.40	-
Coastline Between Pier 6&7	Rubble Mound	0.40	-
Rubble Mound Coastline North of Pier 9	Rubble Mound	0.40	-
Northern Beach	Gently Sloping Beach	0.35	-

In order to be on the safe side, all piled piers which are backed up by land (sheetpiles) have a reflection ratio of 1 which corresponds to full reflection. In the model, to avoid stability problems, one grid layer of porosity with a 0.99 porosity value is located in front of all fully reflective structures. By doing so, the structures behave still fully reflective while preventing instabilities due to full reflection.

In all simulations, sponge layers are placed behind the generation lines and the southwest outer part of the domain (Figure 6-9). The blue areas represent sponge layers.

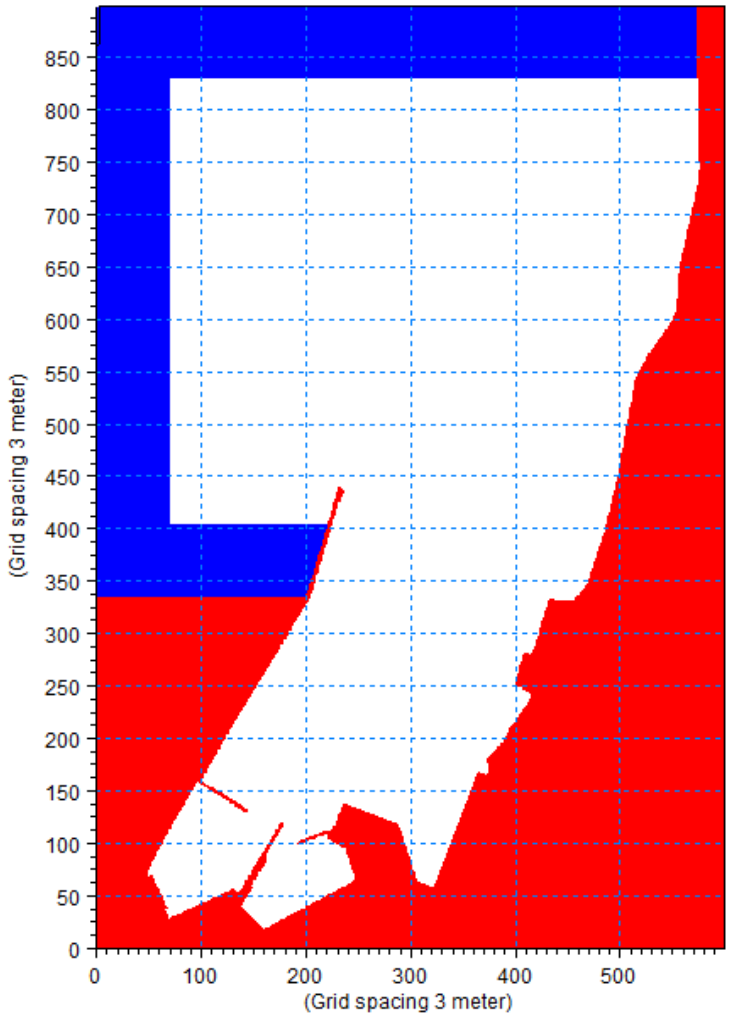

Figure 6-9: Sponge Layer Map. Blue zones denote sponge layers

6.3 Evaluation of Cases and Model Outputs

The model is simulated and run for each case with the input parameters described in Section 6.2. Each simulated scenario is run for 30 minutes which allows the wave agitation inside the harbor to reach a steady state. As explained in previous sections, 4 different wave conditions for the present layout of the harbor. In total, there are 4 different simulations. Each case scenario is listed in Table 6-1.

The results of the simulations are presented mainly as three categories:

1) Deterministic Parameters
2) Phase Averaged Parameter
3) Wave Disturbance Parameters

In Deterministic Parameters, the surface elevation at each grid is obtained for each second during the simulation. Thus the propagation, refraction, diffraction, reflection etc. of the waves can be plotted or animated. This is a strong tool to visualize the general wave propagation inside the domain. The output can be selected to represent a point, a line, the whole domain or the combinations of these.

In Phase Averaged Parameters, cumulative statistics of the domain is obtained. The statistical output parameters are significant wave heights. The update interval of the Phase Averaged Parameters is selected as 60 seconds. The output can be selected to represent a point, a line, the whole domain or the combinations of these. In this model, a total of 8 gauges are placed in front of Piers 1, 2, 3, 4, 7, 8, 9, 10,. Also an area type output representing the significant wave height over the whole domain is obtained.

In Wave Disturbance Parameters, the wave disturbance coefficient, which is defined as the ratio of the significant wave height at a certain point relative to the incoming significant wave height, is obtained. The update interval is 60 seconds, and the output represents the whole domain. This is a very useful tool, output of which illustrates the possible problematic zones inside the harbor very clearly. Wave Disturbance Parameters output yields the most indicative results among all outputs of the simulation.

All the layout cases are the same and they are the present layout of the existing Iskenderun Port. The bathymetry is the same in all cases as well.

Also note that, there is no site data available for comparing the model results to.

6.3.1 Case 1

The direction of the waves modeled in this case is NNE (See Table 6-1). The type of the wave modeled in this case is irregular. The last time step is illustrated in Figure 6-10 which represents the time step when the waves inside the port have fully built up. Reflections from rubblemound breakwater and the piers are presented as well as the refraction and diffraction of the waves around pier 8.

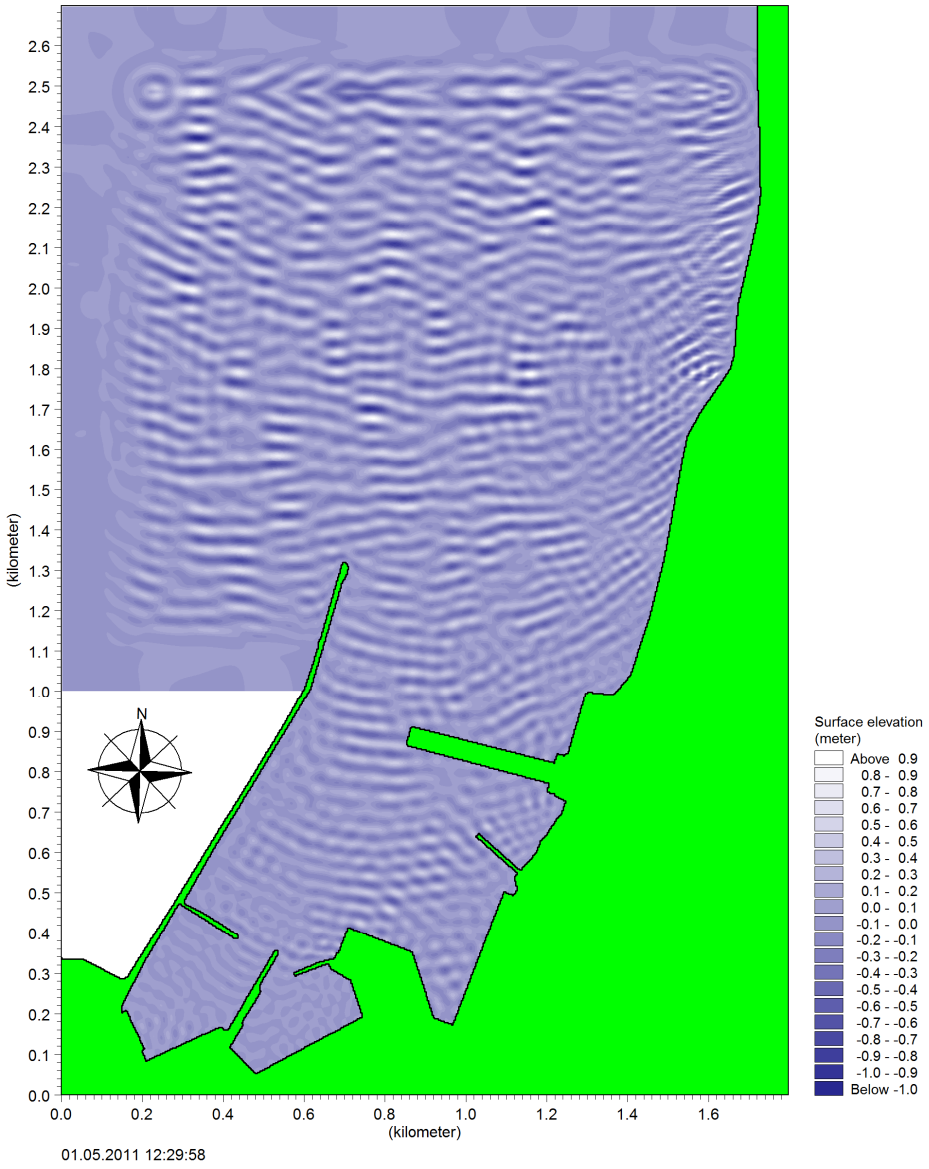

Figure 6-10: Propagation of Waves, 29:58 After Start

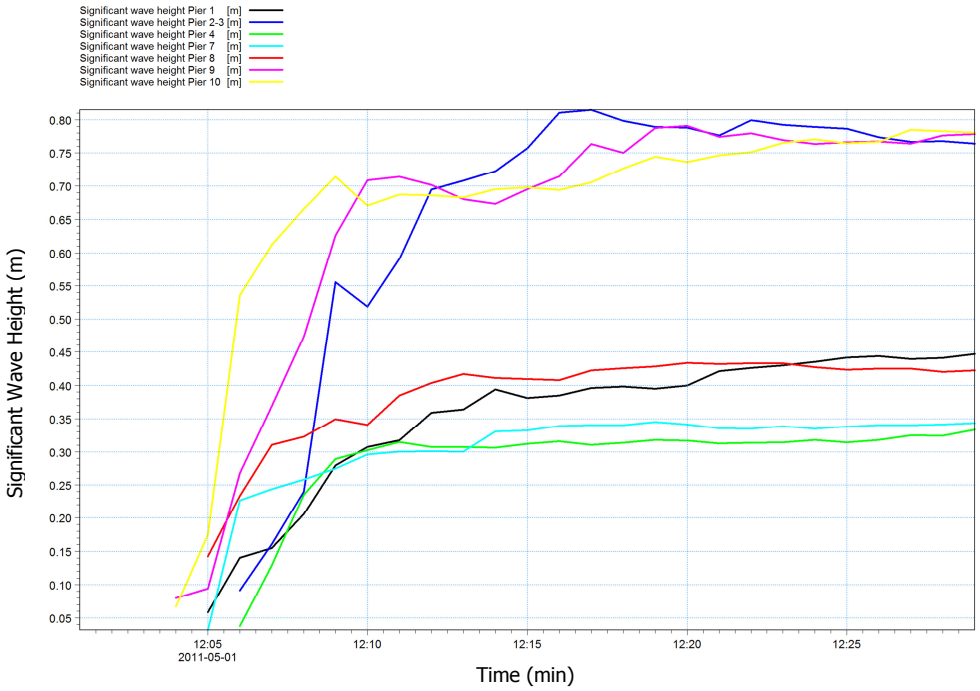

Figure 6-11: Significant Wave Heights In Front of Piers

Table 6-4: Significant Wave Heights for Case 1

Pier #	Significant Wave Height (m)
Pier 1	0.45
Pier 2-3	0.76
Pier 4	0.33
Pier 7	0.34
Pier 8	0.42
Pier 9	0.78
Pier 10	0.78

In Figure 6-11 and Table 6-4, the significant wave heights in front of piers are presented. As expected, since Pier 9 and 10 are exposed to the NNE waves, the significant wave heights in these zones are higher compared to the inner port. However, the significant wave height is also high near Pier 2-3, which is most probably due to the reflection and re-reflection around these areas.

In Figure 6-12, the ratio of the incident wave heights inside the harbor relative to the incoming significant wave height is illustrated. This wave disturbance map represents most of the storms which cause waves from NNE direction.

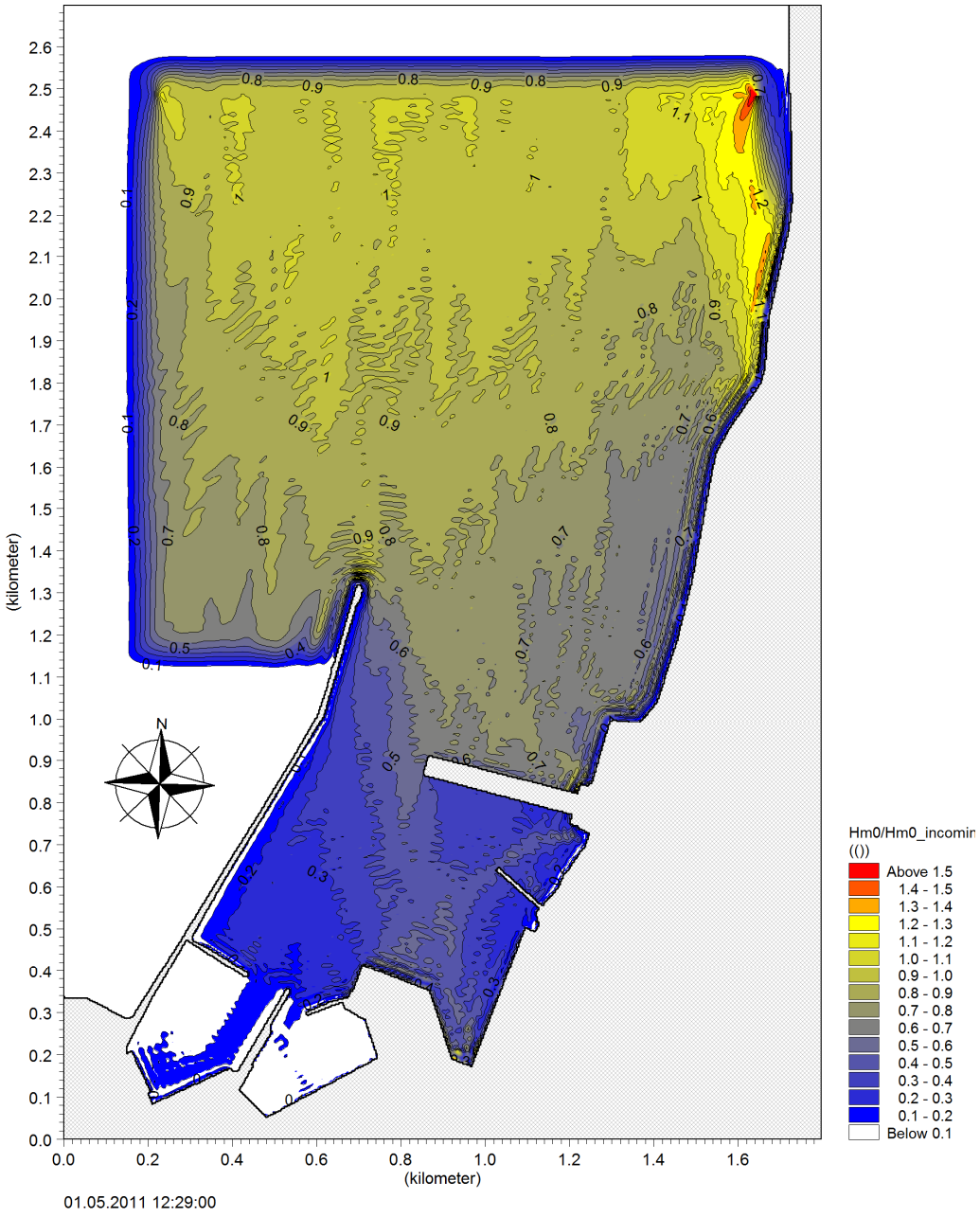

Figure 6-12: Wave Disturbance Map After 29 Minutes

6.3.2 Case 2

The direction of the waves modeled in this case is NNE (See Table 6-1). The type of the wave modeled in this case is regular. The last time step is illustrated in Figure 6-13. Since the waves are regular in this case, reflections from rubblemound breakwater and the piers and the refraction of the waves near the coastline can be seen more clearly compared to the irregular wave case.

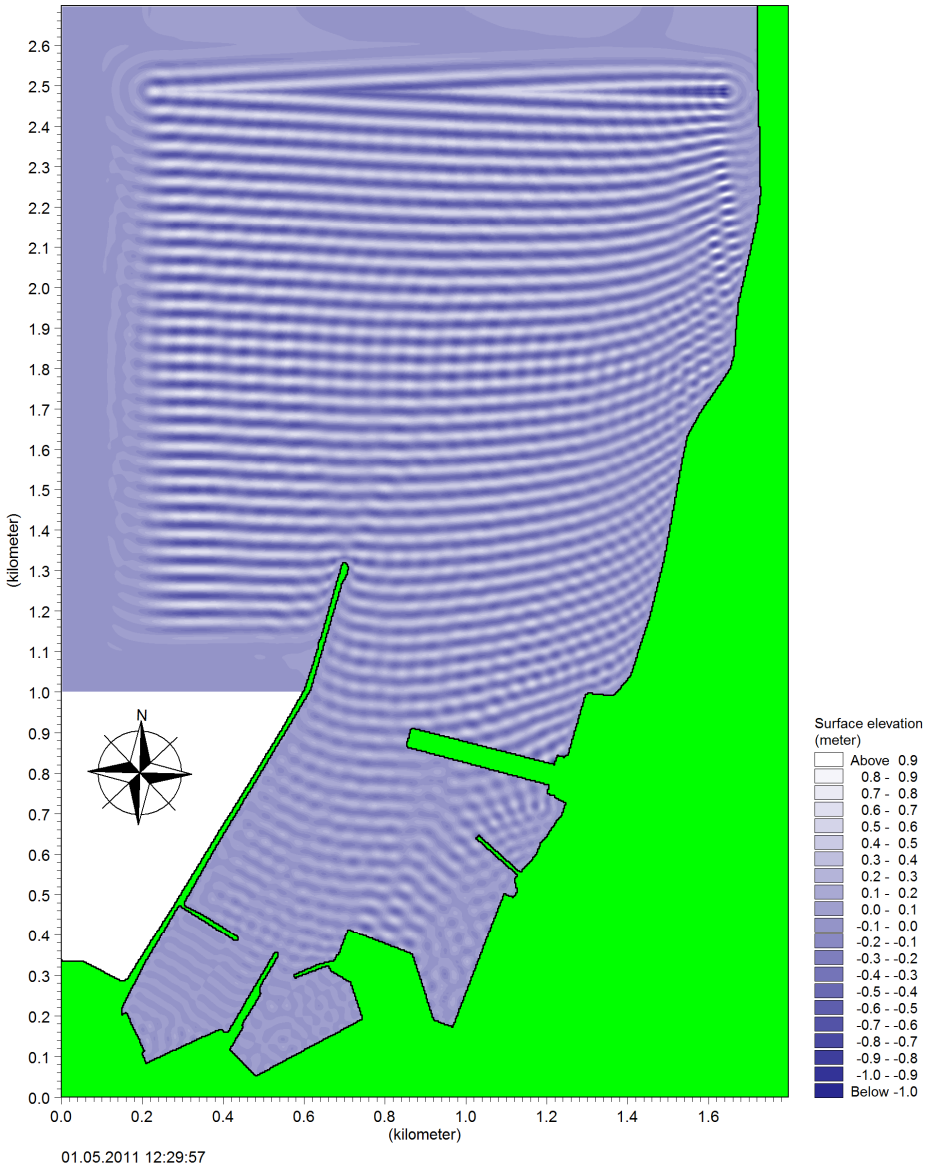

Figure 6-13: Propagation of Waves, 29:57 After Start

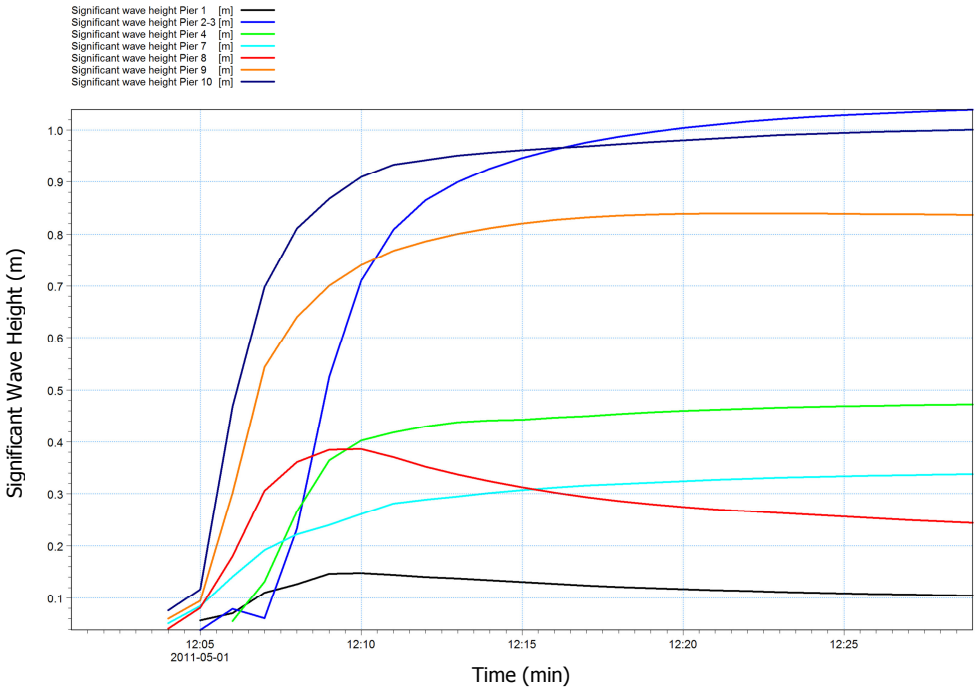

Figure 6-14: Significant Wave Heights In Front of Piers

Table 6-5: Significant Wave Heights for Case 2

Pier #	Significant Wave Height (m)
Pier 1	0.10
Pier 2-3	1.03
Pier 4	0.47
Pier 7	0.34
Pier 8	0.24
Pier 9	0.84
Pier 10	1.00

Similar to Case 1, the highest significant wave heights are observed around piers 2, 3, 9 and 10.

In Figure 6-15 although a majority of the harbor has a disturbance coefficient of less than 0.3, the coefficient in the zone in front of Pier 2-3 can go up to as high as 1 which indicates that the wave height in this zone can be built up by reflection from the piers to form waves with heights equal to the incoming wave height.

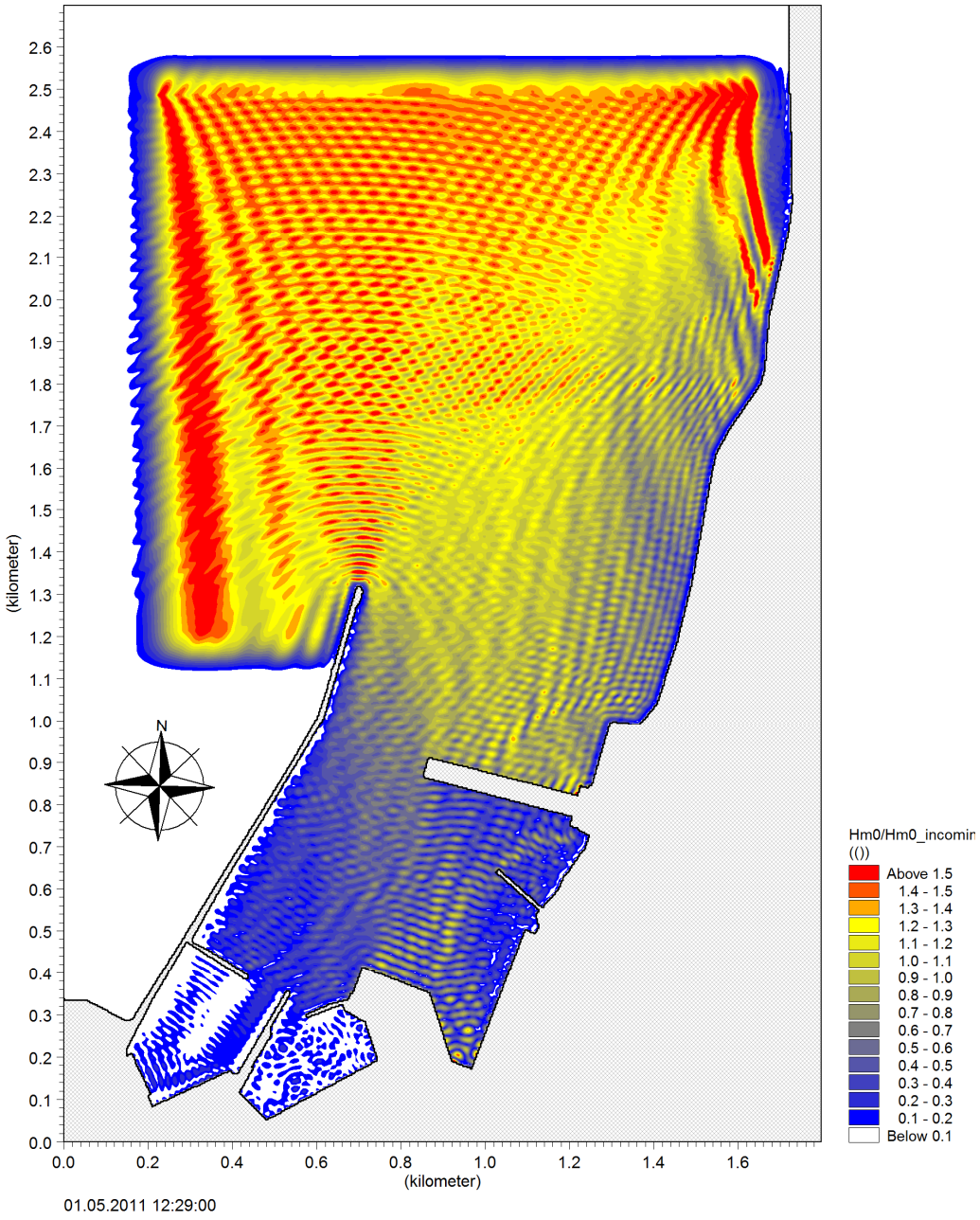

Figure 6-15: Wave Disturbance Map After 29 Minutes

6.3.3 Case 3

The direction of the waves modeled in this case is W (See Table 6-1). The type of the wave modeled in this case is Irregular. The controlling factor that causes agitation inside the harbor is the diffraction of the incoming waves around the main breakwater head. It is clearly observed that only a small part of the incoming wave energy is transmitted to the inside of the port in this scenario. Other wave phenomena such as refraction and reflection can also be observed.

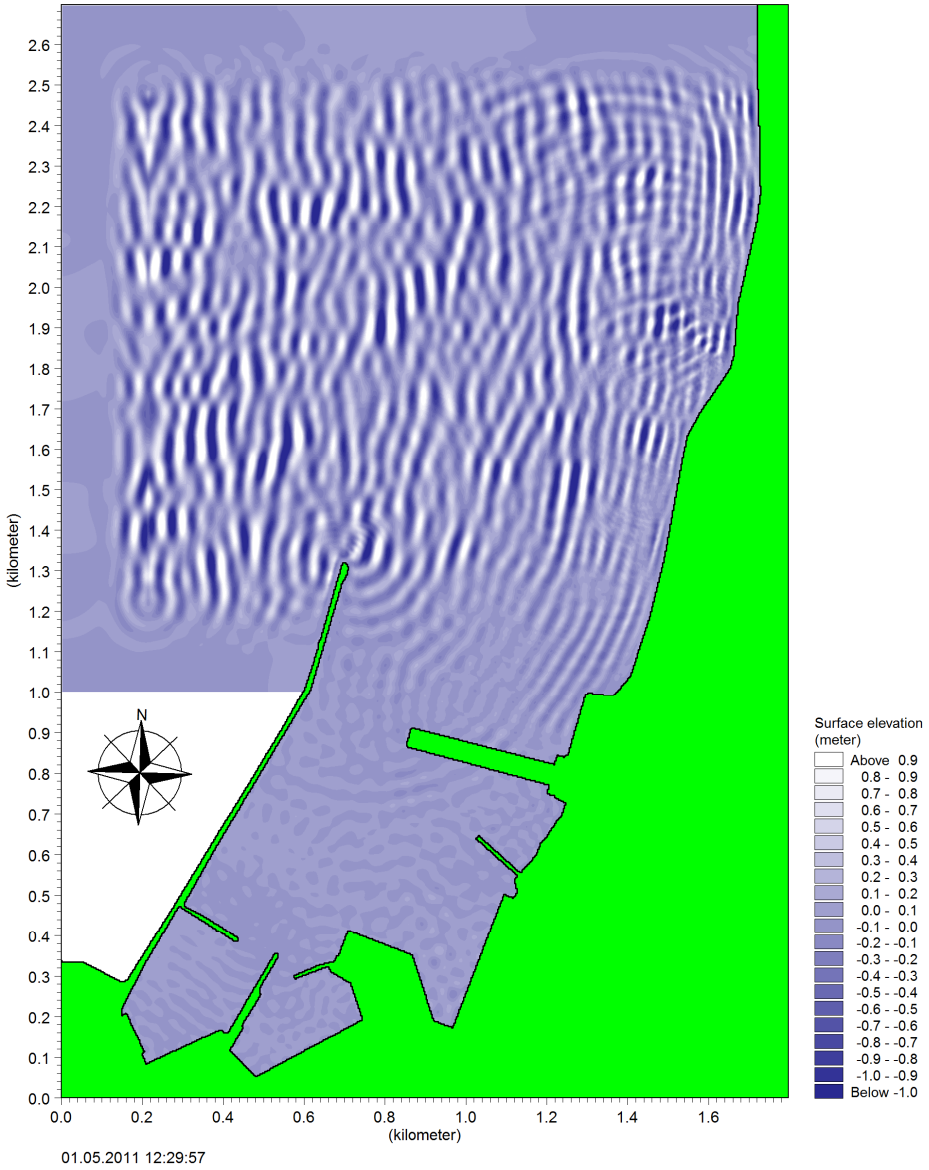

Figure 6-16: Propagation of Waves, 29:57 After Start

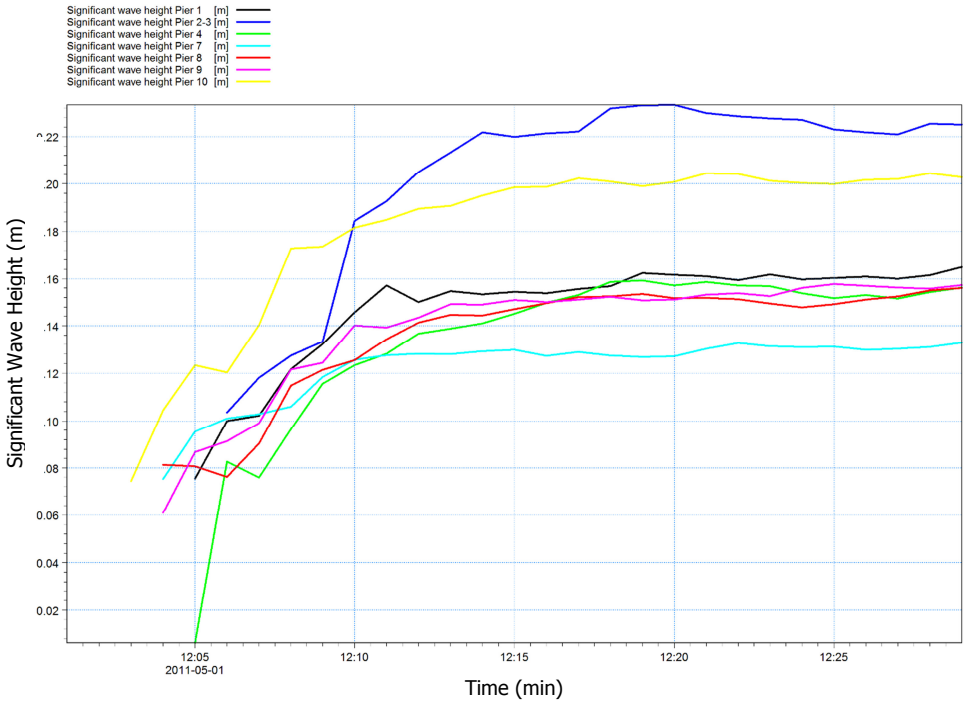

Figure 6-17: Significant Wave Heights In Front of Piers

Table 6-6: Significant Wave Heights for Case 3

Pier #	Significant Wave Height (m)
Pier 1	0.17
Pier 2-3	0.23
Pier 4	0.16
Pier 7	0.13
Pier 8	0.16
Pier 9	0.16
Pier 10	0.20

Compared to Cases 1&2, the significant wave heights in Case 3 are very low, as expected. There are no critical zones in this case with respect to significant wave height.

This wave disturbance map represents most of the storms which cause waves from WEST direction. For the westerly waves, the breakwater provides an excellent shelter for the inner harbor. For irregular westerly waves case, the wave disturbance coefficient inside the harbor is below 0.1 almost everywhere.

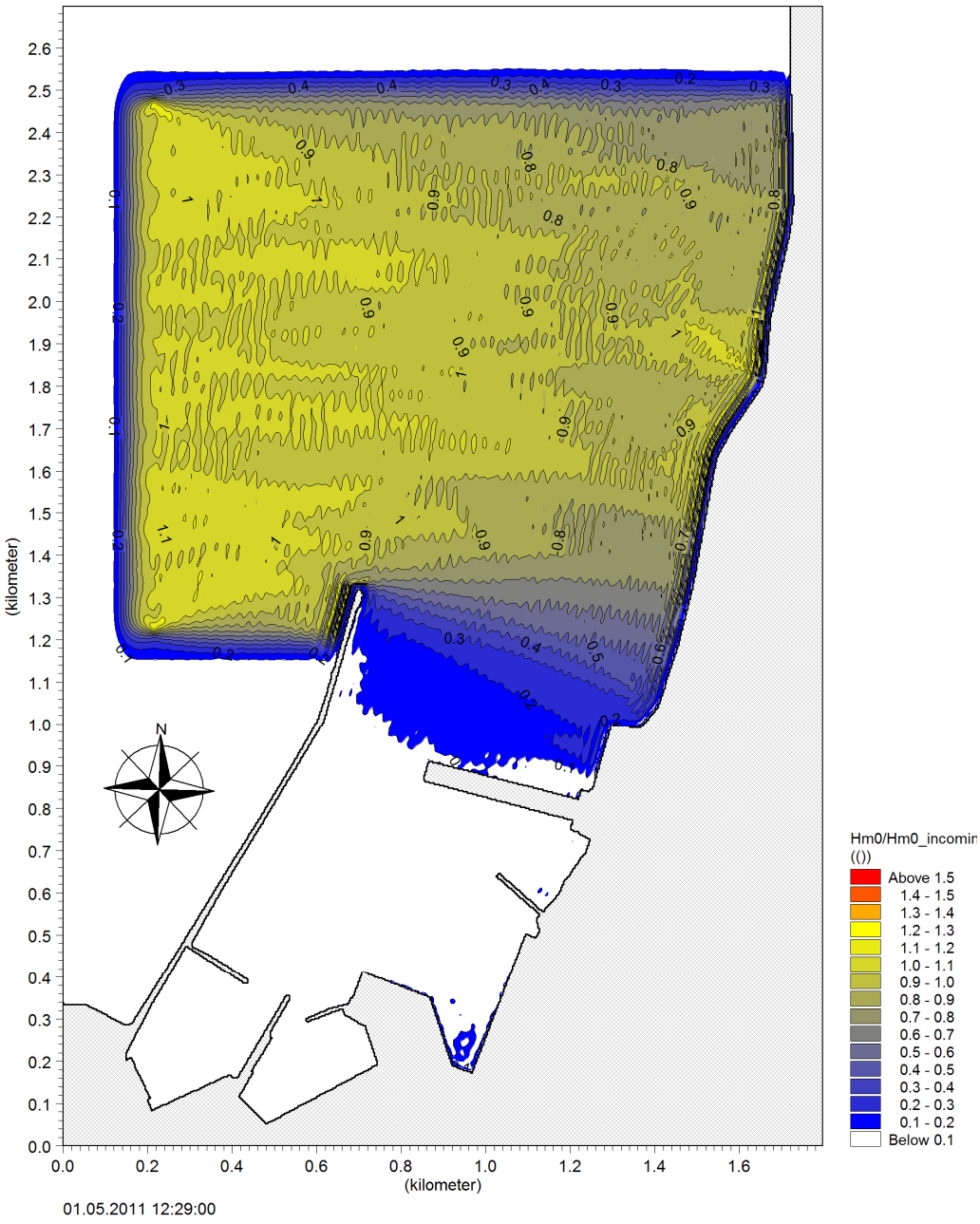

Figure 6-18: Wave Disturbance Map After 29 Minutes

6.3.4 Case 4

The direction of the waves modeled in this case is W (See Table 6-1). The type of the wave modeled in this case is regular. The diffraction around the main breakwater head can be clearly observed very clearly in Figure 6-19. Reflection can also be observed around the semi-headland along the shoreline.

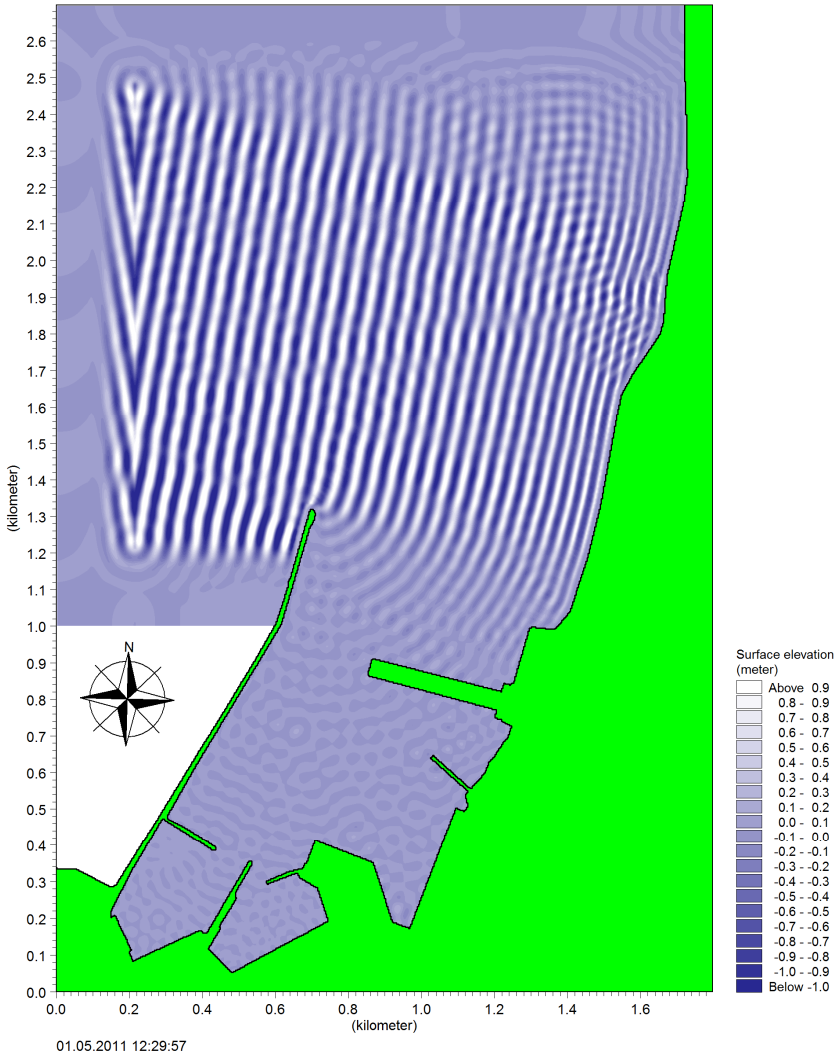

Figure 6-19: Propagation of Waves, 29:57 After Start

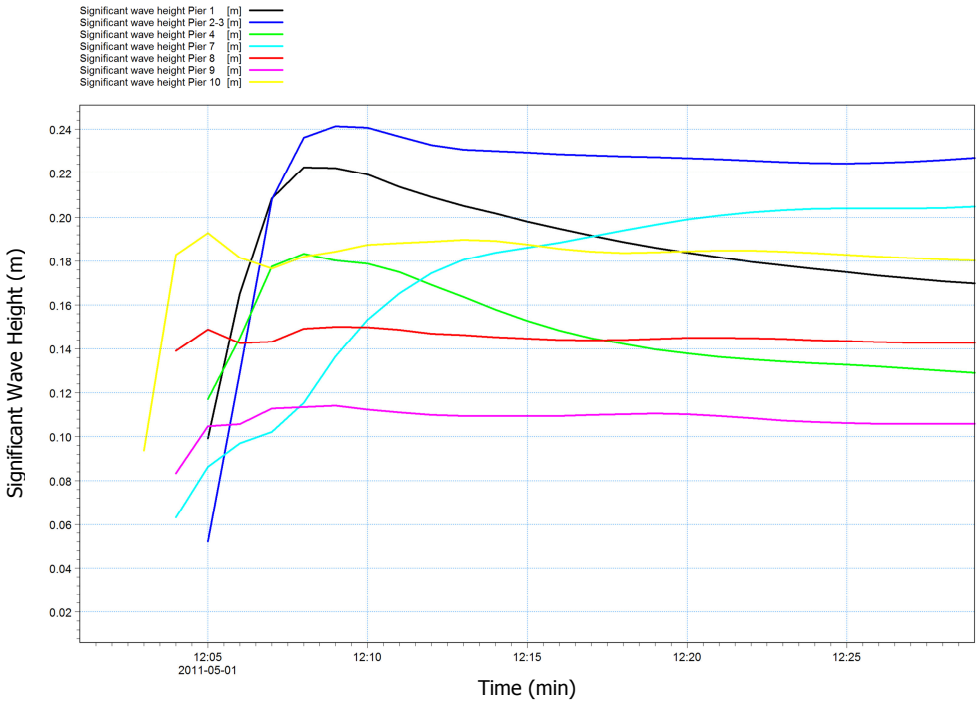

Figure 6-20: Significant Wave Heights In Front of Piers

Table 6-7: Significant Wave Heights for Case 4

Pier #	Significant Wave Height (m)
Pier 1	0.17
Pier 2-3	0.23
Pier 4	0.13
Pier 7	0.21
Pier 8	0.14
Pier 9	0.11
Pier 10	0.18

As in Case 3, the significant heights inside the port are very low and insignificant. The breakwater provides a very good shelter against westerly waves.

In Figure 6-21, the wave disturbance map of the Iskenderun Port for westerly regular waves is observed. The inner harbor is very tranquil in this scenario. Compared to the irregular westerly wave case (Case 3), some spots of inside the harbor have higher disturbance coefficients which are probably due to the periodic and directional regularity of the incoming waves. The reflected waves from the piers may be building up at certain spots to form higher spot wave heights.

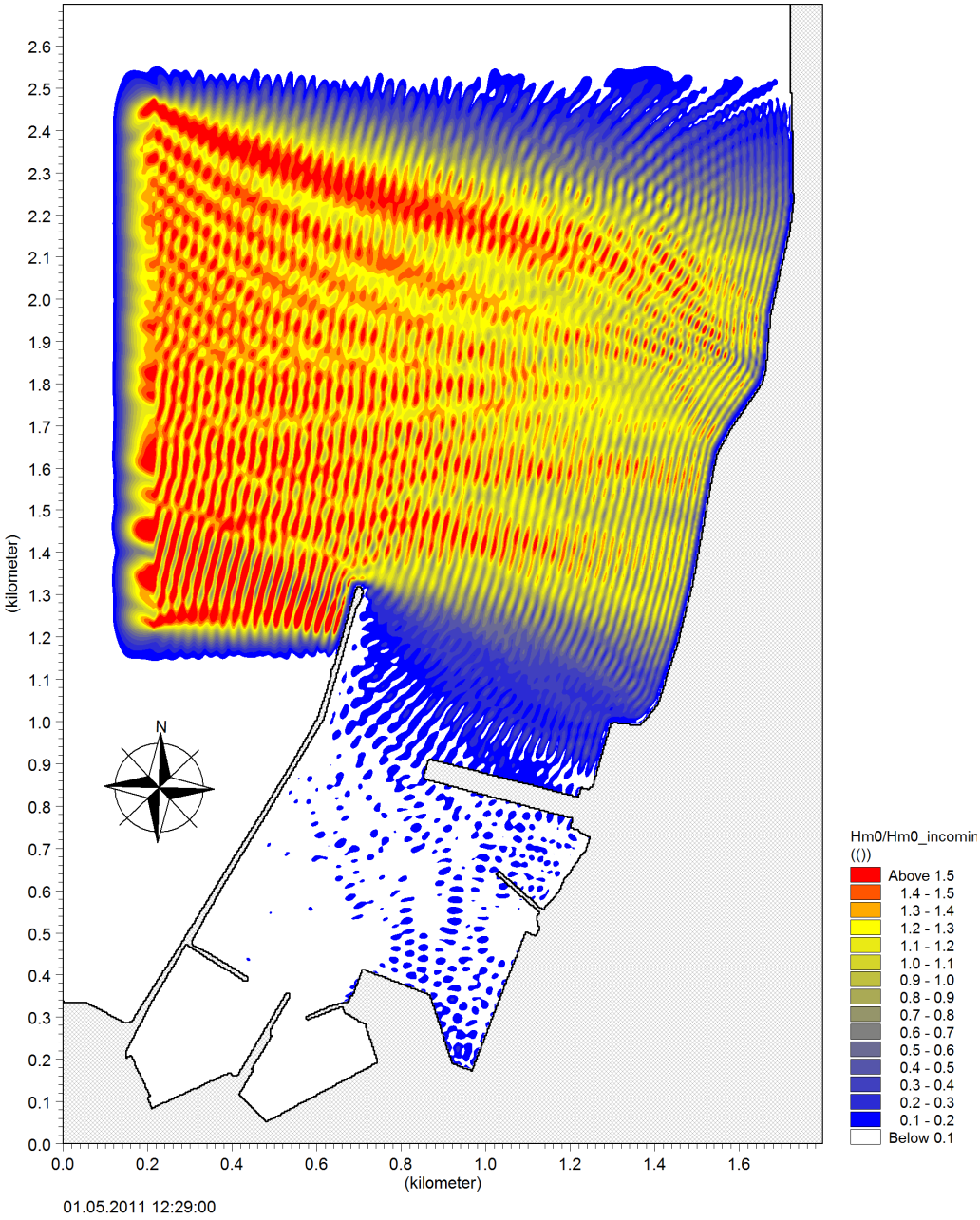

Figure 6-21: Wave Disturbance Map After 29 Minutes

CHAPTER 7

CONCLUSIONS AND RECOMMENDATIONS FOR FURTHER STUDIES

The latest developments in the field of numerical modeling of water waves have enabled the researchers and engineers to model complex hydrodynamic mechanisms of the ocean more accurately. Together with the increasing processor capabilities of computers, much more detailed outputs can be obtained from the advanced computational tools. Compared to the physical scale models; when setup properly, numerical models save the researcher a tremendous amount of time and money as well as providing flexibility with respect to variable parameters in the model such as layout, bathymetry and scale.

There are several theories and methods to setup models to predict the mechanics and dynamics of water waves. Boussinesq theory is only one of them. Each theory has its advantages-disadvantages, similarities-differences, capabilities-limitations and so on. It is the researcher's responsibility to analyze the engineering problem by using the governing equations which best fit the problem and solve them with proper methods and valid verified numerical methods.

MIKE21 BW, which is developed by Danish Hydraulic Institute, is based on the Boussinesq theory. MIKE21 BW utilizes the enhanced formulations of the Boussinesq equations to setup either 1D or 2D numerical models of water waves which are, in general, of concern in assessment of wave dynamics in ports, harbors and coastal areas.

Nonlinearity and frequency dispersion is included in the enhanced Boussinesq equations. A wide range of wave generation is possible in MIKE21 BW including directional spreading. The model yields good results even for the deep water upto

h/L_0=0.5. MIKE21 BW also reproduces the effects of wave breaking and moving shoreline. These can be listed as the major advantages of MIKE21 BW.

For depths greater than h/L_0=0.5, the error in the results increases and the nonlinear performance of the model decreases. The breaking process may not always be reproduced perfectly in terms of the starting location of the breaking, setup values, decay rates etc. These can be listed as the main disadvantages of MIKE21 BW.

MIKE21 BW has been tested and verified in numerous studies. The model is benchmarked with many different physical experiment results. All the effects of fundamental wave phenomena such as shoaling, refraction, diffraction, reflection and breaking are reproduced well as well as non-linear wave-wave interactions.

MIKE21 BW is compared to NAMI DANCE which is a model based on the nonlinear shallow water equations. A number of plane and composite bathymetries are applied to the models and the propagation and runup of sinusoidal waves are tested. In the plane bathymetry simulations, the gauge reading, the runups and the inundation distances in the results two models are in fairly well agreement. In the composite bathymetry simulations, where the horizontal propagation distance is relatively very long compared to the plane bathymetry simulations, the results of the two models show differences due to dispersion which is not included in NAMI DANCE.

A numerical model of the Datça Yacht Harbor is setup in MIKE21 BW and the results are compared to the results of experimental study of Datça Marina Yacht Harbor. The model is calibrated by adding porosity layers along the coastal boundaries. The disturbance coefficients inside the harbor are in fairly well agreement in both MIKE21 BW and the physical experiment results.

Numerical model tests of Iskenderun Harbor are carried out by using MIKE21 BW as a case study. 4 different input wind waves, i.e. 2 regular and 2 irregular waves, are tested in the model. The wave disturbance maps inside the harbor are plotted.

The followings are developed as for the concluding remarks of this study.

1. It can be stated that MIKE21 BW is a strong, effective and practical tool to study the wave dynamics inside harbors and coastal areas under intermediate and shallow water conditions. The flexible and reliable solution methods based on proven techniques provide the researcher/engineer with the ability to reproduce/predict the nearshore wave parameters for various approaching offshore wave conditions which are predetermined and are readily available as input data.
2. When applied to the problem of determination runup and inundation distances of long waves on plane slope bathymetries, the nonlinear shallow water equations and Boussinesq type equations result in close results of wave shapes. The results are either in fairly well agreement or have minor differences depending on the parameters such as bottom slope and input wave height.
3. The runup and inundation distances increase as the bottom slope gets milder. Also, the leading depression waves cause greater runup and inundation distances on land compared to leading elevation waves.
4. Nonlinear shallow water equations with no dispersion and Boussinesq type equations (with dispersion) reproduce the propagation of 12 min. and 60 min. period long waves on a constant 1000m bathymetry with good agreement. However, when the wave reaches the shelf, the wave profiles begin to differ. While propagating over a constant 50 m depth after the shelf, in NAMI DANCE the wave keeps its initial form while in MIKE21 BW the wave is split into two due to the dispersive terms included in the Boussinesq type equations.
5. Reflection parameters of different coastal boundaries for Datça yacht harbor are determined. Good correlation of disturbance coefficients are obtained in the application to Datça Yacht Harbor for the reflection coefficients given in Table 7-1

Table 7-1: Reflection Coefficients of Coastal Boundaries for Datça Yacht Harbor

Coastal Structure	Reflection Coefficient
Rubble Mound BW	0.40
Rocky Shoreline	0.60
Vertical Wall Piers	0.99

6. The results are generalized and applied to Iskenderun Harbor. The areas inside Iskenderun harbor, where wave agitation becomes critical, are determined under the wave conditions regarding the safe operational time. Under the effect of waves approaching from North-Northeast the significant wave height in front of piers 2-3, 9 and 10 are calculated as 1.03m, 0.84m and 1.00 meters respectively.

The following are the suggestions for further studies.

1. More than one wave with same or different periods should be tested for comparison of results of non-dispersive nonlinear shallow water equations and dispersive Boussinesq type equations.
2. Different bathymetries or coastal slopes can be tested for comparison of the runup of long waves by Boussinesq type equations.

REFERENCES

Abott, M. B., Damsgaard, A. & Rodenhuis, G. S., 1973. System 21 Jupiter. A Design System For Two-dimensional Nearly Horizontal Flows. *J. Hydraulic Resource,* Volume 11, pp. 1-28.

Abott, M. B., Petersen, H. M. & Skovgaard, O., 1978. On The Numerical Modelling Of Short Waves In Shallow Water. *J. Hydr. Res.,* Cilt 16, pp. 173-203.

Agnon, Y., Madsen, P. A. & Schäffer, H. A., 1999. A New Approach To High-Order Boussinesq Model. *J. Fluid Mech.,* Volume 399, pp. 319-333.

Anon., 2010. *NAMI DANCE Version 4.9 Tsunami Simulation / Visualization Code MANUAL.* [Online]
Available at: http://namidance.ce.metu.edu.tr

Battjes, J. A., 1994. Shallow Water Wave Modelling. *Proc. Int. Symp.: Waves - Physical and Numerical Modelling,* pp. 1-23.

Benjamin, T. B., Bona, J. L. & Mahony, J. J., 1972. Model Equations for Long Waves In Non-Linear Dispersive Terms. *Phil. Trans. R. Soc. Lond. A.,* Cilt 272, pp. 47-48.

Boussinesq, J., 1872. Théorie Des Ondes Et Des Remous Qui Se Propagent Le Long D'un Canal Rectangulaire Horizontal, En Communiquant Au Liquide Contenu Dans Ce Canal Des Vitesses Sensiblement Pareilles De La Surface Au Fond. *J. Math. Pures Appl.,* Volume 17, pp. 55-108.

Chen, Q. et al., 2000. Boussinesq Modelling of Wave Transformation, Breaking, and Runup. II:2D. *Journal of Waterway, Port, Coastal and Ocean Engineering,* pp. 48-56.

Deigaard, R., 1989. *Mathematical Modelling Of Waves In the Surf Zone. Prog. Rep. 69. ISVA,* Lyngby: Technical University.

DHI, 2010. *Mike 21 Boussinesq Wave Module Scientific Documentation.* Hørsholm: DHI Water and Environment.

DHI, 2010. *Mike 21 Boussinesq Wave Module User Guide.* Hørsholm: DHI Water and Environment.

Ergin, A. et al., 2011. *İskenderun Limanı Dalgakıran Denge Durumlarının Deneyler Yapılarak Araştırılması Projesi Ara Raporu,* Ankara: Orta Doğu Teknik Üniversitesi İnşaat Mühendisliği Bölümü Deniz Mühendisliği Araştırma Merkezi.

Hamm, L., 1992. *Directional Nearshore Wave Propagation Over A Rip Channel: An Experiment.* Venice, Italy, Proc. 23th Int. Conf. Coastal Eng., pp. 226-239.

Hamm, L., 1992. *Random Wave Propagation In The Nearshore Zone: Experiments In A Directional Wave Basin. Internal Report,* s.l.: MAST-G6M, SOGREAH.

Hamm, L., Mory, M. & Peronnard, C., 1995. *Hydrodynamic Measurements Around A Detached Breakwater In A 3D Wave Basin. Internal Report,* s.l.: MAST-G8M, SOGREAH.

Hansen, J. B. & Svendsen, I. A., 1984. *A Theoretical and Experimental Study of Undertow.* s.l., 19th Coastal Engineering Conference, pp. 2246-2262.

Imamuira, F., Yalçıner, A. C. & Özyurt, G., n.d. *Tunami N2 Tsunami Modelling Manual.* [Online]
Available at: http://tunamin2.ce.metu.edu.tr/

Kennedy, A. B., Chen, Q., Kirby, J. T. & Dalrymple, R. A., 2000. Boussinesq Modelling of Wave Transformation, Breaking, and Runup. I:1D. *Journal of Waterway, Port, Coastal and Ocean Engineering,* pp. 39-47.

Kobayashi, N., De Silva, G. S. & Watson, K. D., 1989. Wave Transformation and Swash Oscillation On Gentle and Steep Slopes. *J. Geophys. Res.,* Volume 94 (C1), pp. 951-966.

Lin, P., 2008. *Numerical Modeling of Water Waves.* London - New York: Taylor & Francis Routledge.

Madsen, O. S. & Mei, C. C., 1969. The Transformation Of A Solitary Wave Over An Uneven Bottom. *J. Fluid Mech.,* Cilt 39, pp. 781-791.

Madsen, P. A., Bingham, H. B. & Liu, H., 2002. A New Boussinesq Method For Fully Nonlinear Waves From Shallow To Deep Water. *J. Fluid Mechanic,* Volume 462, pp. 1-30.

Madsen, P. A., Bingham, H. B. & Schäffer, H. A., 2003. Boussinesq-type Formulations For Fully Nonlinear and Extremely Dispersive Water Waves: Derivation and Analysis. *Proc. R. Soc. Lond. A.,* Volume 459, pp. 1075-1104.

Madsen, P. A. & Fuhrman, D. R., 2010. High-Order Boussinesq-Type Modelling of Nonlinear Wave Phenomena In Deep And Shallow Water. In: *Advances In Coastal And Ocean Engineering Volume 11 - Advances In Numerical Simulation of Nonlinear Water Waves.* Singapore: World Scientific Publishing Company, pp. 245-285.

Madsen, P. A., Fuhrman, D. R. & Wang, B., 2006. A Boussinesq-type Method For Fully Nonlinear Waves Interacting With Rapidly Varying Bathymetry. *Coastal Engineering,* Volume 53, pp. 487-504.

Madsen, P. A., Murray, R. & Sørensen, O. R., 1991. A New Form Of The Boussinesq Equations With Improved Linear Dispersion Characteristics. *Coastal Engineering,* Cilt 15, pp. 371-388.

Madsen, P. A. & Schäffer, H. A., 1998. High-order Boussinesq-type Equations For Surface Gravity Waves: Derivation And Analysis. *Phil. Trans. R. Soc. Lond. A.,* Volume 356, pp. 3123-3181.

Madsen, P. A. & Sørensen, O. R., 1992. A New Form of The Boussinesq Equations With Improved Linear Dispersion Characteristics. Part 2. A Slowly Varying Bathymetry. *Coastal Engineering,* Volume 18, pp. 183-204.

Madsen, P. A., Sørensen, O. R. & Schäffer, H. A., 1997. Surf Zone Dynamics Simulated By A Boussinesq Type Model. Part I. Model Description and Cross-shore Motion Of Regular Waves. *Coastal Engineering,* Volume 32, pp. 255-287.

Madsen, P. A., Sørensen, O. R. & Schäffer, H. A., 1997. Surf Zone Dynamics Simulated By A Boussinesq Type Model. Part II: Surf Beat And Swash Oscillations For Wave Groups And Irregular Waves. *Coastal Engineering,* Volume 32, pp. 289-319.

Mase, H., 1994. *Uprush-backrush Interaction Dominated and Long Wave Dominated Swash Oscillations.* Vancouver, Canada, International Int. Symposium: Waves-Physical and Numerical Modelling, pp. 316-325.

Mase, H., 1995. Frequency Down-shift of Swash Oscillations Compared to Incident Waves. *J. Hydraulic Res.,* Volume 33 (3), pp. 397-411.

Mei, C. C. & Méhauté, B. L., 1966. Note On The Equations Of Long Waves Over An Uneven Bottom. *J. Geophys. Re.,* Volume 71, pp. 393-400.

Mortensen, S. B., 2006. *Numerical Modeling Of The Surf Zone Dynamics In Waimea Bay,* Denmark: Technical University of Denmark.

Mory, M. & Hamm, L., 1997. Wave Height, Setup and Currents Around A Detached Breakwater Submitted To Regular Or Random Wave Forcing. *Coastal Engineering,* Volume 31, pp. 77-96.

Nwogu, O., 1993. Alternative Form of Boussinesq Equations for Near Shore Wave Propagation. *Journal of Waterway, Port, Coastal and Ocean Engineering,* Volume 119(6), pp. 618-638.

Nwogu, O., 1996. *Numerical Prediction of Breaking Waves and Currents with a Boussinesq Model.* Orlando, s.n.

Nwogu, O. G. & Demirbilek, Z., 2001. *BOUSS-2D: A Boussinesq Wave Model for Coastal Regions and Harbors - Report 1 Theoretical Background and User's Manual,* s.l.: US Army Corps of Engineers Engineer Research and Development Center.

Özhan, E., Ergin, A., Yalçıner, A. C. & Abdalla, S., 1999. *Datça Yat Limanı İçin Rüzgar, Dalga, Limaniçi Çalkantı ve Kirlenme Araştırmaları,* Ankara: s.n.

Peregrine, D. H., 1967. Long Waves On A Beach. *J. Fluid Mech.,* Volume 27, pp. 815-827.

Schäffer, H. A., Madsen, P. A. & Deigaard, R., 1993. A Boussinesq Model For Waves Breaking In Shallow Water. *Coastal Engineering,* Volume 20, pp. 185-202.

Sørensen, O. R., Schäffer, H. A. & Madsen, P. A., 1998. Surf Zone Dynamics Simulated By A Boussinesq Type Model. Part III. Wave-induced Horizontal Nearshore Circulations. *Coastal Engineering,* Volume 33, pp. 155-176.

Stive, M. J. F., 1980. *Velocity and Pressure Field of Spilling Breakers.* s.l., 17th Coastal Engineering Conference, pp. 547-566.

Svendsen, I. A., 1984. Wave Heights And Setup In A Surf Zone. *Coastal Engineering,* Volume 8, pp. 303-329.

Ting, F. C. K. & Kirby, J. T., 1994. Observation of Undertow and Turbulence In A Laboratory Surf Zone. *Coastal Engineering,* Volume 24, pp. 51-80.

Wei, G., Kirby, J. T., Grilli, S. T. & Subramanya, R., 1995. A Fully Nonlinear Boussinesq Model for Surface Waves. I: Highly Nonlinear, Unsteady Waves. *Journal of Fluid Mechanics,* Volume 294, pp. 71-92.

Witting, J. M., 1984. A Unified Model For The Evolution Of Nonlinear Water Waves. *J. Comput. Phys.,* Cilt 56, pp. 203-236.

Young, I. R., 1999. *Wind Generated Ocean Waves.* Amsterdam-Lausanne-New York-Oxford-Shannon-Singapore-Tokyo: Elsevier.

APPENDIX A

POROSITY VS. REFLECTION DIAGRAMS

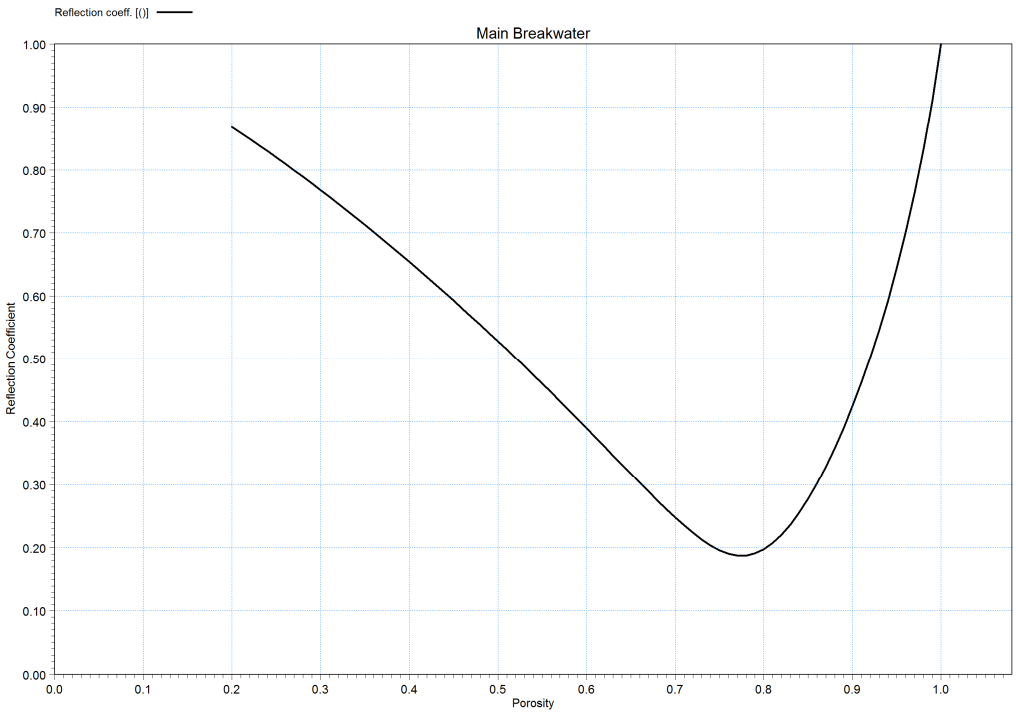

Figure A-1: Porosity vs. Reflection Diagram for Main Breakwater

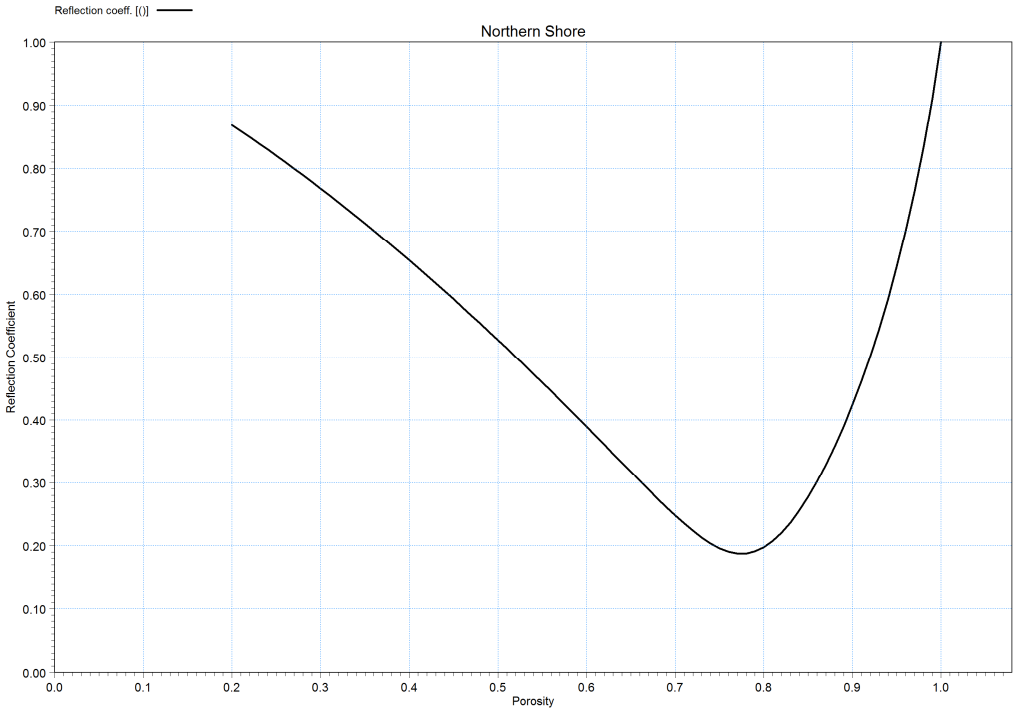

Figure A-2: Porosity vs. Reflection Diagram for Northern Shore

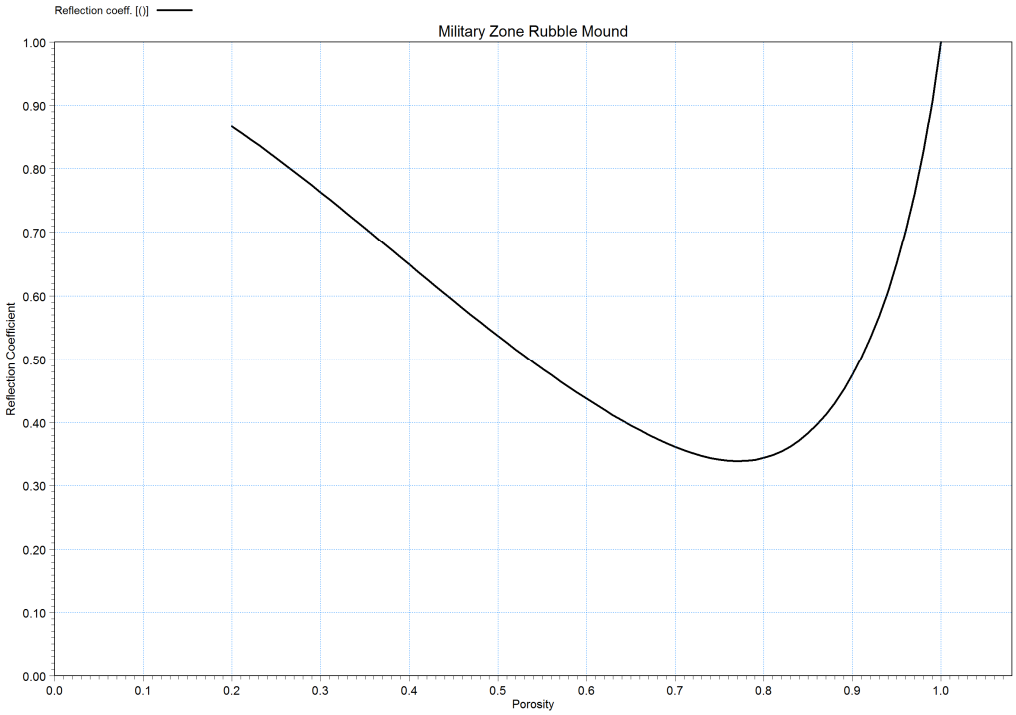

Figure A-3: Porosity vs. Reflection Diagram for Military Zone RM

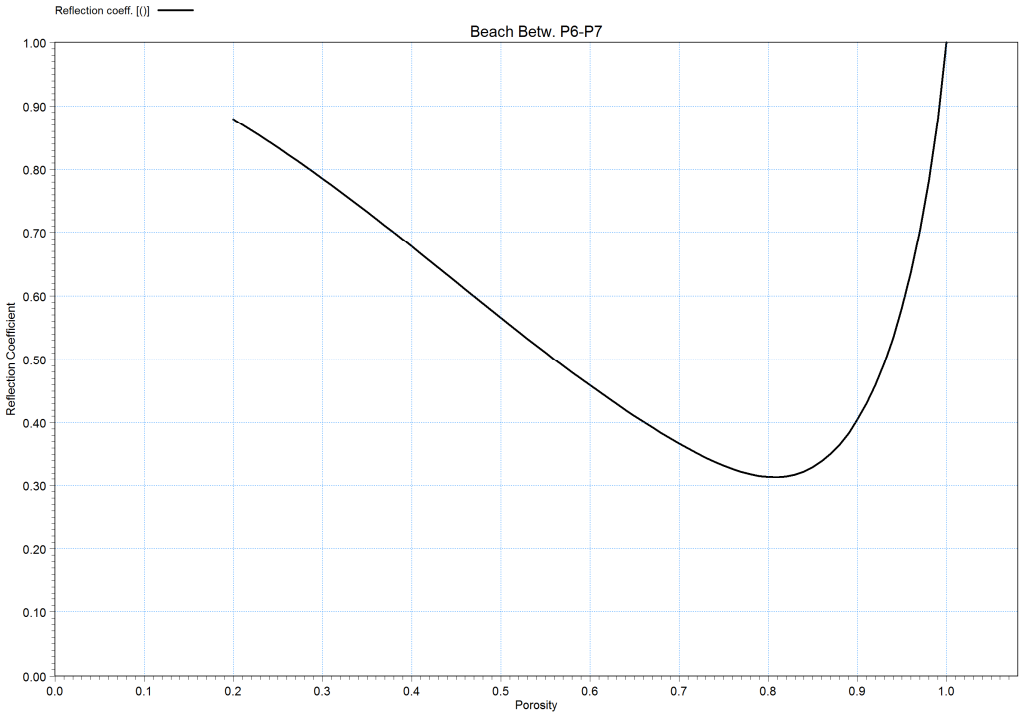

Figure A-4: Porosity vs. Reflection Diagram for Beach Between P6-P7

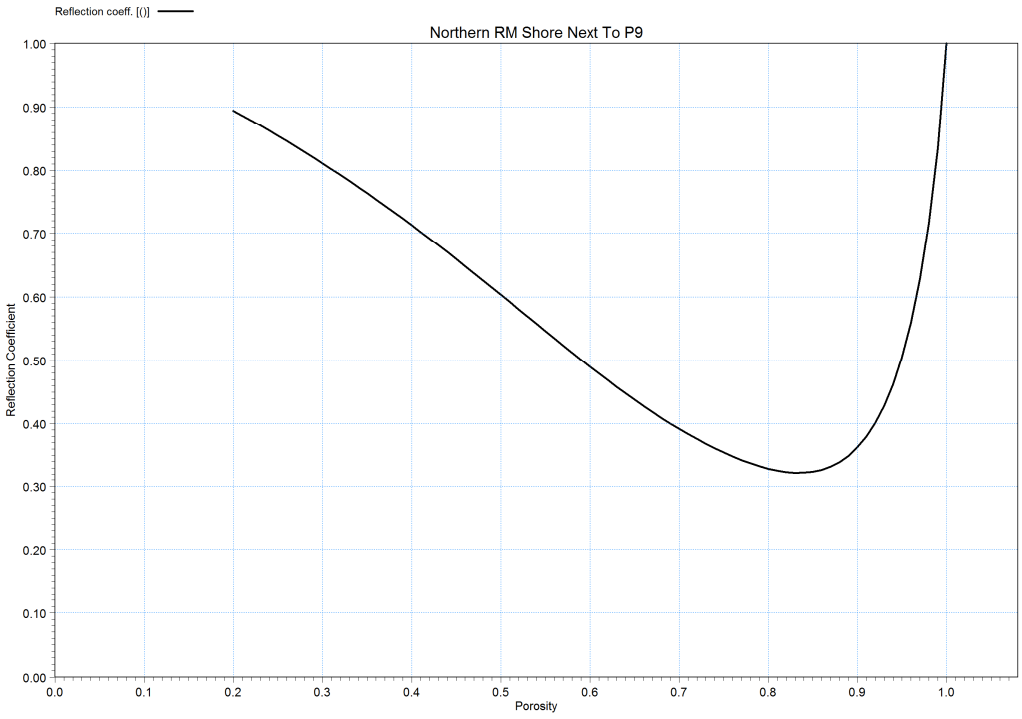

Figure A-5: Porosity vs. Reflection Diagram for Northern RM Shore by P9

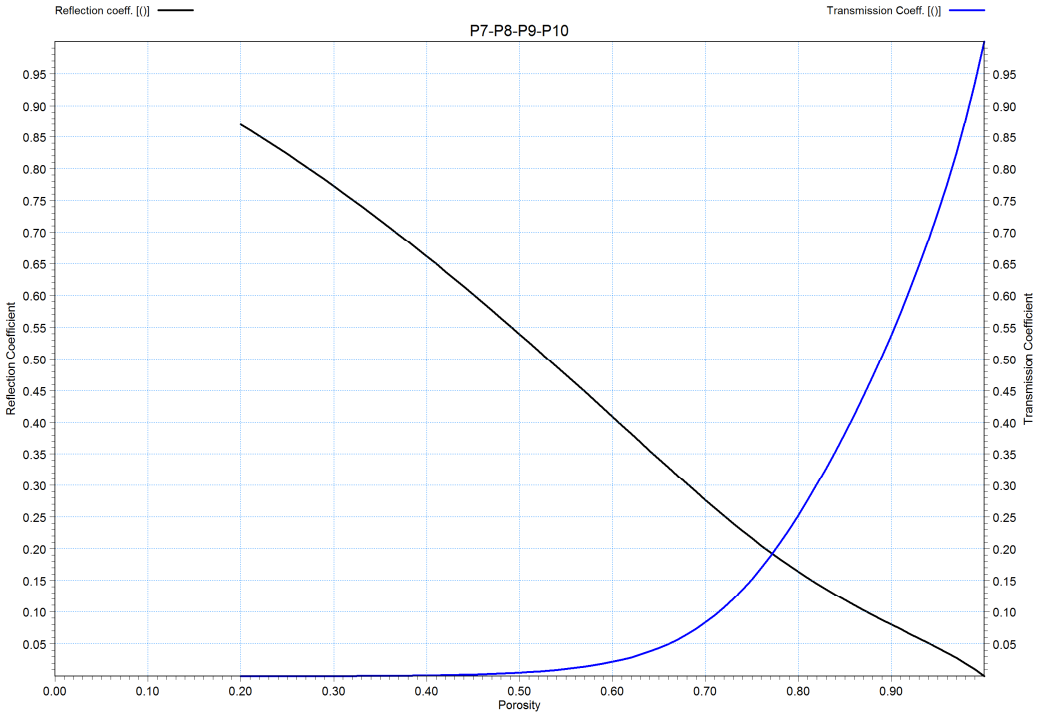

Figure A-6: Porosity vs. Reflection Diagram for P7-P8-P9-P10

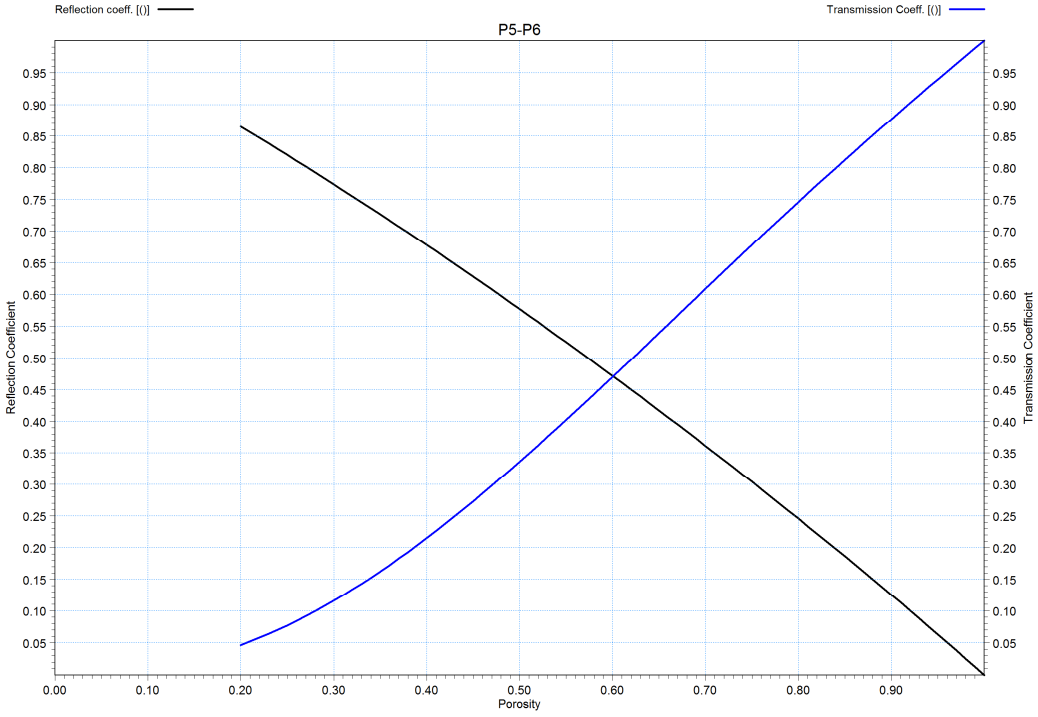

Figure A-7: Porosity vs. Reflection Diagram for P5-P6

APPENDIX B

THEORY OF THE BOUSSINESQ TYPE MODEL

In this appendix, the theory of the Boussinesq type model (MIKE21 BW) is briefly presented.

The following sections are based on the studies carried out in (Madsen & Sørensen, 1992), (Madsen, et al., 1997), (Sørensen, et al., 1998), and (Mortensen, 2006).

B.1 The Enhanced Boussinesq Equations

The numerical model is based on two-dimensional equations of the Boussinesq type using a depth integrated flux-formulation with enhanced linear dispersion characteristics as presented in (Madsen, et al., 1997). The enhanced Boussinesq formulations are as follows:

$$\frac{\partial \eta}{\partial t} + \frac{\partial P}{\partial x} + \frac{\partial Q}{\partial y} = 0 \tag{B-1}$$

$$\frac{\partial P}{\partial t} + \frac{\partial}{\partial x}\left(\frac{P^2}{d}\right) + \frac{\partial}{\partial y}\left(\frac{PQ}{d}\right) + \frac{\partial R_{xx}}{\partial x} + \frac{\partial R_{xy}}{\partial y} + gd\frac{\partial \eta}{\partial x} + \psi_x + \frac{\tau_x}{\rho} = 0 \tag{B-2}$$

$$\frac{\partial Q}{\partial t} + \frac{\partial}{\partial y}\left(\frac{Q^2}{d}\right) + \frac{\partial}{\partial x}\left(\frac{PQ}{d}\right) + \frac{\partial R_{yy}}{\partial y} + \frac{\partial R_{xy}}{\partial x} + gd\frac{\partial \eta}{\partial y} + \psi_y + \frac{\tau_y}{\rho} = 0 \tag{B-3}$$

In the formulations above, η is the surface profile, d is the total water depth (still water depth + instantaneous surface profile), (P,Q) are the depth integrated velocity components (volume flux) in the Cartesian coordinate system where the subscripts denote differentiation with respect to space (Madsen, et al., 1997).

The terms denoted by R_{xx}, R_{yy} and R_{xy} account for the excess momentum originating from the nonuniform velocity distribution due to the presence of roller (Madsen, et al., 1997).

$$\left(R_{xx}, R_{xy}, R_{yy}\right) = \frac{\delta}{1-\delta/d}\left(\left(c_x - \frac{P}{d}\right)^2, \left(c_x - \frac{P}{d}\right)\left(c_y - \frac{Q}{d}\right), \left(c_y - \frac{Q}{d}\right)^2\right) \tag{B-4}$$

The surface roller concept is basically a volume of water which propagates with the wave celerity which results in the vertical distribution of the horizontal particle velocity. It is used to define the breaking phenomena by inserting extra momentum into the equation by R_{xx}, R_{yy} and R_{xy}. In (B-4), δ=(t, x, y) is the roller thickness and (c_x, c_y) are the wave (also roller) celerity (Madsen, et al., 1997).

ψ_x and ψ_y are dispersive Boussinesq terms which were originally derived by (Peregrine, 1967) for shallow water. Later these terms were enhanced by (Madsen & Sørensen, 1992) to provide improved frequency dispersion (Madsen, et al., 1997). In the following parts, the formulation of (Madsen & Sørensen, 1992), which is derived under the mild-slope assumptions, are adopted.

$$\begin{aligned}\psi_x \equiv & -\left(B+\frac{1}{3}\right)h^2\left(\frac{\partial^3 P}{\partial x^2 \partial t}+\frac{\partial^3 Q}{\partial x \partial y \partial t}\right) - Bgh^3\left(\frac{\partial^3 \eta}{\partial x^3}+\frac{\partial^3 \eta}{\partial x \partial y^2}\right) \\ & - h\frac{\partial h}{\partial x}\left(\frac{1}{3}\frac{\partial^2 P}{\partial x \partial t}+\frac{1}{6}\frac{\partial^2 Q}{\partial y \partial t}+2Bgh\frac{\partial^2 \eta}{\partial x^2}+Bgh\frac{\partial^2 \eta}{\partial y^2}\right) \\ & - h\frac{\partial h}{\partial y}\left(\frac{1}{6}\frac{\partial^2 Q}{\partial x \partial t}+Bgh\frac{\partial^2 \eta}{\partial x \partial y}\right)\end{aligned} \tag{B-5}$$

$$\begin{aligned}\psi_y \equiv & -\left(B+\frac{1}{3}\right)h^2\left(\frac{\partial^3 Q}{\partial y^2 \partial t}+\frac{\partial^3 P}{\partial x \partial y \partial t}\right) - Bgh^3\left(\frac{\partial^3 \eta}{\partial y^3}+\frac{\partial^3 \eta}{\partial y \partial x^2}\right) \\ & - h\frac{\partial h}{\partial y}\left(\frac{1}{3}\frac{\partial^2 Q}{\partial y \partial t}+\frac{1}{6}\frac{\partial^2 P}{\partial x \partial t}+2Bgh\frac{\partial^2 \eta}{\partial y^2}+Bgh\frac{\partial^2 \eta}{\partial x^2}\right) \\ & - h\frac{\partial h}{\partial x}\left(\frac{1}{6}\frac{\partial^2 P}{\partial y \partial t}+Bgh\frac{\partial^2 \eta}{\partial x \partial y}\right)\end{aligned} \tag{B-6}$$

In (B-5) & (B-6), B is the dispersion coefficient which provides linear dispersion characteristics corresponding to a Padé [2,2] expansion of the Stokes linear dispersion relation when set equal to 1/15. The bottom friction is also included in the Equations (B-2) & (B-3) by the terms τ_x/g and τ_y/g. (Madsen, et al., 1997).

B.2 Linear Shoaling Characteristics

In this section a brief shoaling analysis of the enhanced Boussinesq equations is demonstrated. The analysis is carried out for the one dimensional type of the equations (B-1), (B-2) and (B-3) for the no bottom friction and nonbreaking case. Under these assumptions the governing equations become:

$$\frac{\partial \eta}{\partial t} + \frac{\partial P}{\partial x} = 0 \tag{B-7}$$

$$\frac{\partial P}{\partial t} + gh\frac{\partial \eta}{\partial x} - Bgh^3\frac{\partial^3 \eta}{\partial x^3} - \left(B + \frac{1}{3}\right)h^2\frac{\partial^3 P}{\partial x^2 \partial t} - \frac{\partial h}{\partial x}\left(2Bgh^2\frac{\partial^2 \eta}{\partial x^2} + \frac{1}{3}h\frac{\partial^2 P}{\partial x \partial t}\right) = 0 \tag{B-8}$$

By inserting (B-7) into (B-8) and by cross-differentiation:

$$\frac{\partial^2 \eta}{\partial t^2} - gh\frac{\partial^2 \eta}{\partial x^2} + Bgh^3\frac{\partial^4 \eta}{\partial x^4} - \left(B + \frac{1}{3}\right)h^2\frac{\partial^4 \eta}{\partial x^2 \partial t^2} = \frac{\partial h}{\partial x}\left(g\frac{\partial \eta}{\partial x} + (2B+1)h\frac{\partial^3 \eta}{\partial x \partial t^2} - 5Bgh^2\frac{\partial^3 \eta}{\partial x^3}\right) \tag{B-9}$$

The solution is in the form:

$$\eta(x,t) = A(x)e^{i(\omega t - \varphi(x))} \tag{B-10}$$

Where A is the local wave amplitude, ω is the cyclic frequency and φ is the phase function which is expressed in terms of wave number as:

$$\frac{\partial \varphi}{\partial x} = k(x) \tag{B-11}$$

For a case where the water depth, the wave number and the wave amplitude are assumed to vary slowly with respect to x, the higher derivatives of these terms can be neglected (Madsen & Sørensen, 1992). By inserting (B-10) into (B-9) and neglecting all derivatives of h, k and A to the lowest order, the linear dispersion relation is obtained as:

$$-\omega^2 + \ ghk^2 + Bgh^3k^4 - \left(B + \frac{1}{3}\right)k^2h^2\omega^2 = 0 \tag{B-12}$$

Equation (B-12) can be expressed as:

$$\omega^2 = \frac{3(gk^2h + Bgk^4h^3)}{3 + k^2h^2 + 3Bk^2h^2} \tag{B-13}$$

The linear dispersion relation for the linear wave theory is given by: (Mortensen, 2006)

$${\omega_{stokes}}^2 = g \cdot k \cdot \tanh(kh) \tag{B-14}$$

By combining (B-13) & (B-14), the ratio is obtained as:

$$\frac{\omega^2}{{\omega_{stokes}}^2} = \frac{3kh\left(1 + \frac{1}{15}(kh)^2\right)\coth(kh)}{3 + \frac{18}{15}(kh)^2} \tag{B-15}$$

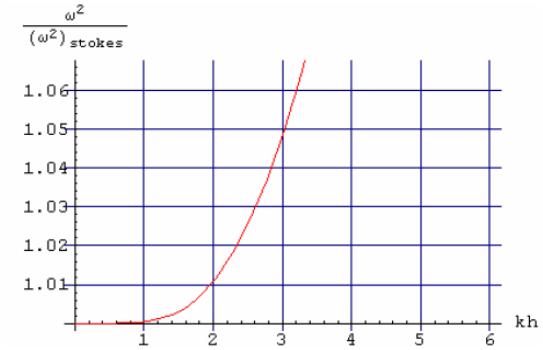

Figure B-1: Comparison of Linear Dispersion Characteristics of Boussinesq Equations with Linear Wave Theory (Mortensen, 2006)

In Figure B-1, it is observed that the Boussinesq equations yield results which are almost exact matches of the linear theory results' in terms of linear dispersion characteristics up to a kh (wave number) value of around 1. After this point the deviation increases rapidly and goes beyond acceptable limits around kh=3.15 for which there is a difference of around 5.7%. This value (kh=3.15) is also the recommended upper limit for the enhanced Boussinesq equations as stated in (DHI, 2010). (Mortensen, 2006).

B.3 Wave Celerity

In (Madsen & Sørensen, 1992), the celerity is calculated interactively from the local wave field. However, since the feedback to the mass and momentum equations through the roller model makes it a recursive system, instabilities may occur in the form of "noise". Due to this fact in (Sørensen, et al., 1998) the celerity is given as a two dimensional expression of the linear formulation $c = 1.3\sqrt{gh}$ (Mortensen, 2006).

$$\begin{pmatrix} c_x \\ c_y \end{pmatrix} = \begin{pmatrix} \frac{\partial \eta}{\partial x} \\ \frac{\partial \eta}{\partial y} \end{pmatrix} \cdot \frac{1.3 \cdot \sqrt{gh}}{\sqrt{\left(\frac{\partial \eta}{\partial x}\right)^2 + \left(\frac{\partial \eta}{\partial y}\right)^2}} \qquad \text{(B-16)}$$

where η is the surface elevation and h is the still water depth. Although this approximation was shown to yield good results for regular waves, it does not represent some processes such as the deceleration of primary waves due to downrush of long waves in the swash zone very well. (Sørensen, et al., 1998).

B.4 Wave Breaking

The roller concept was first suggested by (Svendsen, 1984). As mentioned in Appendix B.B.1, the basic principle is that a roller is a volume of water being propagated with the wave celerity, adding an extra momentum to the formulation in order to account for the breaker whose characteristics are inherited from a spilling one (Madsen, et al., 1997).

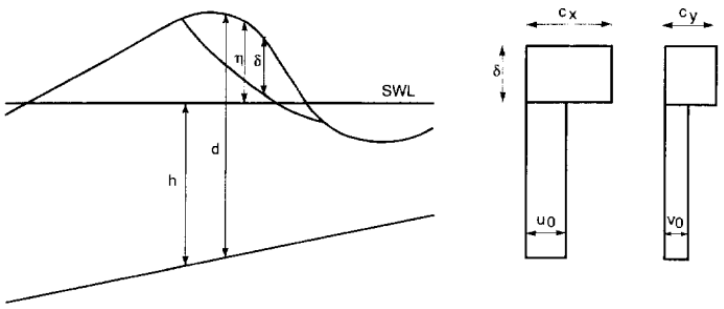

Figure B-2: Cross-section of a breaking wave and assumed vertical profile of the horizontal particle velocity components (Madsen, et al., 1997)

The breaking is assumed to start when the local slope of the surface profile exceeds an initial threshold value, $\tan\phi_B$ as suggested by (Deigaard, 1989). According to the results of the research carried out by (Schäffer, et al., 1993) for spilling breakers on plane sloping beaches, using $\phi_B = 20°$ yields acceptable results although this value may not represent all types of breakers adequately (Madsen, et al., 1997).

After the breaking starts, the initial threshold angle, ϕ_B, gradually decreases to a terminal angle ϕ_0. This is due to the transition from the initial breaking to a bore-like stage in the inner surf zone. Henceforth, the value of ϕ constantly varies with time. In other words ϕ depends on the age of the roller (Madsen, et al., 1997). The decay function is as follows:

$$\tan\phi(t) = \tan\phi_0 + (\tan\phi_B - \tan\phi_0)exp\left[-ln2\frac{t-t_B}{t_{1/2}}\right] \quad \text{(B-17)}$$

where $t_{1/2}$ is the time scale for the development of the roller (i.e. half time for the decay of ϕ_B to ϕ_0.)

As observed in Figure B-2, the roller is the water mass above the tangent of slope $\tan\phi$ and the breaking stops when the maximum local slope becomes less than $\tan\phi$.

Before inserting the roller thickness into the governing equations, it is multiplied by a shape factor f_δ following the determination of the roller at each time step. (Madsen, et al., 1997).

B.5 Bottom Friction

The bottom shear in the model is defined as:

$$(\tau_x, \tau_y) = \frac{1}{2} f_m \rho \frac{\sqrt{P^2+Q^2}}{d^2}(P,Q) \quad \text{(B-18)}$$

where f_m is the friction factor, (P,Q) are depth integrated velocities (volume fluxes) and d is the instantaneous water depth.

B.6 Moving Shoreline

In order to simulate the runup of waves onto the shore, the shoreline has to change for each time step. But this procedure is usually problematic and the solution may vary among different models. The approach followed in MIKE21 BW is straightforward and is as follows: The computational domain (wet grids) is extended artificially into the shore by replacing the solid beach by a permeable one which has a very small porosity. Thus, near the moving shoreline, the water surface intersects with the sea bed and continues into the porous beach. This intersection line gives the instantaneous position of the moving shoreline. (Madsen, et al., 1997).

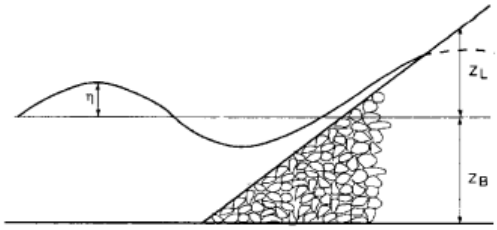

Figure B-3: Definition sketch of a beach including an artificial porous regime (Madsen, et al., 1997)

In order to avoid numerical instabilities, an exponential transition is introduced between the physical regime and the porous flow regime:

$$\gamma(z) = \begin{cases} 1, & Z_L \leq z \\ \varepsilon + (1-\varepsilon)e^{\beta(z-Z_L)/(Z_L-Z_B)}, & Z_B \leq Z \leq Z_L \end{cases} \quad \text{(B-19)}$$

where $\gamma(z)$ is the porosity, ε is the minimum value of γ, β is a constant shape factor, z is the vertical coordinate, $Z_L(x,y)$ defines the physical seabed and Z_B is the lower limit of the porous zone. The resulting effective water depth is determined by integration as follows: (Madsen, et al., 1997)

$$A(x,y,t) \equiv \int_{Z_B}^{\eta} \gamma(z)dz \quad \text{(B-20)}$$

For the porous flow formulation, this effective water depth replaces the physical water depth *d* in the depth-integrated momentum equations (B-2) & (B-3). (Madsen, et al., 1997)

The nature of the formulation above is the combination of the physical flow regime of clear water with an artificial porous flow regime for which the depth term in the momentum equations is dealt with in a straightforward method. Yet, introducing the porosity in the continuity equation (B-1) is not as straightforward.

The new form of the continuity equation for the porous flow is:

$$\alpha \frac{\partial \eta}{\partial t} + \frac{\partial P}{\partial x} + \frac{\partial Q}{\partial y} = 0 \qquad \text{(B-21)}$$

where α is the representative porosity value. α is the function of the local surface elevation, and it is unity in clear water and it decays exponentially to the value of ε whenever the water surface disappears into the porous beach (Madsen, et al., 1997). Instead of using a depth averaged porosity, which would result in porous flow conditions over the whole domain, α is defined as such.

$$\alpha(x, y, t) \equiv \gamma(\eta) \qquad \text{(B-22)}$$

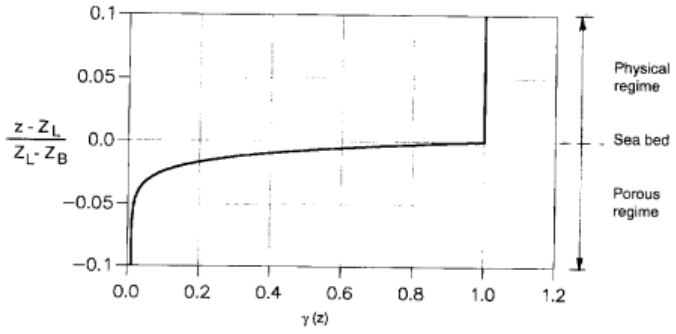

Figure B-4: Vertical variation of the porosity, $\gamma(z)$ (Madsen, et al., 1997)

This method for moving shoreline explained so far is very practical and easy to apply to 2D formulations yet it underestimates the uprush and downrush on impermeable slopes due to minor errors in the mass balance (Madsen, et al., 1997).

B.7 Numerical Scheme

2D Boussinesq Wave Module of MIKE21 utilizes a numerical method which is based on the so-called SYSTEM 21. It was (Abott, et al., 1973) who first introduced the SYSTEM 21 and later it was (Abott, et al., 1978) who extended it to short wave modeling. Since then, this numerical method has been under constant enhancement such as in (Madsen, et al., 1991) and (Madsen & Sørensen, 1992).

"The differential equations are discretized by using a time-centered implicit scheme with variables defined on a space-staggered rectangular grid. Scalar quantities such as water surface elevation are defined in the grid nodes, whereas flux components are defined halfway between adjacent grid nodes in the respective directions. The finite-difference approximation of the spatial derivatives is a straightforward mid-centering, except for the convective terms, which are described in detail in (Madsen & Sørensen, 1992)." (DHI, 2010).

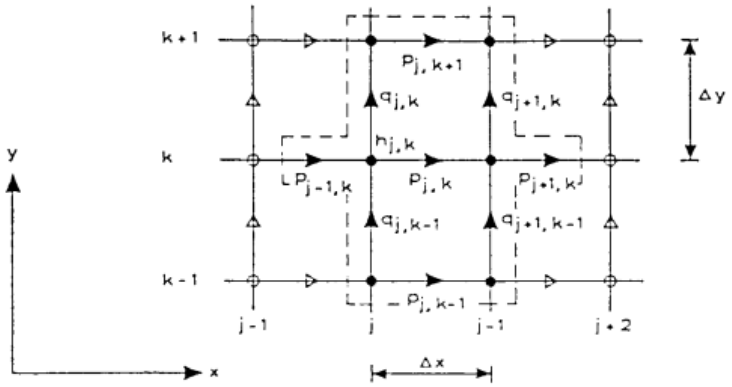

Figure B-5: Grid notation used for x-momentum equation (Madsen & Sørensen, 1992)

"The applied algorithm is a non-iterative Alternating Direction Implicit algorithm using a fractional step technique and side-feeding (semi-linearization of non-linear terms)." (DHI, 2010)

The result is a system of finite difference equations which are reduced to a three-diagonal system and solved by the Double Sweep algorithm (Madsen & Sørensen, 1992).

In zones with steep gradients, the model may become unstable due to artificial high frequency oscillations, or so-called noise. In these regions, a simple unwinding scheme is applied to avoid instabilities (Mortensen, 2006).

The standard representation of the solution of the cross Boussinesq terms requires a back centering of these terms half a time step. This procedure results in artificial attenuation of the waves propagating with an angle to the grid. In order to avoid this effect, a linear extrapolation scheme is applied. However, time-centering the

cross terms as discussed above may again cause instabilities. In order to prevent this, a time extrapolation factor is utilized in the model. The value of the time extrapolation factor varies between 0 and 1 where 1 means a correct time centering and 0 means a backward centering. (Mortensen, 2006). In cases where there is a stability problem in the model, decreasing the time extrapolation factor will aid the problem. However, using a time extrapolation factor of 0 should be used a last resort since the waves over the domain are going to be artificially dissipated to a certain extent due to backward centering.